Transient Photoconduction in Amorphous Materials.

A thesis presented by

John Berkin

(Sponsoring establishment

Dundee Institute of Technology

Collaborating establishment

Philips Research Laboratories)

to the CNAA

in partial fulfilment of the

requirments for the degree of

Doctor of Philosophy

May 1989

DECLARATION

I declare that while registered as a candidate for the degree for which this thesis is presented I have not been a candidate for any other award. I further declare that except where stated the work contained in this thesis is original and was performed by the author. The author is grateful to the Dundee University Amorphous Materials Group who kindly supplied the amorphous silicon used.

signed 

Advanced Studies

In addition to the original research presented in this thesis the author attended the Chelsea Meeting on Amorphous and Liquid semiconductors in 1985, 1986 and 1987. The author also attended the International Conference on Amorphous and Liquid Semiconductors in Prague 1987.

ACKNOWLEDGMENTS

The author is greatly indebted to and wishes to thank the following without whose help this work would not have been possible.

Dr. Charles Main and Dr. Joseph M. Marshall for their supervision, encouragement and friendship during this investigation.

Dr. Anthony R. Hepburn and Dr. Charles Bullock for helpful discussions to numerous to mention.

Dr. R.R. Gardener for extending to the author the use of the facilities of the Department of Electronic Engineering at Dundee Institute of Technology.

Mr. J.C. Anderson and all the technical staff of the former Department of Physics for their help and advice during the course of this study.

The staff of the Computing Centre Dundee Institute of Technology for helping with many strange requests.

Dundee Institute of Technology for providing the finacial assistance which made this work possible.

Most of all to my wife Gaenor for putting up with strange working hours during both the research and the preparation of this thesis.

TRANSIENT PHOTOCONDUCTION IN AMORPHOUS MATERIALS

JOHN BERKIN

Abstract.

Much of the work presented within this thesis is concerned with the development of computer programs capable of simulating the transient current pulses that would be expected for amorphous materials possessing known density of states distributions. Two simulation methods are used, the Monte Carlo technique and the finite difference method. While the Monte Carlo method makes few basic assumptions, the transients produced are noisy and the computer execution times are long. The newly developed finite difference method circumvents both of these problems. Comparison of the finite difference results with those obtained from Monte Carlo simulations shows that the transients produced are essentially the same. The finite difference method can therefore be used to produce accurate, noise free simulated transients in relatively short times.

The simulation programmes are used to investigate the accuracy of three methods proposed as techniques for obtaining the functional form of the density of states from 'time of flight' current transients. The three analysis methods used are the Marshall - Allen technique, the 'TROK' method and the integral technique. The last of these was developed during the course of this work. These three methods were each used to analyse the transients that would be produced by an amorphous semiconductor possessing either an exponential or linear distribution of tail states. These two distributions were chosen as they are both currently proposed in the literature as possible candidates for the density of states within amorphous silicon.

Examination of the results produced when each of these analytical methods was applied to the same transients revealed major differences in the calculated results. The TROK method could not distinguish between the two different types of tail state distribution, and interpreted linear tail simulated data in terms of an exponential distribution of characteristic temperature 312K, a figure very close to that frequently quoted in the literature. The Marshall - Allen technique could differentiate between the two distributions but could not reproduce the correct functional forms. The integral technique distinguished between the two distributions and also gave them their correct functional form.

To complement the computer simulation work above, an experimental computerized 'time of flight' measurement system was developed and constructed by the author. This system was used to obtain transients over a wide range of field and temperature, as is required by the integral technique. Unfortunately, due to the nature of the sample used, only a small energy range within the tail states could be studied. When analysed, two functional forms for the distribution proved to be possible; these were an exponential tail (T_c = 93K) and a linear tail (ΔE = 0.165eV). The exponential tail would, however, not be consistent with the observation of anomalously dispersive transients above 100K so it was rejected as an option.

Contents.

1 Electronic Transport in Amorphous Materials.

1.1 Crystalline Materials.

An ideal crystalline material is a substance which is arranged in a three dimensional periodically repeating array, so that any given lattice point is in exactly the same enviroment as any other equivalent lattice point. This array of points extends infinitely in all directions. Such a crystal is said to possess infinite long range order. The immediate surroundings of any given atom will be identical to any other corresponding atom in any other unit cell. This correspondence is termed short range order.

As real crystals are materials of finite dimensions they do not possess *infinite* long range order. However the long range order is still maintained over a distance that is much greater than the dimensions of the unit cell. The perturbations caused by the lack of infinite long range order are sufficiently small that many of the theories of ideal crystals can be used with real materials. Specifically the theory of the band structure of crystalline materials can be developed from consideration of an ideal lattice.

The theory of band structure in crystalline materials is well established. There are certain universal features in the structure of crystalline solids. These features include :-

Figure 1.1 Energy bands separated by a forbidden gap.

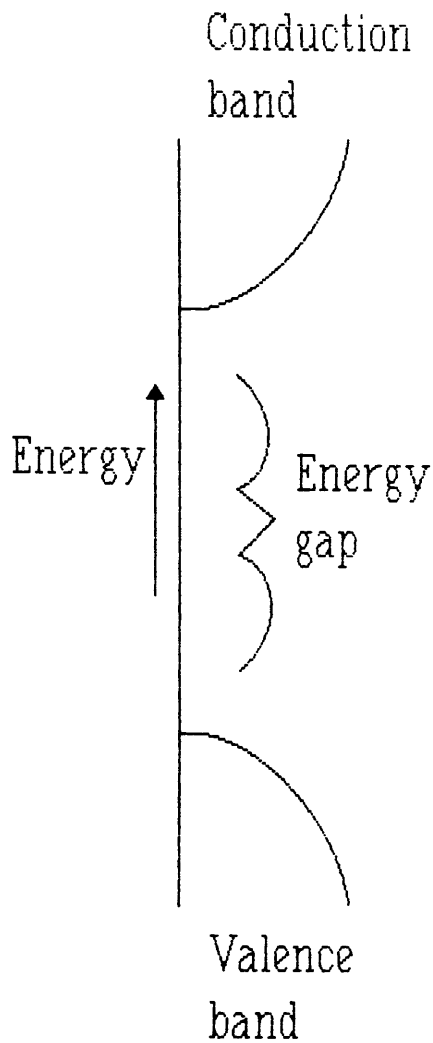

1. The presence of energy bands *separated* by forbidden gaps. (see figure 1.1).

2. The fact that the crystal momentum is a good quantum number.

3. The electron wavefunction has the form of a plane wave modulated by a function which has the same periodicity as the lattice.

The electron wavefunction will extend throughout the entire crystal. In a perfect lattice at absolute zero the electron wavefunction would maintain coherence over the entire lattice. This would mean that the electrons would not be scattered at all. However, in a real crystal at finite temperature the electrons will be scattered from imperfections in the crystal or from interaction with phonons. An electron will therefore only travel a certain distance, the mean free path λ, before it is scattered. This scattering typically results in an electron mobility $\mu \geq 100$ $cm^2V^{-1}s^{-1}$.

Using this model as a starting point it is possible to form a theory of electronic transport mechanisms in amorphous materials. (A review of electronic transport in both crystalline and amorphous materials can be found in either Roberts et al [1] or Nagels [2])

1.2 Amorphous Materials.

In an amorphous material the long range order, that is so important in crystalline theory, no longer exists. There is no long

term periodicity within the material and the concept of a regular lattice must be abandoned. However, the atoms forming the material still have the same bonding requirements. Therefore the short range order about any particular atom will be essentially the same as within the crystalline material.

The amorphous analogue of the ideal crystal is the *continuous random network* (CRN). In a CRN all of the bonds between atoms are satisfied and there are no vacancies. Many theoretical studies of amorphous materials are based on the CRN. Real materials, however, have structures which deviate considerably from the idealised CRN. Therefore there will be an appreciable density of defect states. The defects mainly consist of vacancies or unsaturated bonds. The electronic states associated with these defects can completely dominate the transport properties of the material, so leading to major disagreements with theoretical models.

The loss of long range order and the presence of defects within an amorphous material leads to a finite density of states at energies that would normally be forbidden in a crystalline substance. A proposed density of states for amorphous silicon is presented in figure 1.2 as an example of this phenonmenon. The spreading of the band edges is a product of the disorder within the material. Features within the energy gap are usually associated with specific defects, such as the dangling bond (see figure 1.3)

The spreading of the band tails into, and the occurrence of features within, the energy gap can have a marked effect on charge

Figure 1.2 The density of states for amorphous silicon as proposed by Marshall et al. The techniques used to obtain the results at different energy ranges are shown. Bremsstrahlung Isochromat Spectroscopy (BIS), Deep Level Transient Spectroscopy (DLTS), Time of Flight (TOF) and X-ray Photoelectron Spectroscopy (XPS)

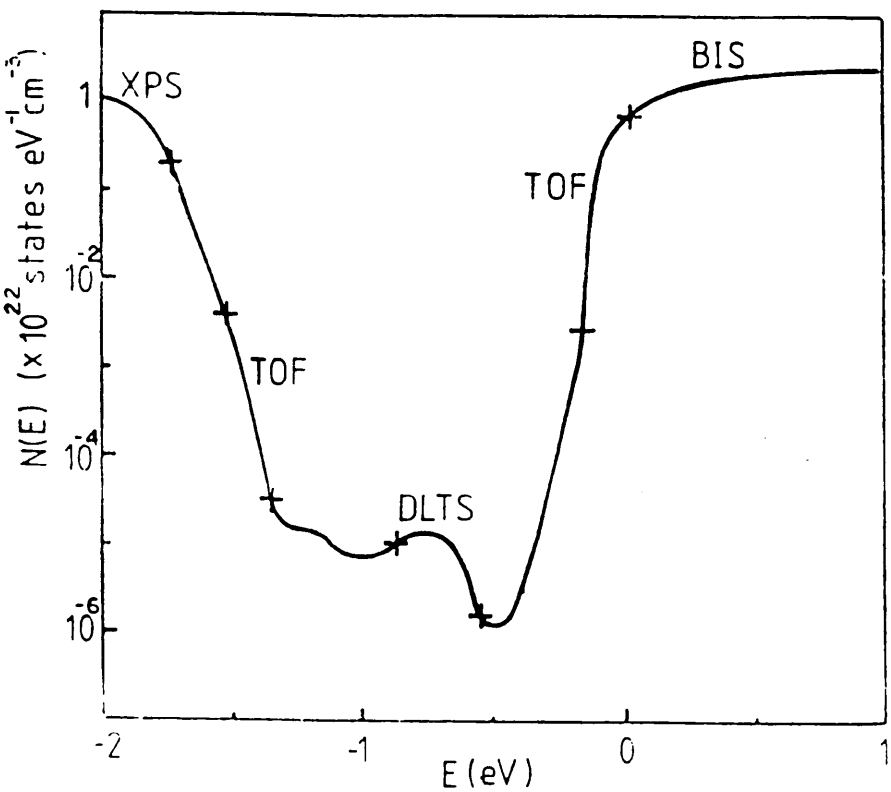

Figure 1.3 Many features within the distribution of trapping states can be associated with specific defects, for instance the dangling bond.

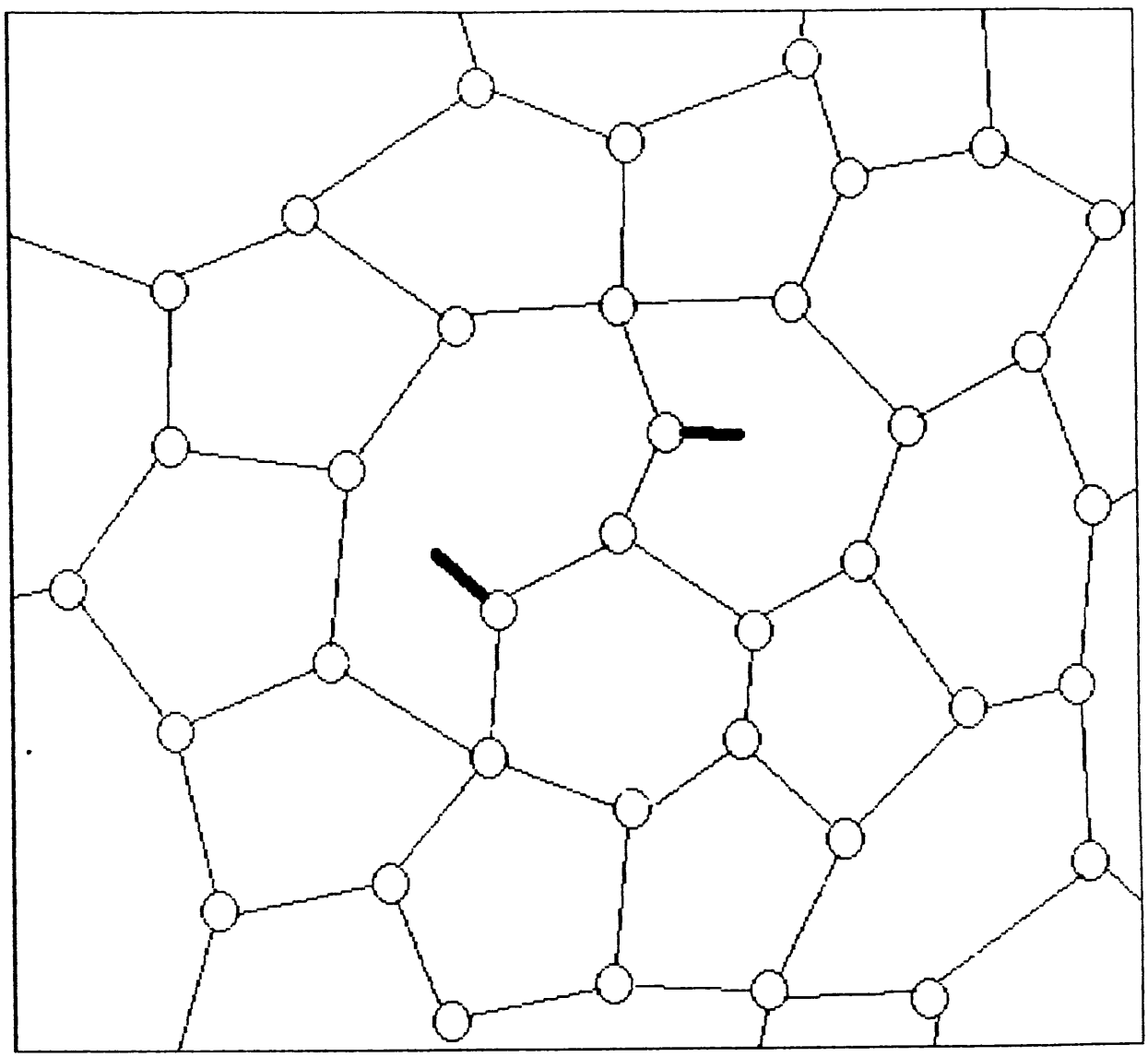

transport within the material. The mid-gap states are *localised* (see later) therefore any carrier in them will not contribute to the charge transport in a similar fashion to those still in the extended states. These states can also act as recombination centres, this will reduce the lifetime of carriers.

Knowledge of the exact distribution of trapping states is very important for device fabrication, as it will limit speed of response and efficiency. However, an exact determination of the density of states has not proved possible, even for a technologically important material such as amorphous silicon. Much work has been undertaken in trying to determine the shape of the band tails in this material. There are currently two models which have a wide spread acceptance, these are either an exponential or linear dependence of the electron trapping state distribution with energy. The marked difference between these two models may well arrive from the fact that the amorphous silicon used is prepared at different sites and under different conditions. As the density of states is critically dependent on the deposition conditions it may well be that different energy dependences can arise in samples which are formed under different conditions.

One experimental technique which is useful in the determination of the density of states will be discussed in the next chapter. Below is presented a basic outline of the electronic transport processes which are thought to occur in amorphous materials.

1.3 Electronic Transport in Amorphous Materials.

A simple model of the features common to all disordered systems was proposed by Mott [3]. This model can be considered to be an extrapolation of the crystalline work, with the disorder treated as a small perturbation. This perturbation will cause the scattering of the electrons after they have travelled a distance λ. As the perturbing disorder is gradually increased the mean free path will decrease. However, when λ becomes equal to the lattice spacing, a, this decrease will cease, because this is the limiting case. From the Heisenberg uncertainty principle :-

$$\Delta k \Delta x \simeq 1 \qquad (1.1)$$

Therefore if an appropriate value is chosen for k, eg k = 1/a the above becomes :-

$$\frac{\Delta k}{k} = \frac{a}{\Delta x} \qquad (1.2)$$

This shows that the phase of the wavefunction will change randomly over a distance of the order of the lattice spacing. Note however that the wavefunction will still extend *throughout* the entire lattice.

If there is further increase in the disorder this will lead to a dramatic change in the nature of the electron wavefunction. Instead of extending throughout the structure the electron wavefunction will

now be modulated by an exponentially decaying envelope. This means that the electron wavefunction will have become localised. The concept of localisation is discussed in more detail in the next section.

1.3.1 Anderson Localisation.

A theoretical treatment of the problem of localised states was proposed by Anderson [4]. His treatment was based on the tight-binding approximation. Note that his treatment only considered random fluctuations in potential and not in spatial separation.

The tight-binding approximation is applicable when the electron wavefunctions are only weakly overlapping and the bands are narrow. It can be shown that the band width, B, is given by :-

$$B = 2zJ \tag{1.3}$$

where z = the coordination number

J = the overlap integral.

Using scattering theory and the effective mass approximation along with the tight-binding approximation Anderson was able to show that :-

$$a/L = \frac{4z^2}{16\pi}\left[V_o/B\right]^2 \tag{1.4}$$

In the limiting case considered above (when $a/L \simeq 1$) the value

of $V_o/B \simeq 0.6$, if a typical value for z of 6 is used. At this point the electron wavefunction is still completely delocalised, so at what point does complete localisation occur ? Anderson suggested that localisation would set in when :-

$$V_o/B \geq 5 \qquad (z = 6) \tag{1.5}$$

Later work has suggested that this value may be somewhat restrictive and that a more reasonable value would be $V_o/B = 2$.

The Anderson criterion is only applicable to narrow bands so how can it be applied to the wide bands normally found in amorphous materials ? It is noted at this point that the value of the overlap integral is critically dependent on the separation of the sites. This will mean that the overlap will be much smaller in the 'tails' of the band as the density of states has a relatively low value at this point. So V_o/B will reach the critical value for localisation first in the tail states. The wavefunctions of the states in the centre of the band will still be delocalised. This co-existence of localised and delocalised states leads to the definition of a very important quantity, the mobility edge. If states below a certain energy, E_c, are localised then when the temperature reaches zero the ensemble average of the conductivity, $\langle\sigma\rangle$, will be zero and the mobility, μ, will also be zero. However, in the extended states above E_c conduction can take place even at $T = 0$. This critical energy E_c is called the mobility edge [5] and in many cases can take the place of the band edge used in crystalline semiconductors.

1.4 Electronic Transport Mechanisms in Amorphous Semiconductors.

There are two main types of iso-electronic transport mechanism in amorphous semiconductors. These are extended state conduction in the states above E_c and various forms of 'hopping' conduction in the states below E_c.

1.4.1 Extended State Conduction.

Consider first extended state conduction. This will occur in the extended states above the mobility edge. Although these states are delocalised the mean free path length is of the order of the lattice constant and the effects of random variations in potential are adding to the disorder. This implies that transport just above E_c can no longer be regarded as band motion which suffers occasional scattering. It was suggested that the transport in this region will have a diffusive form somewhat akin to Brownian motion [6]. The diffusion coefficient is given by :-

$$D = 1/6\ \nu a^2 \qquad (1.6)$$

where D = diffusion coefficient

ν = electronic frequency

a = interatomic spacing

then the mobility in this region can be found using the Einstein relation:-

$$\mu_e = eD/kT \qquad (1.7)$$

giving :-

$$\mu_e = \frac{ea^2\nu}{6kT} \qquad (1.8)$$

If a typical value for ν is taken (= $10^{15}s^{-1}$) then the estimated extended state drift mobility is $\simeq 10\ cm^2V^{-1}s^{-1}$.

If it is assumed that the Fermi level E_F is situated in mid-gap, so that it is sufficiently far away from E_c that Boltzmann statistics can be used to describe the occupancy of states then the conductivity due to the extended states will have the following form:-

$$\sigma = \sigma_o \exp\left[-(E_c - E_F)/kT\right] \qquad (1.9)$$

where $\sigma_o = e\mu_o g(E_c)kT$

$g(E_c)$ = density of states at E_c

1.4.2 Hopping Conduction.

Electron transport in states below the mobility edge, at an energy E within the band tails, can occur via a mechanism known as 'hopping'. This is a process whereby an electron can move from one

localised state to another, provided that the wavefunctions overlap. The carrier is said to 'hop' from the first state to the second. If the two states involved in the hop lie at different energies the electron must interact with a phonon before it can move. This electron - phonon interaction will be the rate limiting process for transport via hopping.

The theory of hopping was developed, by Miller and Abrahams [7], for use with impurity conduction mechanisms in doped crystalline semiconductors . This theory proposed that a carrier would usually jump to an unoccupied site situated at energy ΔE above its current location. Note that in this case the electron wave function will fall off rapidly so the hop will normally be to the nearest neigbouring site. ΔE will be given by :-

$$\Delta E \simeq \frac{1}{a^3 N(E)} \qquad (1.10)$$

where $N(E)$ = density of states at energy level E

E = energy level at which hopping is occuring.

The hopping probability is then given by :-

$$p = \nu_{ph} \exp(-2\alpha R - \Delta E/kT) \qquad (1.11)$$

where ν_{ph} = phonon frequency (typically 10^{13}Hz)

α = a measure of the localisation of the wavefunction

R = distance hopped.

This leads to an expression for the hopping mobility of :-

$$\mu_{hop}(E) \simeq (1/6)(eR_o^2(E)/kT)\nu_{ph}\exp(-2\alpha R_o)\exp(-\Delta E/kT) \qquad (1.12)$$

where R_o = average distance hopped.

Using a typical value for ν_{ph}, a value of $R_o \simeq \alpha^{-1}$ and a value of $\Delta E \simeq kT$ (average phonon energy) this gives a maximum hopping mobility of the order of $10^{-2}cm^2V^{-1}s^{-1}$. By comparison with the above result for extended state mobility it can be seen that the expected mobility drops by at least two orders of magnitude. This drop can be identified with the mobility edge.

The conductivity due to transport via hopping in states at energy E is found to be :-

$$\sigma_{hop} = \sigma_o'\exp\left[-(E-E_F+\Delta E)/kT\right] \qquad (1.13)$$

As the temperature decreases, thus reducing the average phonon energy, the nature of the hopping mechanism will change.

At sufficiently low temperatures, given a non-zero N(E) at E_F, the hopping mechanism will change over to nearest neighbour hopping at the Fermi level. This process is only weakly activated. The carriers are hopping from just below the Fermi level to just above it when they interact with a low energy phonon. The conductivity in this case will

be given by :-

$$\sigma(E_F) = (1/6)e^2R_o^2g(E_F)\nu_{ph}\exp(-2\alpha R_o - \Delta E/kT) \qquad (1.14)$$

where $g(E_F)$ = the density of states at the Fermi level.

Another transport mechanism may dominate at low temperatures depending on the amount of overlap between the electron states [8]. This phenomenon is called variable range hopping. In this case the electron will hop to a site further away than its nearest spatial neighbour so as to minimise the amount of energy that it is required to gain from phonons. Conductivity from variable range hopping follows a $T^{-1/4}$ law and so is easily identified. The form of the conductivity is given by :-

$$\sigma_{vrh} = (1/6)e^2g(E_F)R_{opt}^2\nu_{ph}\exp\left[-\left(18\alpha^3/g(E_F)kT\right)^{1/4}\right] \qquad (1.15)$$

where R_{opt} = optimum value of R

$$= \left(\frac{9}{8\pi g(E_F)kT\alpha}\right)^{1/4}$$

The temperature at which variable range hopping becomes predominant depends on the extent of the overlap between the sites. If there is little overlap variable range hopping can occur at reasonably high temperatures (>100K).

2 Review of 'Time of Flight' Techniques.

2.1 Measurement of Carrier Mobility.

In crystalline materials there are two major techniques for measuring carrier mobility. These two methods are Hall effect measurements and the Haynes-Shockley technique [9]. The usefulness of these techniques will now be discussed with respect to amorphous materials.

Although probably the most useful technique for measuring mobilities in crystalline materials, the Hall effect is of limited use when applied to amorphous substances. The Hall mobilities are usually one to two orders of magnitude lower than conductivity mobilities and often exhibit an anomalous sign reversal. That is the charge carrier predicted by the sign of the Hall mobility is not in agreement with data on the majority carrier obtained from other experimental measurements (thermo power for example) on the same sample. For these reasons Hall effect measurements are rarely used on amorphous materials.

The Haynes-Shockley technique for measuring the drift mobility of the minority carriers is, in a modified form, useful in characterisation of amorphous materials. The Haynes-Shockley technique employs a sample which has an electric field applied along it. A charge packet is then created at one end of the sample by either illumination or injection. This packet drifts down the sample

Figure 2.1 The Haynes-Shockley Experiment.

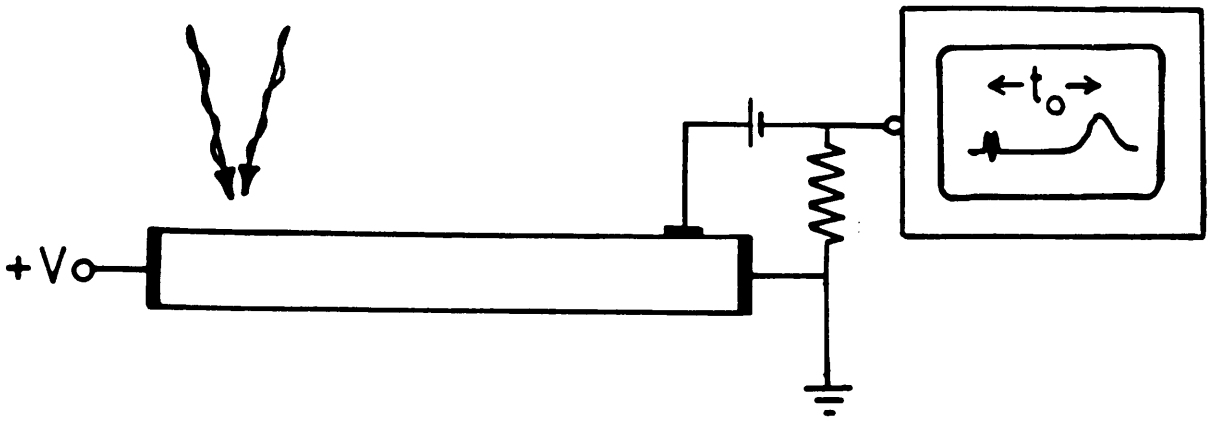

under the action of the applied field as seen in figure 2.1. A majority charge carrier packet will spread out in a time equal to the dielectric relaxation time τ_{rel}. τ_{rel} is frequently shorter than is experimentally measureable therefore no information can be gained about the drift of the majority carriers. However, minority carriers will not spread in this way because of the screening effect of the majority carriers.. Provided that the minority carriers have a sufficiently long lifetime that they can drift down the sample, under the action of the applied field before recombination occurs, then information on the drift mobility can be obtained.

In many amorphous materials the dielectric relaxation time is sufficiently long that neither minority or majority carrier charge packets will spread within the experimental time. However, the free lifetime of the carriers is much often lower in amorphous materials so recombination starts to occur after much shorter periods. As carrier mobility is low in amorphous materials the charge packet will not travel very far before recombination begins. However by making the sample very thin it is still possible to extract the charge packet before recombination dominates. Therefore a variation of the Haynes-Shockley technique can be used to study both minority and majority carriers. This modified Hyanes-Shockley technique is the 'time of flight' experiment [10]. Similar results to those obtained for the pre-transit regime of the 'time of flight' experiment can be obtained by use of the transient photodecay technique. Experimental layouts for both techniques can be seen in figure 2.2. The 'time of flight' technique will be described in more detail below. A general review of time of flight techniques and the analysis of the results

Figure 2.2 Transient photoconductivity techniques.

a) The 'time of flight' experiment

b) The transient photodecay experiment.

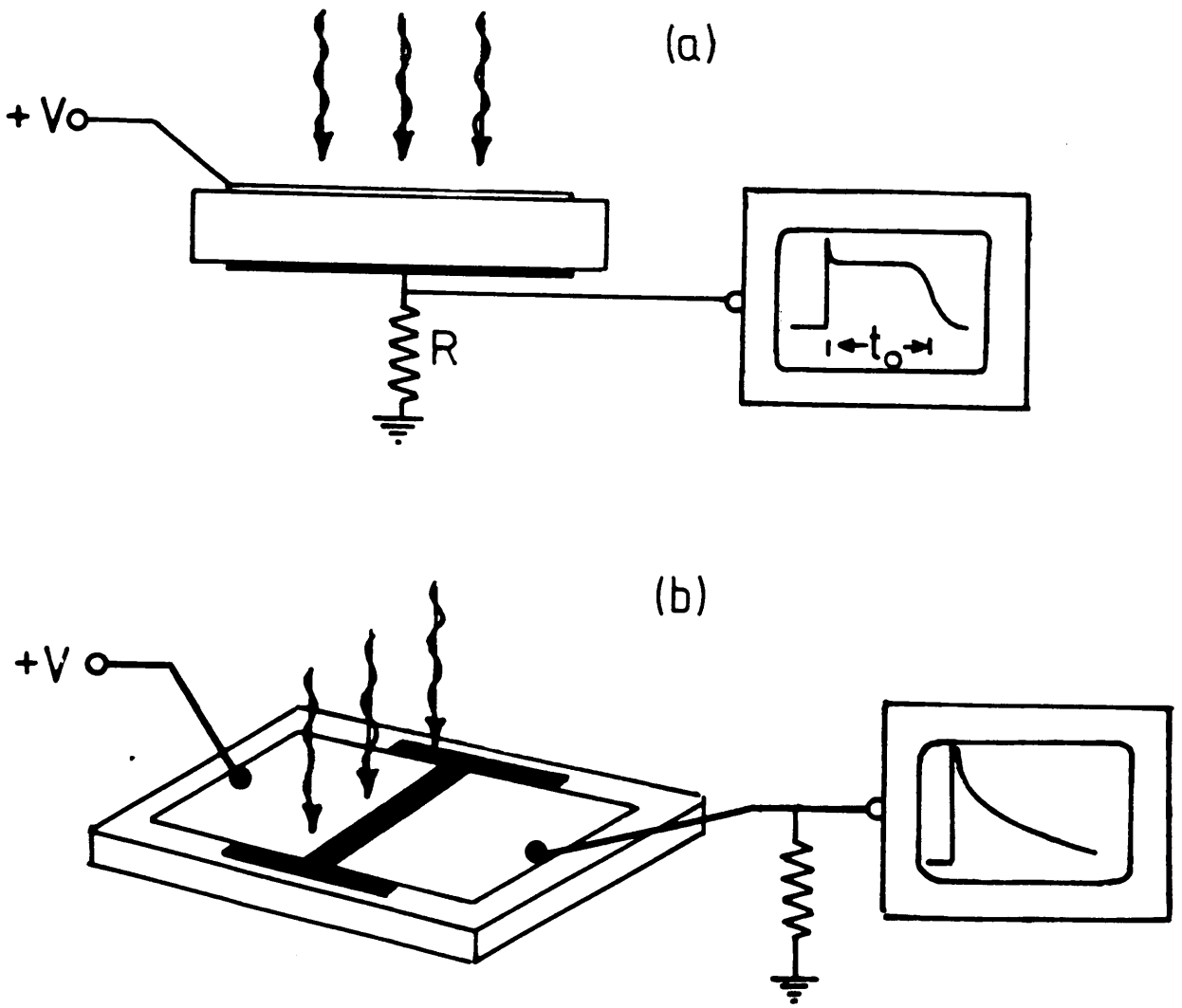

can be found in Marshall [11,12]. The transient photodecay technique uses a sample with coplanar electrodes. This configuration allows the study of the photocurrent with time after a short pulse of illumination. The transient that results should be similar in behaviour to the pre-transit regime of a 'time of flight' pulse (see later).

The 'time of flight' technique uses a layer of amorphous material sandwiched between two electrodes. The electrodes must be blocking (non-injecting) so as to prevent undesirable injection or re-injection of charge. The packet of charge carriers is usually created by optical excitation through a transparent electrode. The amount of excess charge introduced must be kept within certain limits if the results are to be valid. The limit for the amount of excess charge is set by the requirement that the field across the sample must remain essentially constant while the packet is drifting across the sample. This requirement means that the total charge injected into the sample must be considerably less than the capacitance applied voltage product for the sample. This may be stated as :-

$$Q_{excess} \ll CV$$

where C = capacitance of sample

V = voltage applied across sample.

Provided that the above criterion is satisfied the time taken for the charge packet to drift across the sample can be found from the observation of either the current or induced charge on the opposite

Figure 2.3 Schematic of the charge sheet and electric fields present in the 'time of flight' experiment.

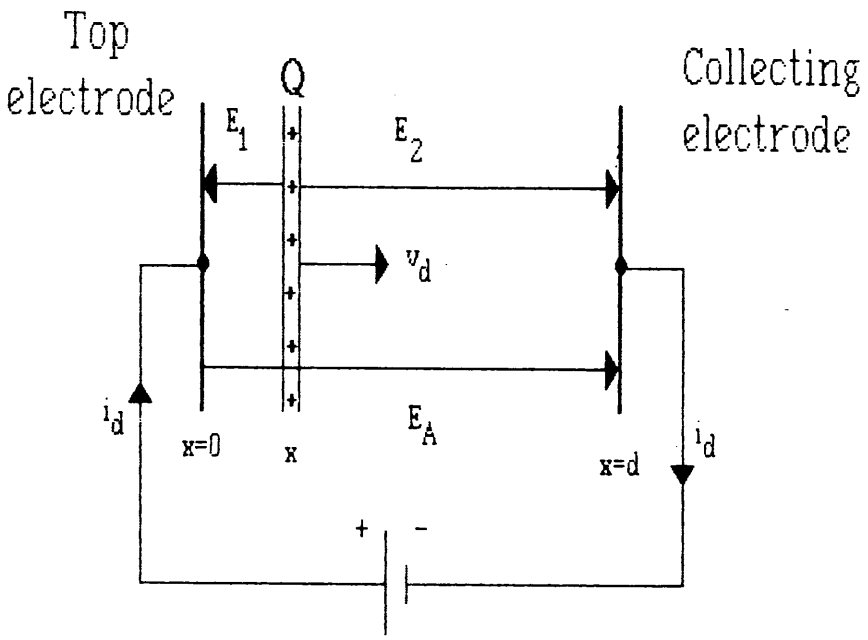

electrode. Figure 2.3 shows the charge sheet and the fields normally associated with it for a standard time of flight experiment[10,13]. The incremental fields E_1 and E_2 are time dependent and their values are given by :-

$$E_1 = -\frac{1}{\epsilon\epsilon_o}\frac{Q}{A}\left[1-\frac{x}{d}\right] \qquad E_2 = \frac{1}{\epsilon\epsilon_o}\frac{Qx}{Ad} \tag{2.1}$$

As the sheet drifts across the sample these fields will give rise to a displacement current in the external circuit. An integrated charge transit will be observed if the external CR is greater than the transit time and an approximately rectangular current transient will be observed if the external CR is much less than the transit time. Examples of idealised transit pulses for both cases can be seen in figure 2.4. In both cases the point that corresponds to the time for the carriers to transit the sample can be clearly seen.

Given the transit time of the carriers, the drift mobility can be easily calculated from :-

$$\mu_d = d/Ft_t \tag{2.2}$$

where μ_d = the drift mobility

d = the sample thickness

t_t = the transit time.

Figure 2.4 Idealised transient pulses for :-

a) external CR > transit time

b) external CR < transit time

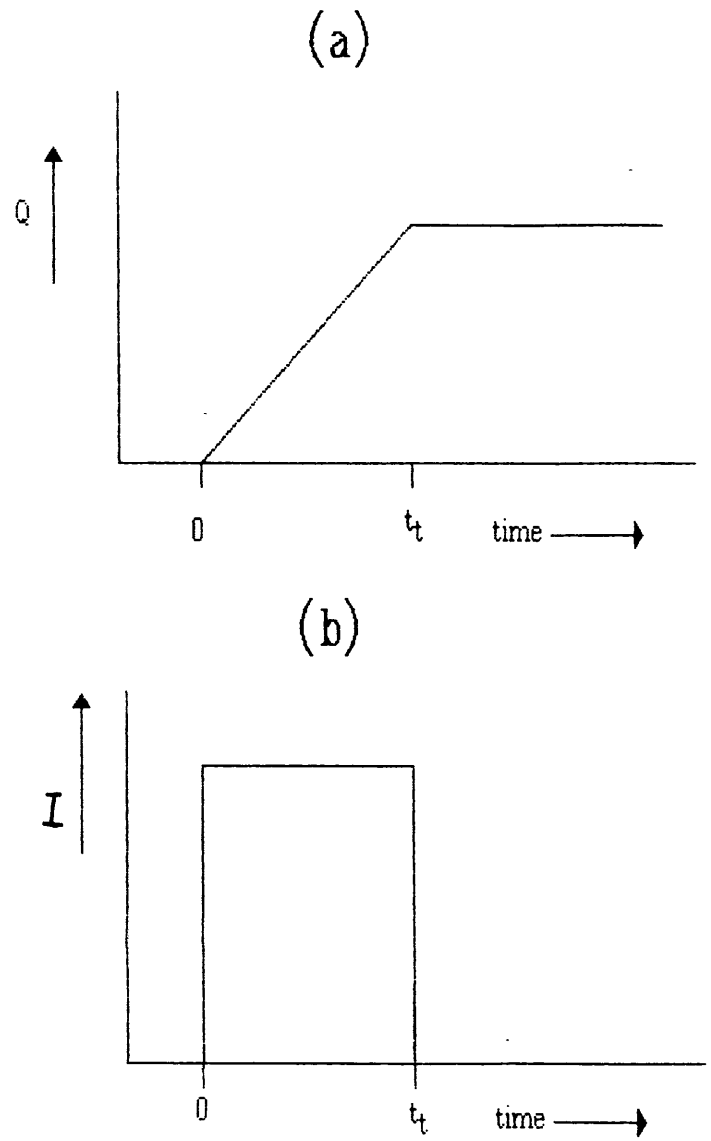

2.2 Conventional Dispersion.

An idealised current transient without dispersion would have the following features. There would be a rapid rise in current after the excitation pulse, then the current would remain on a plateau until the transit time of the carriers and would then fall away to zero as all of the carriers, travelling at the same velocity, arrive at the extraction electrode together. In real samples this is not observed. Firstly, even if the carriers travel only in the extended states, the carrier pulse will spread out because of diffusion, giving a spread of arrival times. The diffusion arises from statistical variations in the scattering processes. It can be described in terms of a diffusion coefficient, D, which is given by the Einstein relation :-

$$D = (kT/e)\mu \qquad (2.3)$$

The statistical variations will cause the charge packet to assume a Gaussian profile. The root mean square deviation of the electron displacement from the mean position is given by :-

$$\Delta l = (2Dt)^{1/2} \qquad (2.4)$$

Now if t_o is the mean time for the packet to cross the sample then the spread of arrival times for the individual carriers is of the order of :-

$$\Delta t = \Delta l/\mu\epsilon \qquad (2.5)$$

So the relative degree of dispersion observed is given by :-

$$\Delta t/t_o = \Delta l/l \propto (2D/\mu)^{1/2}(El)^{-1/2} \qquad (2.6)$$

The above equation shows that the relative degree of dispersion should be less in thicker samples, for a given field.

When the carriers spend some time in localised states an additional dispersion may be expected to arise from the statistical variation of trapping and release times even when the free and trapped charge are in thermal equilibrium.. The effect that this dispersion has on a transit pulse can be seen in figure 2.5. It should be noted that, although the transit pulse is no longer of the ideal form, the transit time can still be readily identified.

2.3 Anomalous Dispersion.

Although the above description of dispersion is approached for some amorphous materials at high temperatures, all materials at low temperatures exhibit a degree of dispersion that cannot be explained in such terms. Pulses which exhibit this high degree of dispersion are said to be 'anomalously dispersive'. As the temperature is lowered for a material that has an anomalously dispersive transient the pulse departs more and more from the ideal rectangular shape. Eventually, if the pulse is displayed on linear axis of I and t, it becomes almost impossible to decide where the transit time occurs. However, if the pulse is displayed on logarithmic axis of current and time, a well defined breakpoint, associated with the transit time, can

Figure 2.5 The effect of diffusion on conventionally dispersive transit pulses.

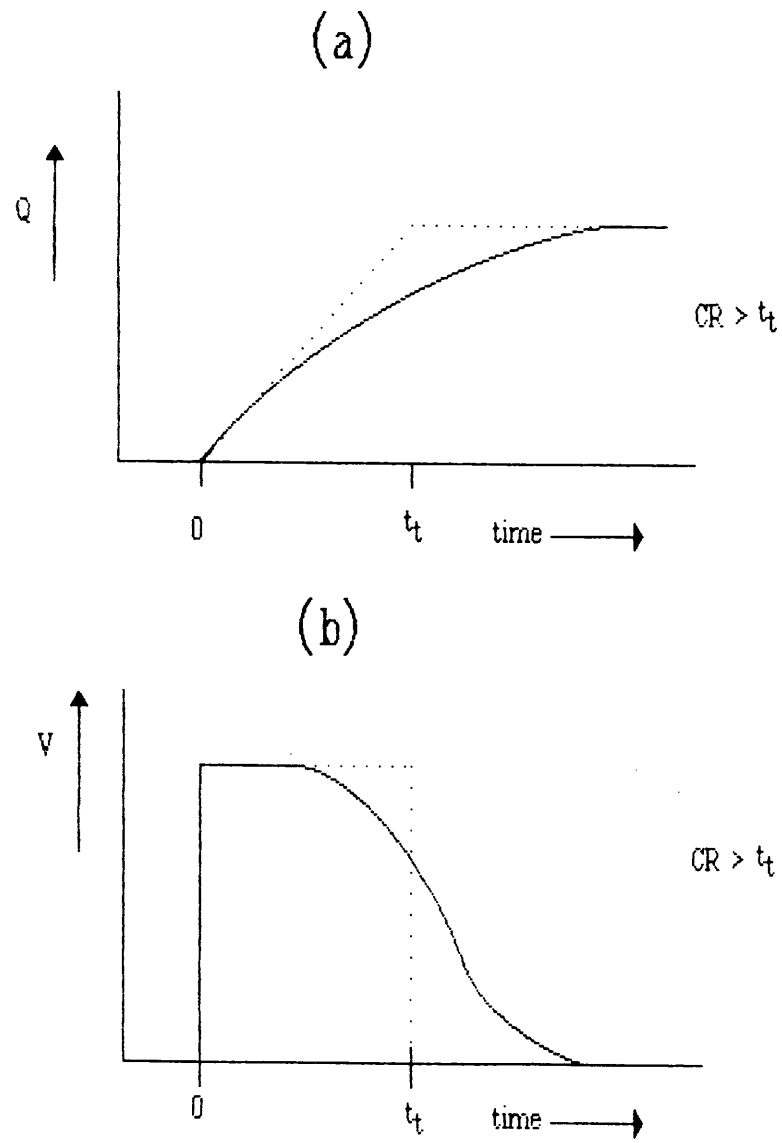

Figure 2.6 An example of an anomalously dispersive transit pulse.

a) On linear axes

b) On logarithmic axes

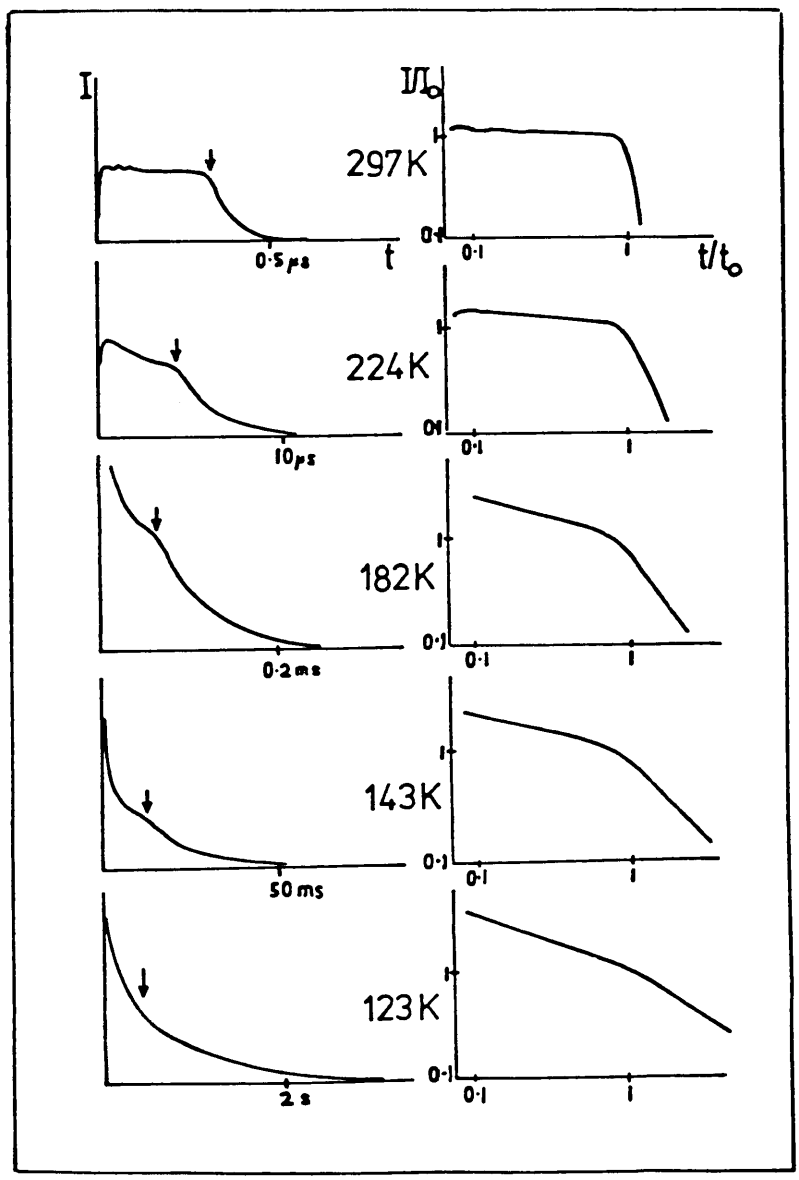

still be observed. Note that the transit time given by this breakpoint is not the average transit time of the carrier packet as for conventional dispersion, but is the transit time of the leading edge of the charge packet. Examples of these anomalously dispersive transients can be seen in figure 2.6. Study of these transits can provide information about the transport mechanism involved. The theory behind this will be considered in the following sections.

2.4 Transport Models.

2.4.1 Experimental Evidence.

Shortly after the first anomalously dispersive transit pulses were reported it was claimed that all the pulses seemed to be characterised by 'universality' of pulse shape against variations in applied field and temperature [14,15]. That is, pulses measured at different fields and, sometimes, temperatures all seemed to exhibit the same degree of relative dispersion. It was also noted that the current pulse displayed an approximately algebraic time dependence of excess current. When plotted on logarithmic axes of current and time the transit pulses showed two approximate linear regions. One of these existed at times less than the "transit time", t_t, and the other at times greater than t_t. This is shown in figure 2.7. The power law dependence can be represented by:-

$$I_1 \propto t^{-(1-\alpha_1)} \qquad 0 < t < t_t \tag{2.7}$$

$$I_2 \propto t^{-(1+\alpha_2)} \qquad t > t_t \tag{2.8}$$

Figure 2.7 A set of transit pulses showing the proposed universality of shape with temperature and the presence of two power laws. (from Scher and Montroll)

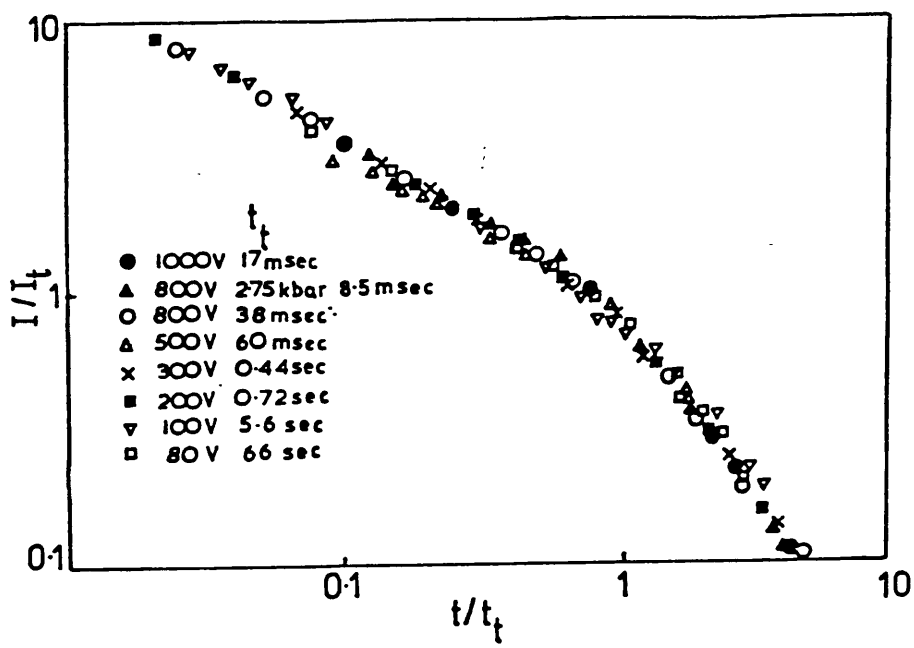

Experimental evidence from arsenic selanide suggested that the two parameters α_1 and α_2 seemed to be equal.[16]

2.4.2 The Scher and Montroll Model.

Making use of the above experimental facts Scher and Montroll [16] (SM) advanced the first major theoretical treatment of anomalously dispersive transport. The model they proposed was based on the assumption that transport occurred by hopping between iso-energetic sites which have a random spatial distribution, though they did note that any mechanism capable of providing the required $\psi(t)$ (see below) would be equally valid. The range of each hop will vary from site to site (this is termed 'r-hopping'). The theoretical analysis of this model has so far proved to be extremely difficult and to date no exact solution has been advanced.

The SM model develops in the following manner. Firstly a global waiting time distribution, $\psi(t)$, is calculated. This is made up in the following manner. For each occupied site within the sample there exists the possibility of a transition to various neighbouring sites. The probability, $p(t)$, of any particular hop between two sites occuring in unit time is given by :-

$$p(t) = \exp(-2R/R_o) \qquad (2.9)$$

where R = the intersite distance

R_o = the localisation radius of the centre.

It can be seen from this that widely different escape probabilities may arise if the average site separation $\bar{R}$ is large compared with R_o.

$\psi(t)$ represents an average of p(t) taken over all the sites in the array. So if a carrier becomes localised somewhere at t=0, the probability that it will hop to another site in the time interval t=t to t = t+dt is represented by $\psi(t)dt$.

Given the form of $\psi(t)$ SM then make the significant assumption that this function can be transferred onto a regular lattice, as the distribution itself will contain all of the information on the randomness of the system. This implies that each site on the regular array may be viewed as having a release distribution function equal to $\psi(t)$. By making this assumption the mathematical complexity of the problem is considerably reduced. From this more tractable problem, SM are able to predict certain characteristics.

SM find that the form of the averaged waiting time distribution is given by:-

$$\psi(t) = \frac{\text{const}(\ln(\tau))^2}{\tau(1+(\eta/3)\ln(\tau)^2)} \qquad (2.10)$$

where τ = a normalised time

$\eta = (R_o/R)^3$

As the logarithmic terms in the above will vary rather slowly (over the time range accessible in a 'time of flight' experiment) SM suggest that a convenient approximation to $\psi(t)$ will be:-

$$\psi(t) = \text{constant } t^{-(1+\alpha)} \qquad (2.11)$$

with $\alpha = 1/3\eta\ln(\tau)^2 \simeq$ constant

From this form of $\psi(t)$ SM show that the excess carrier transit pulse generated by a continuous random walk mechanism on a regular lattice will possess two power-law regimes, as seen experimentally. Furthermore, the predicted values of α_1 and α_2 are found to be identical and equal to the value α, again as observed for As_2Se_3. From the form of $\psi(t)$ it can also be seen that, provided τ is not varied enough to cause a significant change in α, the universality of pulse shape with field is predicted. The universality of pulse shape with temperature was also predicted as $\psi(t)$ is not temperature dependent. This model therefore covers all of the features of the anomalously dispersive transit pulses described above.

After the SM model had been published further experimental evidence was obtained which cast doubt on two of the basic assumptions upon which the model was based. The new experimental results did not show the universality of pulse shape observed earlier [17,18] and also they suggested that the equivalence of α_1 and α_2 [19,20,21,22] was not in general followed.

2.4.3 The Multiple Trapping Model.

At this time another model for explaining the dispersive transport was proposed. This was an extension of the existing trap limited band transport, or multiple trapping (MT) model. The basis of the MT model is simply that a carrier initially in the extended states will be trapped in a localised state after some trapping time. It will then be released back into the extended states after a release time dependent upon the energy depth of the trap. This process then repeats itself until the carrier has crossed the sample.

The transit time in the MT model is not simply the time that it takes a carrier to cross the sample. Most of the transit time will come from the time that the carriers spend immobile in trapping states. So the drift mobility will not be the actual free carrier mobility. Instead it will be greater than the actual mobility by a temperature dependent factor which is related to the density of trapping states. The free mobility and the drift mobility can be related in the following fashion (for a more detailed description see Mott and Davis [5]).

Assume that carriers are only trapped in a single set of states at energy E_t and that a quasi-thermal equilibrium is established between E_c and E_t in a time that is much shorter than the transit time. Then the ratio of free to trapped carriers will be given by :-

$$n_f/n_t = \left[N(E_c)/N(E_t)\right] \exp\left[-(E_c - E_t)/kT\right] \qquad (2.12)$$

now the conductivity can be given by either :-

$$\sigma = n_f e\mu_o \qquad \text{(free carriers no traps)} \tag{2.13}$$

or $$\sigma = (n_f+n_t)e\mu_d \qquad \text{(carriers being trapped so more required)} \tag{2.14}$$

dividing 2.14 by 2.13 gives

$$\mu_d/\mu_o = n_f/(n_f+n_t) = 1/[1+(n_t/n_f)] \tag{2.15}$$

If it is assumed that $n_f \ll n_t$ then

$$\mu_d/\mu_o \simeq n_f/n_t \tag{2.16}$$

so $$\mu_d \simeq \mu_o\left[N(E_c)/N(E_t)\right]\exp\left[-(E_c-E_t)/kT\right] \tag{2.17}$$

It should be noted from equation 2.17 that the trap depth, E_t, can be found from a plot of $\log_e(\mu_d)$ versus 1/T.

The single trapping level considered above will not produce an anomalously dispersive transient pulse as the trapping state will rapidly reach equilibrium with the band. However anomalously dispersive transients can be shown to result if the free carriers are interacting with a distribution of traps wider than $\simeq$ kT. Note that for amorphous semiconductors any trapping level would be expected to be disorder broadend by at least this amount. The use of a distribution of trapping states can lead to an anomalously dispersive transient in the following manner: If it is assumed that states at

all energy levels have the same capture cross section then the trapping probability into any state will be equal. However, the release probabilities from the trapping states will increase with increasing energy depth. This factor will produce a waiting time distribution function $\psi(t)$ which will be of a form that will cause an anomalously dispersive transient to be produced. The general form of the waiting time distribution function will be given, in this case, by :-

$$\psi(t) = \int [N(E)/N_o] p(t,E) dE \qquad (2.18)$$

where $N(E)$ = density of states at depth E

N_o = total density of traps in the distribution

$p(t,E)$ = probability of release from a trap at depth E in time t to t+dt

It was shown, via computer simulation [23,24,25] and theoretical analysis [26,27,28,29] that this mechanism could produce the observed transit pulses provided that the localised DOS extends over more than a few kT. The final results that are predicted by the MT model were very similar to those predicted by SM. This similarity occurs because although the MT model provides a different way of generating $\psi(t)$, the form of the end result is similar.

2.4.4 R-Hopping versus Trap Limited Band Transport.

R-hopping and multiple trapping represent the two different models of the transport mechanism responsible for the anomalous

dispersion observed in amorphous semiconductors. The SM model is based purely on spatial considerations and so predicts a pulse shape that is constant with temperature. The experimental evidence shows that the shape of the transit pulse varies with changing temperature so supporting the MT model. However, it was further proposed that the transport mechanism can still be via hopping, provided that the localised states are distributed in energy (e-hopping). In the e-hopping model a carrier hops through a set a of states that are energetically distributed over a wide (greater than kT) range.

The debate between these two models has been, a great extent, answered by Pollak [30], who performed an analysis of the hopping models in terms of percolation theory. He finds that for the r-hopping case the sites with the anomalously long release times, which are responsible for the dispersion, will also have anomalously long capture times. Hence, these sites will not play a significant role in the transport as they will tend to be unoccupied. For the e-hopping case it can be shown that any highly isolated site, such as will be required to give the necessary long release time constant, will be surrounded by centres of much higher energy. Therefore, any carrier approaching the isolated site is likely to take a route of least possible energy thereby avoiding the trapping site. Pollak states that, in general, *for a site to contribute significantly to the phenomenon of anomalous dispersion it must have a long release time but must not have a correspondingly long capture time.* MT mechanisms readily satisfy this criterion, but the various hopping models do not. Further evidence in favour of MT is provided by the computer simulations of Marshall which show that in both the r-hopping case [31]

and the e-hopping case [21] anomalously dispersive transients will not normally be produced.

2.4.5 The Validity of the Multiple Transport Model.

Monroe [32] has recently expressed doubts about the validity of the MT model. He has proposed a system that is a mixture of band transport and hopping. In his proposed scheme carriers which are initially free are trapped as in the MT model. However, they then hop to lower energies without re-emission to the extended states. When a carrier reaches an energy level below a predicted 'transport energy' it will preferentially hop back up to the transport energy. The main features of this model are that hopping is the dominant process at low temperature and that the transport energy, where most of the current is carried, is sited in the localised states below E_c rather than in the delocalised states above the mobility edge.

This model predicts results which are similar to those obtained from the MT model except at very low temperature. At low temperature the Monroe model predicts that the current curve will drop below the expected power law. Some deviations,of this type, have been observed experimentally [33,34,35].

3 'Time of Flight' and the Analysis of the Density of States.

Once the MT model had achieved widespread acceptance consideration was given to the formulation of methods for analysing the dispersive transit pulses with a view to extracting information on the DOS.

Certain features are common to all of the methods to be discussed below. These features are that there will be progressive thermalisation through the localised states and that the capture cross sections of the trapping states are energy independent.

3.1 The Marshall-Allen Technique.

One of the first methods for the analysis of anomalously dispersive transit pulses was proposed by Marshall and Allen [36] (MA). This method of analysis will be described in detail below.

For a density of states that is continuous and decays with energy the deepest centre that a carrier encounters during its transit of a sample will, to a first approximation, determine the time taken for the crossing. This occurs because the release time increases rapidly with increasing energy depth so that the time taken for release from shallower traps will only be a very small fraction of the release time from the deepest trap encountered. It is shown via computer simulation that the first 5% of the carriers in the leading edge of the charge packet have avoided any of the deeper levels that are impeding the progress of the rest of the charge packet and that they

have all been trapped at approximately the same energy level. Then for carriers which have been trapped within kT of an energy E_{th} below E_c, the energy of the mobility edge, the effective drift mobility is given by :-

$$\mu_d \simeq \mu_o[N_c/kTN(E_{th})]\exp[-(E_c-E_{th})/kT] \qquad (3.1)$$

where μ_o = extended state mobility

μ_d = effective drift mobility

N_c = effective DOS at mobility edge

$N(E_{th})$ = DOS at E_{th}.

by re-arrangement this gives :-

$$N(E_{th}) \simeq (N_C/kT)(\mu_o/\mu_d)\exp[-(E_c-E_{th})/kT] \qquad (3.2)$$

As it is possible to evaluate μ_d from the transit time and to calculate E_c-E_{th} from the drift mobility activation energy it becomes possible to determine the DOS in terms of the product $N_c\mu_o$. MA note that this technique was unlikely to be of much use in a practical situation because of the difficulty of varying the sample thickness sufficiently to allow the study of a reasonable range of transit times and hence energies. MA also reject the use of varying the applied field as this may introduce complications to do with field dependent release rates.

MA also introduced a novel way of identifying the transit times of the pulses they considered. All of the pulses are superimposed one

Figure 3.1 The superimposition technique proposed by Marshall and Allen

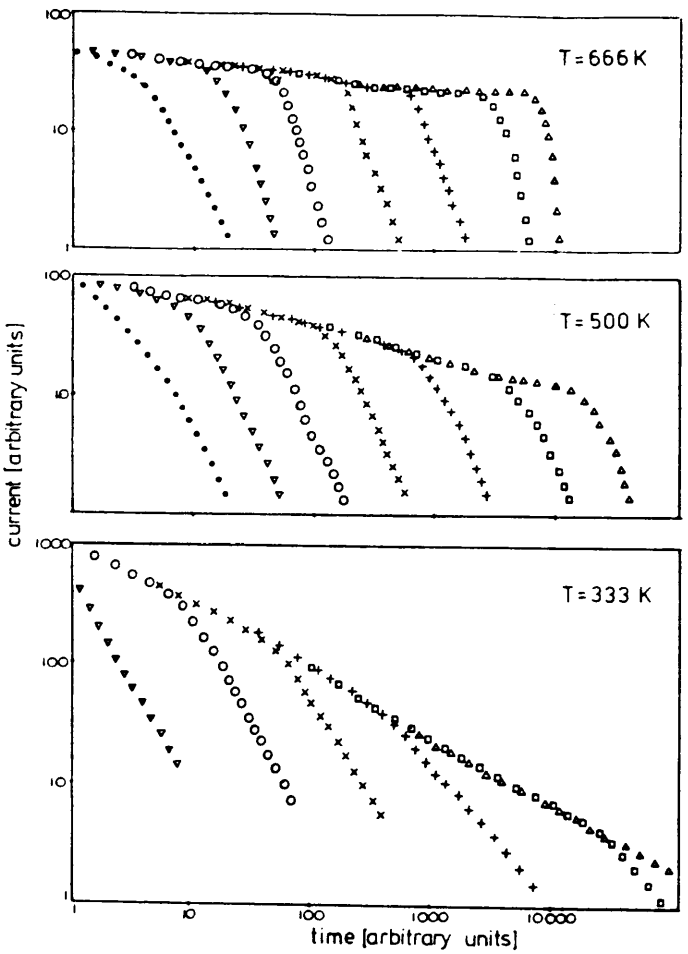

upon another so as to give a single extraction free curve, with each of the post-transit curves peeling away from it after their respective transit times (see figure 3.1).

3.2 The TROK Method.

A different method of determining the DOS from a dispersive transient was proposed separately by Tiedje and Rose [37], and Orenstein and Kastner [38] (TROK). TROK start by considering an exponential density of tail states of the form:-

$$N(E) = N(E_c)\exp(-E/kT_c) \qquad (3.3)$$

where E = energy depth of trapping state

T_c = characteristic energy of exponential tail.

They then attempt to deal with the entire population of excess carriers by the introduction of a thermalisation energy, E_{th}. The thermalisation energy separates 'shallow' from 'deep' trapping centres. The energy E_{th}, measured relative to E_c (the band edge), is defined in this model as the energy at which the release time constant of a trap is equal to the total elapsed time since the creation of the excess charge. From this definition *shallow* states, *above* E_{th}, will be in quasi-thermal equilibrium with the extended states and deep states, below E_{th} will be populated only in terms of trapping kinetics. As time passes more states will reach equilibrium with the band states so E_{th} will move down through the distribution. The position of E_{th} is given at any time by:-

$$E_{th} = kT\ln(\nu t) \qquad (3.4)$$

where ν = attempt to escape frequency

t = total elapsed time.

TROK argue that, for a rapidly decreasing DOS (such as the exponential they considered), the density of trapped carriers will show a pronounced peak close to E_{th}. A simplifying assumption is also introduced at this point. This assumption is that all of the trapped charge at a given energy will be released after the mean release time, rather than being released over a range of times statistically distributed about the mean. They show from this that the waiting time function for this distribution can be given by :-

$$\psi(t) = \text{constant } t^{-(1+\alpha)} \qquad (3.5)$$

where $\alpha = T/T_c$

As this form of $\psi(t)$ is algebraically the same as the SM formulation, and since the transformation from $\psi(t)$ to I(t) is model independent, this shows that the above will also give the appropriate power law decays. The above model suggests a method for obtaining g(E) from I(t) without assuming an exponential DOS. With the simple approximation that the trapped charge lies mainly within kT of E_{th}, and if the quasi-thermal equilibrium between the shallow trapped charge and the free charge is also assumed then the following may be obtained :-

$$n_t/n_f = [kTN(E_{th})/N_c]\exp(E_{th}/kT) \quad (3.6)$$

$$= [kTN(E_{th})/N_c]\nu t \quad (3.7)$$

where n_t = trapped charge density

n_f = free charge density

E_{th} given by equation 3.4

After the initial trapping time most of the excess charge is assumed trapped at E_{th} so $n_t \simeq N_o$, the number of injected carriers. This gives :-

$$N(E_{th}) = (N_c N_o/\nu kT)(n_f t)^{-1} \quad (3.9)$$

The current is proportional to the free charge density so :-

$$N(E_{th}) = \text{constant } (I(t).t)^{-1} \quad (3.10)$$

where E_{th} is given by equation 3.4 .

This also shows that if an amorphous semiconductor possesses an exponential distribution of states then the observed transit pulse will show a power law decay.

Various authors [39,22] have concluded from this result, that if a transient for a material exhibits an approximate power law decay, then the material must have a exponential DOS. The validity of this conclusion has been called in to question on a number of counts.

Firstly it was shown, via computer simulation, that other

Figure 3.2 Schematic of the four distributions used in the simulations of Marshall et al.

a) Rectangular b) Exponential tail

c) Linear tail d) $E\exp[-(E/kT_c)^2]$

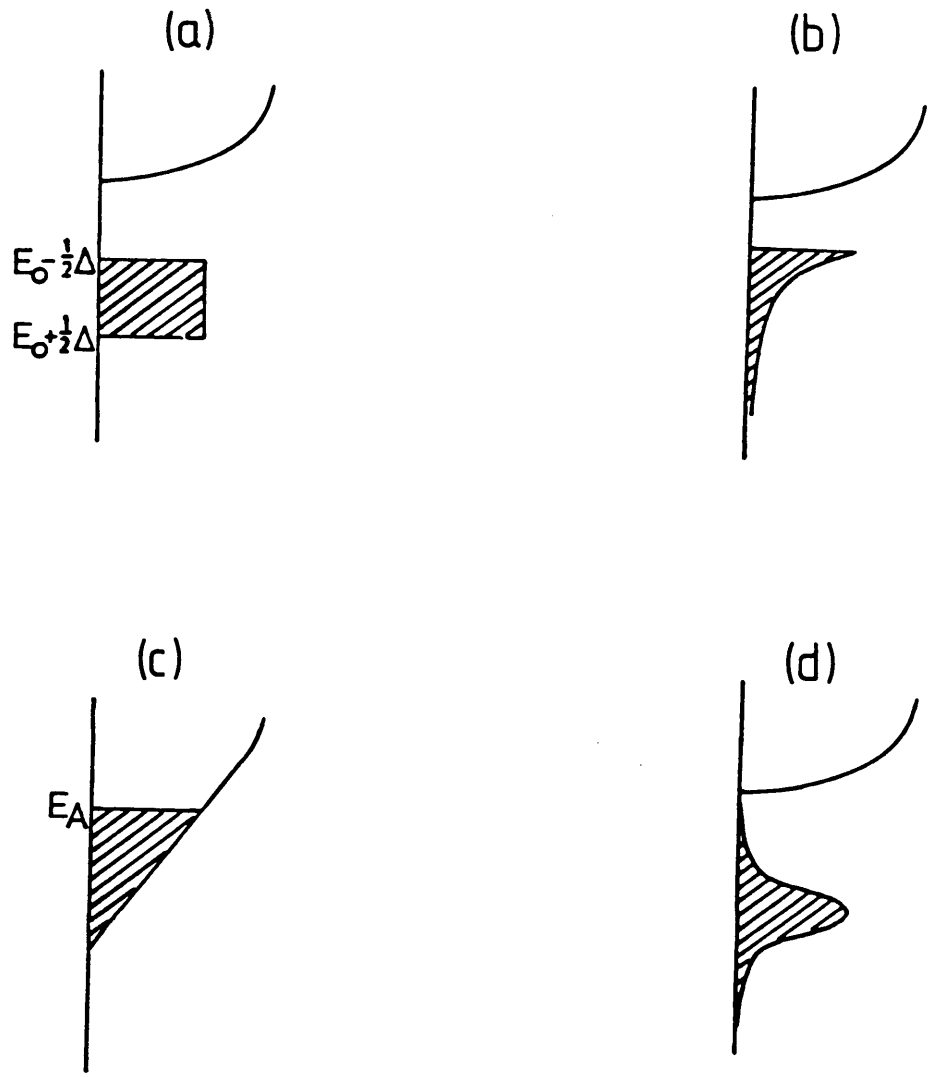

Figure 3.3 The transit pulses calculated for the four distributions shown in figure 3.2.

a) Rectangular b) Exponential tail

c) Linear tail d) $E\exp[-(E/kT_c)^2]$

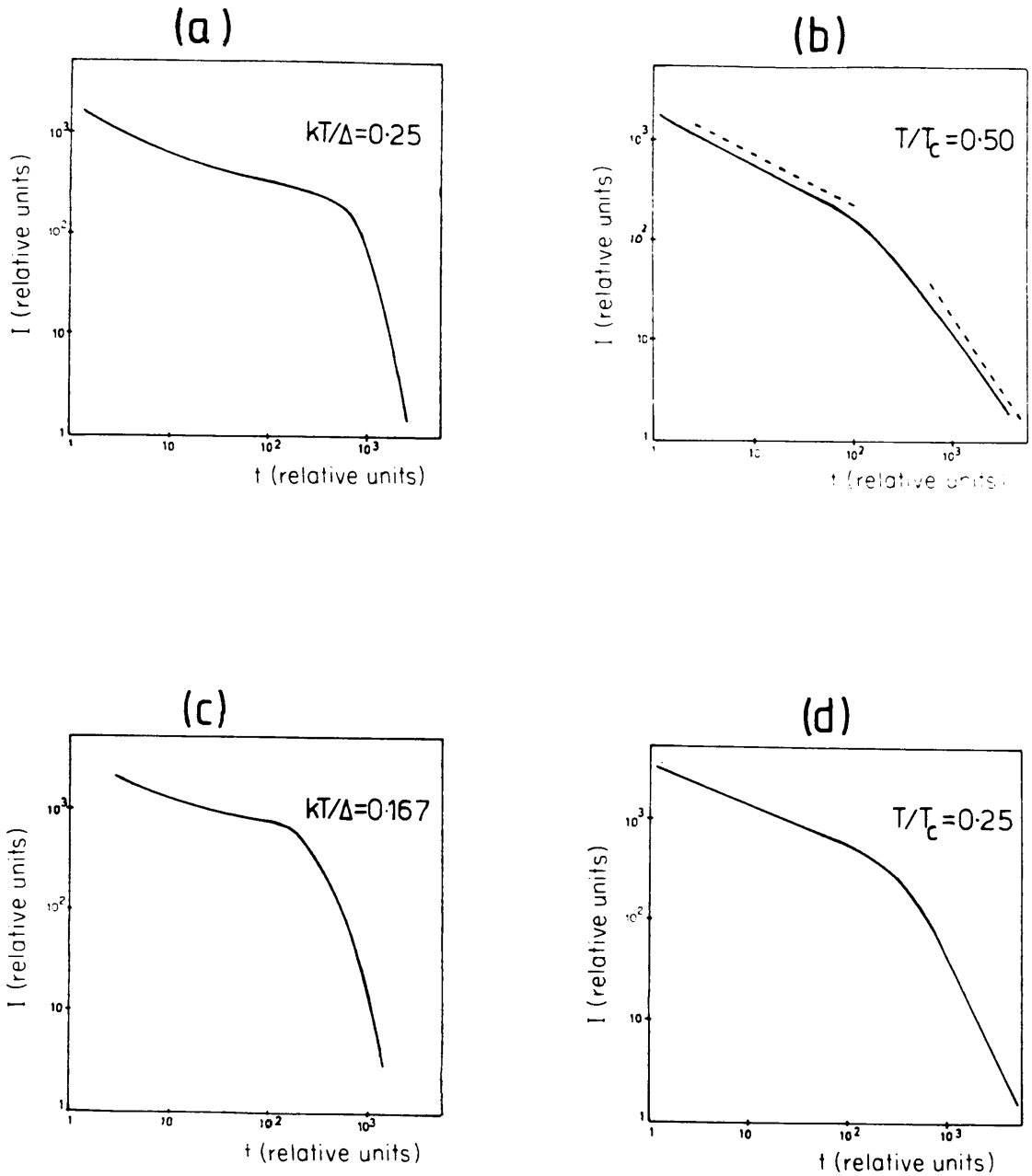

distributions, apart from the exponential tail, could produce broadly similar transit pulses [40]. The authors [40] use computer simulation techniques to find the form of the carrier transit pulse that would be expected for four different distributions of trapping states. The four distributions considered are rectangular, exponential, linear and $E\exp[-(E/kT_c)^2]$. The latter distribution is similar in form to a half gaussian. These distributions are shown in figure 3.2 and the calculated transit pulses are shown in figure 3.3.

The simulation data clearly show that all four of the distributions can produce transit pulses that are an approximate power law. The authors note that the post-transit dispersion parameter α_2 is much more sensitive to any variation of the trap distribution than the pre-transit parameter α_1. They also note that with all of the distributions, except the exponential, the log/log characteristic will show signs of curvature. This will occur when the distribution is approaching a steady free to trapped carrier ratio. However, this curvature is very slight and may not be noticable over the normal time range of a time of flight experiment. If this curvature is observed then this can be taken as evidence that the trapping state distribution does not have an exponential form.

The thermalisation energy concept itself as also been questioned. Marshall and Main [41] consider the predictions made by the thermalisation energy concept if the density of trapping states is made up simply of two discrete levels. Each of these levels has a trapping and release time, T_1, T_2, R_1 and R_2, associated with it. It is shown that the free carrier density for this particular

distribution is given by :-

$$n_f = A + B\exp(-t/\tau_a) + C\exp(-t/\tau_b) \qquad (3.11)$$

where A,B and C are constants determined from the trapping and release times.

Now the first exponential term in 3.11 is derived from the initial trapping of free carriers into the ensemble of trapping states. The constant τ_a is then given by :-

$$\tau_a = \left(T_1^{-1} + R_1^{-1} + T_2^{-1} + R_2^{-1}\right)^{-1} \qquad (3.12)$$

The authors then associate the second exponential term with the redistribution of carriers between the two levels of trapping states as equilibrium is approached. It is predicted from this result that the rate of decay of the free carrier density will decrease once the initial trapping regime is past. This occurs because carriers that were originally trapped in the shallow states when released will *not necessarily* be trapped in the lower states right away. They calculate that the time constant for this regime is :-

$$\tau_b \simeq \tau_a^{-1}\left[\left(T_1R_2\right)^{-1} + \left(T_2R_1\right)^{-1} + \left(R_1R_2\right)^{-1}\right]^{-1} \qquad (3.13)$$

When $R_1R_2 \gg T_1R_2 \gg T_2R_1$ as is often the case of the most interesting cases then equation 3.13 may be simplified to :-

$$\tau_b \simeq R_1(T_2/\tau_a) \qquad (3.14)$$

So the time constant for this regime is not R_1 as would be expected but is in fact modified by a factor dependent on the trapping times for the system. If the trapping time into both set of traps is similar then the above effect will be small. However, if the trapping times are widely dissimilar, possibly due to lower densities or variations in capture cross-section, then the decay time constant would be significantly increased.

Further work is presented on a system possessing three trapping levels. The distribution of free and trapped carriers in this case is found by use of a Monte Carlo simulation of the system. It is found that a true quasi-thermal equilibrium between the free carriers and the various trap levels is not established until all the important sets of deeper lying states also approach quasi-thermal equilibrium. This occurs because the free carrier density is constantly being perturbed by the loss of carriers into the deeper lying states, which are initially acting just as traps (i.e. without release).

Given the details of the time dependence of the free carrier density the authors could now apply the TROK analysis method (see equation 3.8) to see if it would give a correct construction of the density of states.

Figure 3.4 shows the results obtained. It can clearly be seen that the discrete levels used have been broadened, that the energies of the peaks do not correspond to the actual positions of the traps (there has in fact been an inversion of the density of states

Figure 3.4 The result obtained when the TROK analysis method is applied to a distribution consisting of three discrete levels.

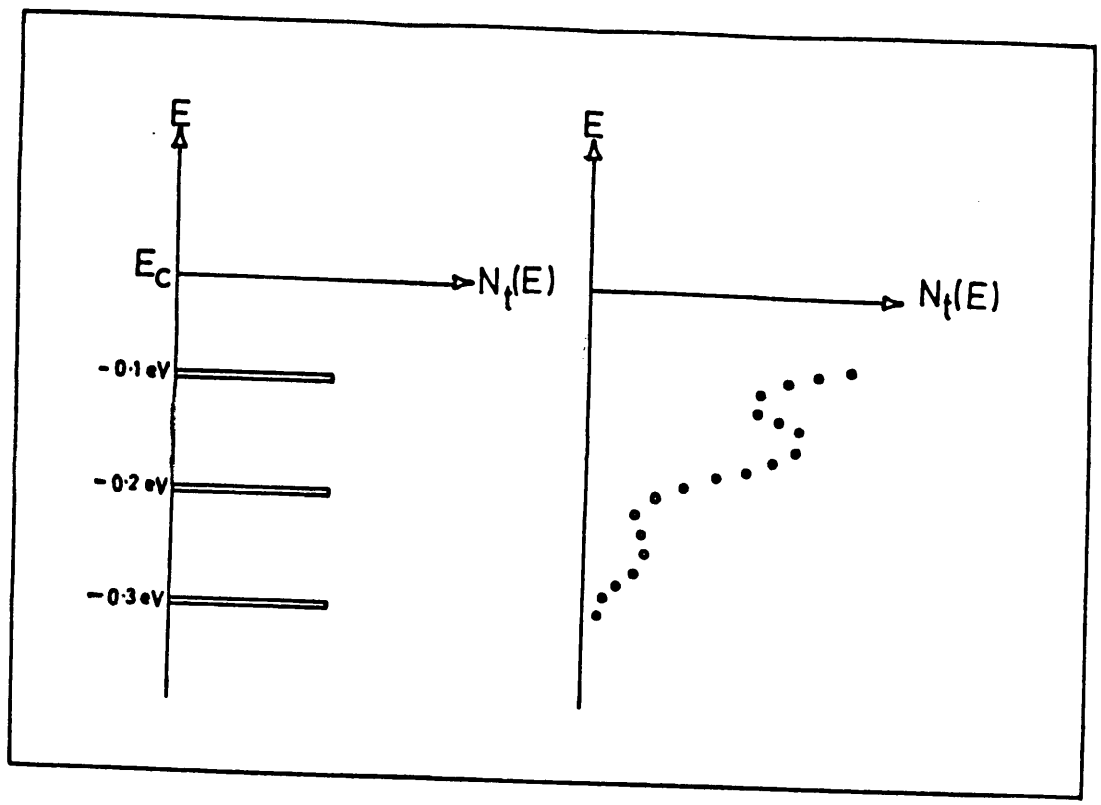

distribution see later) and that the actual calculated density of states decreases with increasing energy depth relative to the actual density.

The authors also note that if the three discrete levels used were to be replaced by some form of disorder broadened trap distribution then the above procedure would give an almost featureless decaying tail state distribution. This shows that the TROK model is likely to suggest an exponential distribution even if one does not exist.

It was also shown that the use of the thermalisation energy concept in the analysis of a highly structured distribution could result in the calculated profile being the *inverse* of the expected result [42]. The relationship between the density of states and the transit pulse and time has already been shown above (equation 3.10). The authors use the formulation of Michiel Marshall and Adriaenssens[43] (see below for further details) that links the density of states with the global waiting time distribution. This relationship may be expressed as :-

$$N(E_{th}) \simeq \text{constant } \psi(t)t \qquad (3.15)$$

Here the energy depth E_{th} is evaluated from $E_{th} = kT\ln(\nu t)$ as in TROK. However the detailed assumptions required by TROK are not used. The authors note that, for a set of discrete traps similar to those described above, except during the initial trapping regime and the approach to final equilibrium, the current I(t) and $\psi(t)$ correspond closely to one another. So for this highly structured distribution it becomes possible to replace $\psi(t)$ with I(t) giving :-

$$N(E_{th}) \simeq \text{constant } I(t)t \qquad (3.16)$$

Comparison of this result with equation 3.10 shows that for a structured distribution the TROK formulism can lead to a total inversion of the calculated density of states.

An assessment of the validity or otherwise of the thermalisation energy is presented by Marshall and Barclay [44]. The authors consider the detailed derivation of the thermalisation concept. They show that the carrier transit time for a time of flight experiment is built up in the following fashion :-

$$t_{trans} \simeq t_f + \sum(t_f/t_{tn})t_{rn} \qquad (t_f/t_{tn} > 1) \qquad (3.17)$$

where t_f = free carrier transit time

t_{tn} = carrier trapping time for states at level n

t_{rn} = release time from states at level n

Note that the above formalism does not necessarily order the trapping states in terms of their release time constants.

The authors then proceed to study the thermalisation energy concept as used by TROK. For the exponential tail the trapping states may, in fact, be ordered so that their trapping times increase continuously with increasing energy depth. It is then shown that the deepest set of traps, m, with which the carriers will interact is $t_{tm} = t_f$ and that the carriers will only interact with these states

once during the transit. The experimental transit time will therefore be of the order of the release time from these states. This gives rise to a measured drift mobility for the carriers that is reduced from the free mobility value by the ratio :-

$$t_t/t_{rm} \simeq t_{tm}/t_{rm} \simeq n_f/n_t \qquad (3.18)$$

This is as predicted by the TROK model. The authors conclude from this that the thermalisation energy concept will only be valid for trap distributions which decay continuously and at a suitable rate with increasing depth, such as the exponential tail. This occurs because with other distributions the carriers may interact with the deepest states encountered *several* times. It is further noted that the criterion of only encountering the deepest state once is that proposed by Schmidlin [26] for the observation of anomalously dispersive transients. The authors therefore go on to state that the thermalisation energy concept is only valid for materials having transit pulses which display a *high-anomalous* degree of dispersion.

3.3 The Michiel, Marshall and Adriaenssens Technique.

A further method of determining the density of states from the carrier transit was proposed by Michiel, Marshall and Adriaenssens [43]. The authors treat the pre-extraction transit of the conventional time of flight experiment. This region is similar to that observed for the transient photocurrent decay seen when a sample with co-planar electrodes is used. Further assumptions are made that carrier loss through the electrodes and by recombination are negligible and that

the transport is of a homopolar nature.

Then if, at time t = 0, n_o carriers are injected into the sample the free carrier density will be given by :-

$$dn_f/dt = n_t f(t) - (n_f/\tau) \tag{3.19}$$

where n_f = the number of free carriers

n_t = the number of trapped carriers $(n_o - n_f)$

τ = free carrier trapping time

f(t) = a function describing the release probability of trapped carrier.

After manipulation the authors find that the function f(t) is given by :-

$$f(t) = \int_0^t \left[\frac{n_f(t-t')}{n_o \tau}\right] \psi(t')dt' \tag{3.20}$$

Now the number of free carriers in the specimen is directly proportional to the excess current. Using this fact and substituting with the above equation 3.19 becomes :-

$$\frac{dI(t)}{dt} + \frac{I(t)}{\tau} = \int_0^t \left[\frac{I_o - I(t)}{I_o \tau}\right] I(t-t')\psi(t')dt' \tag{3.21}$$

where I_0 = the excess current at zero time

Equation 3.21 has the form of a Volterra integral of the first kind and can be solved by numerical methods. The authors then go on to find a relation between the waiting time distribution and N(E). This is :-

$$\psi(t) = [\nu kT/\int_{\substack{\text{all trapping}\\ \text{states}}} N(E)dE]\int_0^1 N[-kT\ln(z)]\exp(-\nu tz)dz \qquad (3.22)$$

where $z = \exp(-E/kT)$

When $\psi(t)$ is known, the above equation is a Fredholm integral of the first kind for N(E). This type of integral is 'ill posed' and difficult to solve. However, an approximate solution can be found by assuming that all the traps at depth E release their carriers after a time exactly equal to their mean release time after capture. The authors note that the introduction of this approximation will lead to a 'blurring' in the calculation of the localised states energy of about ± kT. So finally the density of states may be found from :-

$$N(E) = (N_o/kT)t\psi(t) \qquad (3.23)$$

where $N_o = \int_{\text{all trapping states}} N(E)dE$

and $E = kT\ln(\nu t)$

Although the energy in equation 3.23 is similarly expressed to

that of TROK's thermalisation energy no assumption has been made in this case that the states above E are in quasi-thermal equilibrium.

Michiel Marshall and Adriaenssens then go on to show that application of the above technique will, in fact, yield an accurate representation of the trapping state distribution. The technique is checked for two model distributions, the first of which is the exponential tail and the other being three discrete sets of traps. The results they obtain are reproduced in figure 3.5. These results clearly show that the method accurately reproduces the shape of the model distribution. The 'blurring' effect due to the approximation of equal release times can also be seen. On the same figure is shown what variation in the calculated distribution would arise if the values of two important initial conditions I_o and τ are not accurately known. The fact that the method appears to be relatively insensitive to reasonable variations in these parameters is important as experimentally it would be frequently be impossible to get anything other than estimates for them. In fact, further modelling work [45] has shown that, given sufficient computational time, the errors in these values can be minimised.

Although this technique yields good results the complexity of the method has, so far, tended to limit its application. The main work using this technique [42] is based on the fact that for a structured density of states $\psi(t)$ is closely related to I(t) (see equation 3.16).

Figure 3.5 Computed energy dependence of the density of localised states as proposed by Michiel et al.

(a) The distribution used in the simulations.

(b) The calculated distribution.

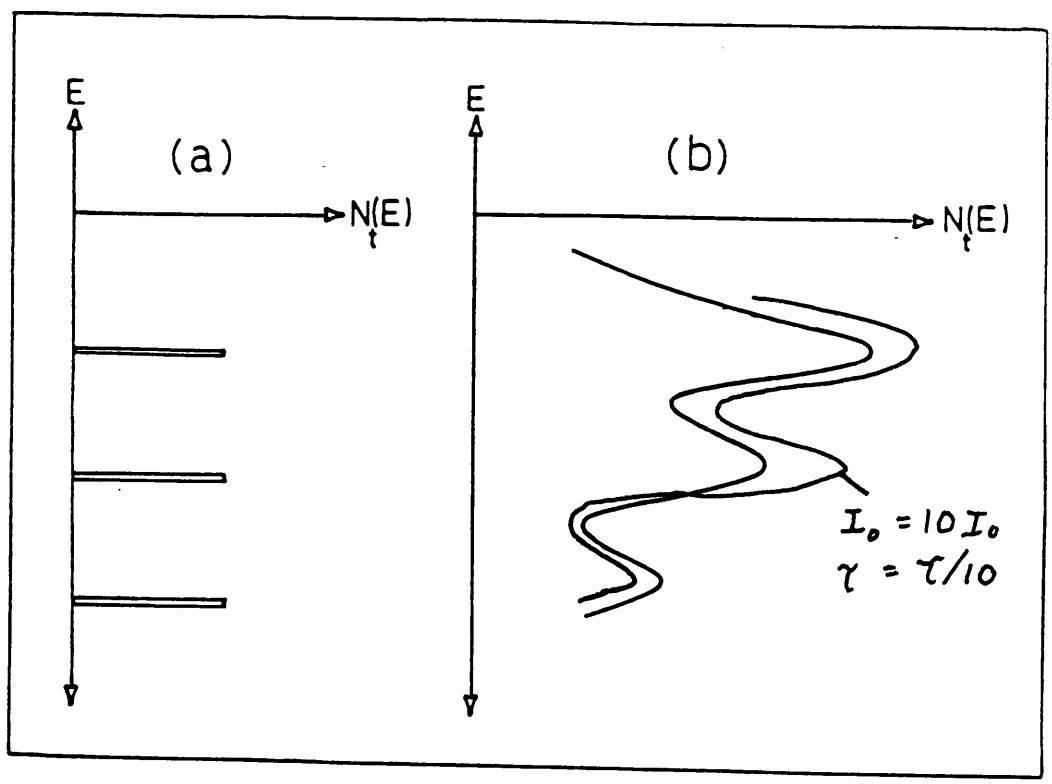

4 The Integral Technique.

The major techniques currently available for the analysis of time of flight results are described in the preceeding chapter. The aim of this present work is to develop and to validate a new analysis technique. This new technique removes problems associated with the previous methods.

The analysis technique proposed in this work is detailed in the literature in a paper by Marshall, Berkin and Main [46]. The new technique considers carrier trapping rather than trap release as considered by TROK. The interaction of free carriers with the trapping states must be of primary importance because a trap must exist and be occupied before any release event can take place. The thermalisation energy E_{th} may now be re-defined in terms of trapping characteristics rather than in terms of equation 3.4. This re-definition gives an E_{th} that successfully identifies the energy depth of the states that are dominating the carrier drift mobility whether the density of states is continuous and monotonically decaying or not. The new definition of E_{th} will also hold true for both anomalous and conventionally dispersive transport. The detailed derivation of this new technique will be considered below.

Start by considering a formalism in which the density of state distribution is sub-divided into strips ($\simeq$ kT) as envisaged by Schmidlin [26]. This process allows the identification of the sites which will have a time constant for capture less than or equal to the

time spent free by the carriers since their initial generation. This will allow the identification of the energy depth of the sites that have been visited once, on average, during the transit. The trapping time into these states is given by :-

$$\tau_{trap} = 1/(\delta N(E_{th})\sigma v_{th}) \simeq t_{free} \qquad (4.1)$$

where τ_{trap} = trapping time

t_{free} = free time

$\delta N(E_{th})$ = $N(E_{th})$ X width of strip at E_{th}

σ = capture cross section

v_{th} = thermal velocity

It should be noted that one problem arising from the use of the above formalism is that the value of $\delta N(E_{th})$ is determined by the width of the strip used. This means that the thermalisation depth can only be defined to within one strip width. A further consequence of the use of a finite strip width is that if the distribution contains structure much of the fine detail will be lost in the discretisation process. Furthermore it is not possible to extend this treatment to situations where the dominant transport states are visited more than once during the transit. This can lead to a situation where the thermalisation energy is predicted to be moving down through a set of states that do not actually exist. For example if the density of states distribution has a linear dependence then E_{th}, as defined by TROK, will move down past the cut-off point of the tail even though there are no states there with which carriers can interact (see figure 4.1). To prevent this obviously erroneous occurrence it is necessary

Figure 4.1 It can clearly be seen in this figure that the thermalisation energy as proposed by TROK can move through non-existent states.

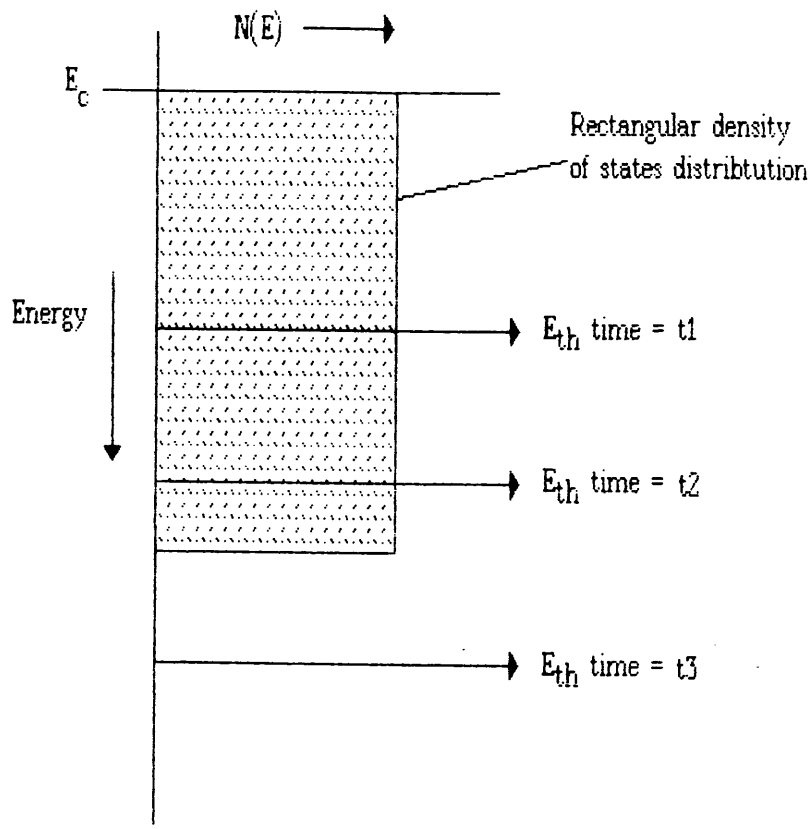

to re-define the thermalisation energy. The new definition must take into account the fact that the density of states distribution is not necessarily continuous, ie the movement downwards of the predicted thermalisation energy must cease if there is a zero density of trapping states. The details of this re-definition are presented below.

To proceed further the definition of the shallow and deep states must be altered from the TROK definition wherein all states below E_{th} are deep and all above are shallow. In the new definition shallow states are those which have been visited at least once during the total elapsed time and deep states are those centres which have been visited less than once in the same time period. It should be noted that this definition of deep states may include some groups of states above E_{th}. These, however, will have release times that are less than the total elapsed time and so can usually be ignored. Deep states below E_{th} will now be populated by some small proportion of the carriers. These deeply trapped carriers are unlikely to be released during the period of the measurement due to their long release time constants. The most important point of the above definitions is that for the deep traps the elapsed free time must not exceed the total time constant for trapping into all of these states. Therefore the trapping time constant into any such states will be equal to the elapsed free time. The net time free may now be calculated from :-

$$t_{free}^{-1} = \int_{\substack{all\ deep \\ traps}} (N(E)v_{th}\sigma)dE \qquad (4.2)$$

Figure 4.2 Schematic of the energy distribution of states as used in the integral technique. Note the direction of the energy axis.

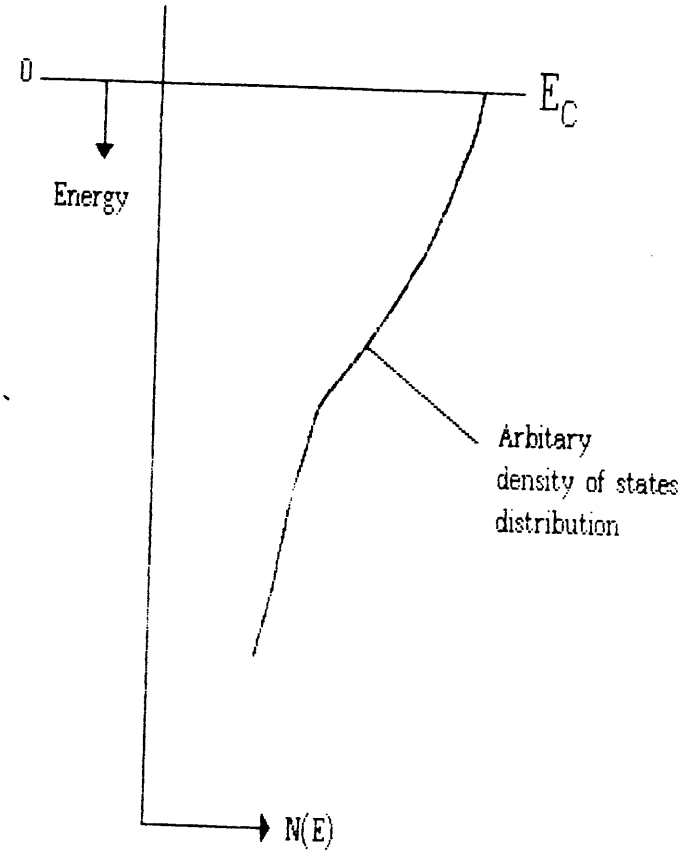

Note that the zero of energy is defined to be at E_c and that for convenience in integration the energy axis is as shown in figure 4.2.

All the states below the thermalisation energy will necessarily be 'deep' traps, so if any 'deep' states above E_{th} are ignored, which they can be because of their short release time constants, equation 4.2 becomes :-

$$t_{free}^{-1} = \int_{E_{th}^{new}}^{\infty} (N(E)v_{th}\sigma)dE \qquad (4.3)$$

Equation 4.3 can be used to re-define the thermalisation energy so that it fits the requirements stated above. It can be seen that the definition of E_{th}^{new} given by equation 4.3 will also solve the problem of non-continuous distributions of trapping states. If the distribution is non-continuous then the progression of the thermalisation energy down the tail will cease until such a time that deeper lying states, if any, have an effect on the transient. The problem of the finite width of the strips is also solved as an integral over all appropriate centres is performed. Note that for the case of an exponentially decreasing density of states, as considered by TROK, it can be shown that $E_{th} = E_{th}^{new}$ (see appendix 1).

The next problem is how to link the above result to factors which may be determined experimentally. To make use of the above equations a value for the free time must be found. It is not normally easy to extract this value from the experimentally determined value of total

elapsed time. However, in the 'time of flight' experiment the free time can be found without much difficulty provided that the value of the free mobility is known. The time spent free by a carrier crossing a sandwich cell will be given by :-

$$t_{free} = w/(\mu_o \epsilon) \qquad (4.4)$$

where w = sample thickness

ϵ = applied field.

Now by using this with equation 4.1 a value for density of states within a certain strip can be found :-

$$\delta N(E_{th}) = (\mu_o/(\sigma v_{th} w))\epsilon \qquad (4.5)$$

whilst use of equation 4.4 with the new approach described by equation 4.3 gives :-

$$N(E_{th}^{new}) = (\mu_o/(\sigma v_{th} w)).d\epsilon/dE \qquad (4.6)$$

The value of E_{th}^{new} will only be very weakly temperature dependent as it will be determined mainly by trapping ballistics. So the value of E_{th}^{new} required to use the above equation can be obtained from the low temperature activation energy of the drift mobility.

Computer simulations have been performed to check the validity of this new technique. The methods used and the results obtained are detailed in the following chapters.

5 Application to Amorphous Silicon.

At the present time the most important electronic non-crystalline material is amorphous silicon. It is already used extensively in the manufacture of solar cells, a-Si photocopiers are starting to appear as are LC display panels which contain a-Si driver transistors. Future applications of this material include scanners, printers and vidicon systems.

In all of the above devices the quality of the material is a paramount consideration. The higher the mobility and the longer the carrier lifetime then the better the performance of the device. Both of these important parameters will be controlled by the density of trapping states within the material. Yet, as shown in chapter 3, present methods of determining the DOS are either inaccurate or very complex.

The rest of this report is concerned with the integral technique described in chapter 4. It will be shown that this technique provides a relatively simple method of determining the DOS for an amorphous substance. However, in view of the technological importance of amorphous silicon the rest of this work will concentrate on it.

5.1 The Density of States in Amorphous Silicon.

The material presented below is not intended to be an exhaustive discussion of all the possible densities of states that have been

Figure 5.1 The calculated drift mobilities as presented by Lecomber and Spear for amorphous silcon.

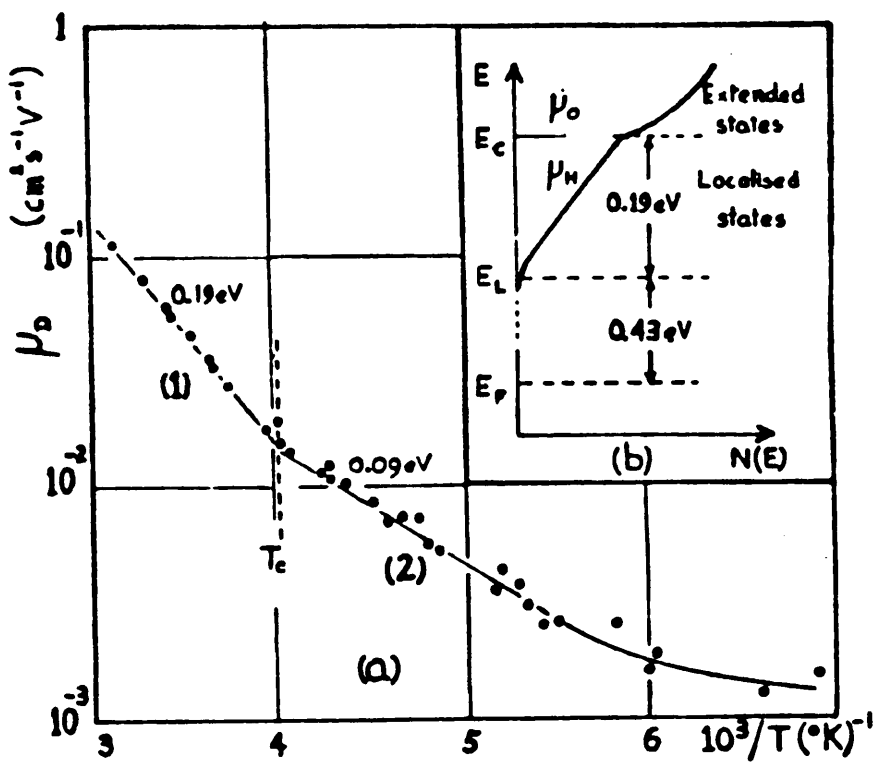

determined for a-Si by many different methods. Only the application of time of flight results to the determination of the DOS will be discussed.

One of the earliest attempts at determining the shape of the density of states in a-Si from time of flight measurements were made by LeComber and Spear [47]. In this paper data were presented from time of flight experiments on several samples over a range of temperatures. The plot of the calculated values of μ_d (see figure 5.1) shows three definite regions. The two lower temperature regions are ascribed to hopping and Fermi level hopping and no information on the DOS is offered. However, in the high temperature region (>240K) the transport is ascribed to the extended states, with multiple trapping in localised states. The mobility in this region is activated with an activation energy of 0.19 eV. From these data three possible models are proposed for the DOS. These are :-

1. A single trapping level at 0.19 eV.
2. A linear distribution of trapping states below the band edge.
3. A linear distribution which continues increasing beyond E_c into the extended states.

It is noted that all of these possible model distributions will give the observed results and so no one of them is preferred.

A different determination of the shape of the density of states distribution was made by Tiedje et al [22]. Details are presented of measurement of both the electron and hole transients of amorphous

silicon. The transients are found to be conventionally dispersive at high (300K) temperatures changing to become anomalously dispersive as the temperature falls. The shape of the DOS distribution is assumed to be exponential with a characteristic temperature T_c. It is shown that at $T > T_c$ conventionally dispersive transport is expected while at $T < T_c$ the trapped carrier packet will thermalise down the distribution giving anomalously dispersive transport. In this way the observed switch from anomalous to conventional dispersion is explained. The value of T_c is predicted either from the temperature at which the dispersion changes from anomalous to conventional or from the temperature dependence of the dispersion parameter.

More recent work by Vanderhagen and Longeaud [48] contains the suggestion that the energy distribution of the trapping states is better described by two exponential tails of characteristic temperature T_{c1} = 390K and T_{c2} = 210K, the higher characteristic tail being closer to the band edge.

The integral technique has been used, in the determination of the density of states, in two papers ,the first by Marshall, Street and Thompson [49] and the second by Marshall, Street, Thompson and Jackson [50]. In the first they consider the shape of the conduction band tail and in the second the shape of valence band tail. The results presented are reviewed below.

The first paper is concerned with the electron drift mobility and so yields results about the shape of the conduction band tail. The authors note that most 'time of flight' data previously presented was

Figure 5.2 Example of the results presented by Marshall et al for amorphous silicon. Fields are as follows :- a, 0.5; b, 1; c, 2; d, 3; e, 5; f, 10; g, 20; h, 30; i, 40; j, 50 $kVcm^{-1}$.

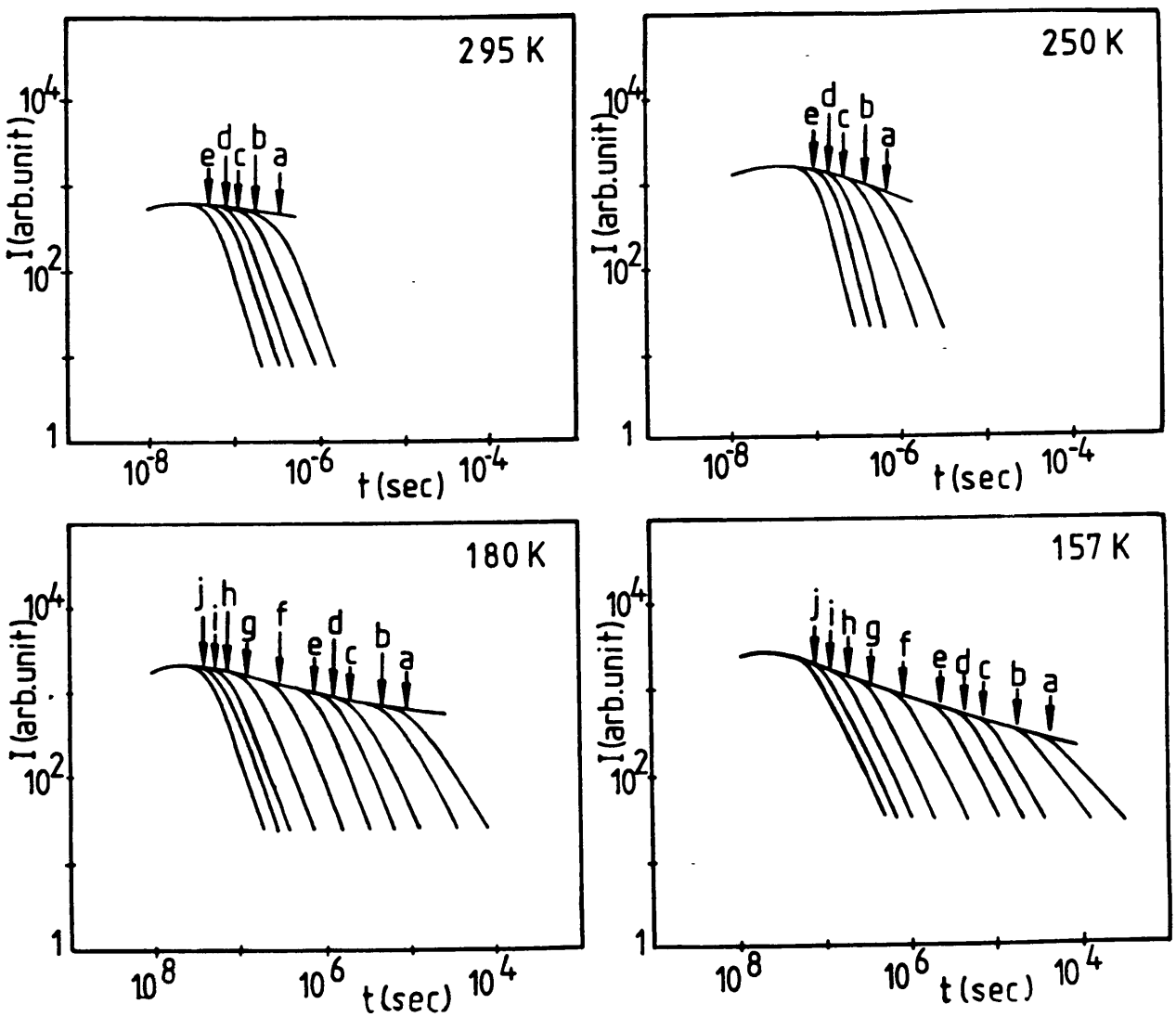

some what fragmentary in that it did not encompass wide ranges of either temperature and field. They correct this lack of data by presenting data for amorphous silicon which covers both parameters extensively. The temperature range covered is 100K to 350K and the field ranges from 5×10^2 to 5×10^4 Vcm^{-1}.

The transit time for the sample is taken to be the point at which the post transit current has fallen to 80% of the extraction free value. To assist in the identification of this point the technique, orginally proposed by Marshall and Allen [36], of superimposing pulses is used. The use of this technique leads to the calculated mobilities being larger by a factor of 30% to 50% than the average drift mobility. An example of the results obtained are shown in figure 5.2.

After presentation of the results the authors note that an estimate can be made of the free carrier mobility, μ_o, from the temperature dependence of the low field mobility. This arises in the following manner. The drift mobility is related to the free mobility by :-

$$\mu_d = \mu_o/(1+[N_t/N_c]\exp(E/kT)) \qquad (5.1)$$

Now as $T \rightarrow \infty$ in the above so $\mu_d \rightarrow \mu_o$. This phenomenon is observed on mobility plots which at high temperature change from an activated form over to a constant value (μ_o). Using this fact and fitting equation 5.1 to the low field data, (figure 5.3) values of $\mu_o = 20$ $cm^{-2}V^{-1}s^{-1}$ and $N_t/N_c \simeq 10^{-2}$ are calculated.

Figure 5.3 Results obtained from the analysis of the results for the high temperature low field regime for a-Si:H. (from Marshall et al.)

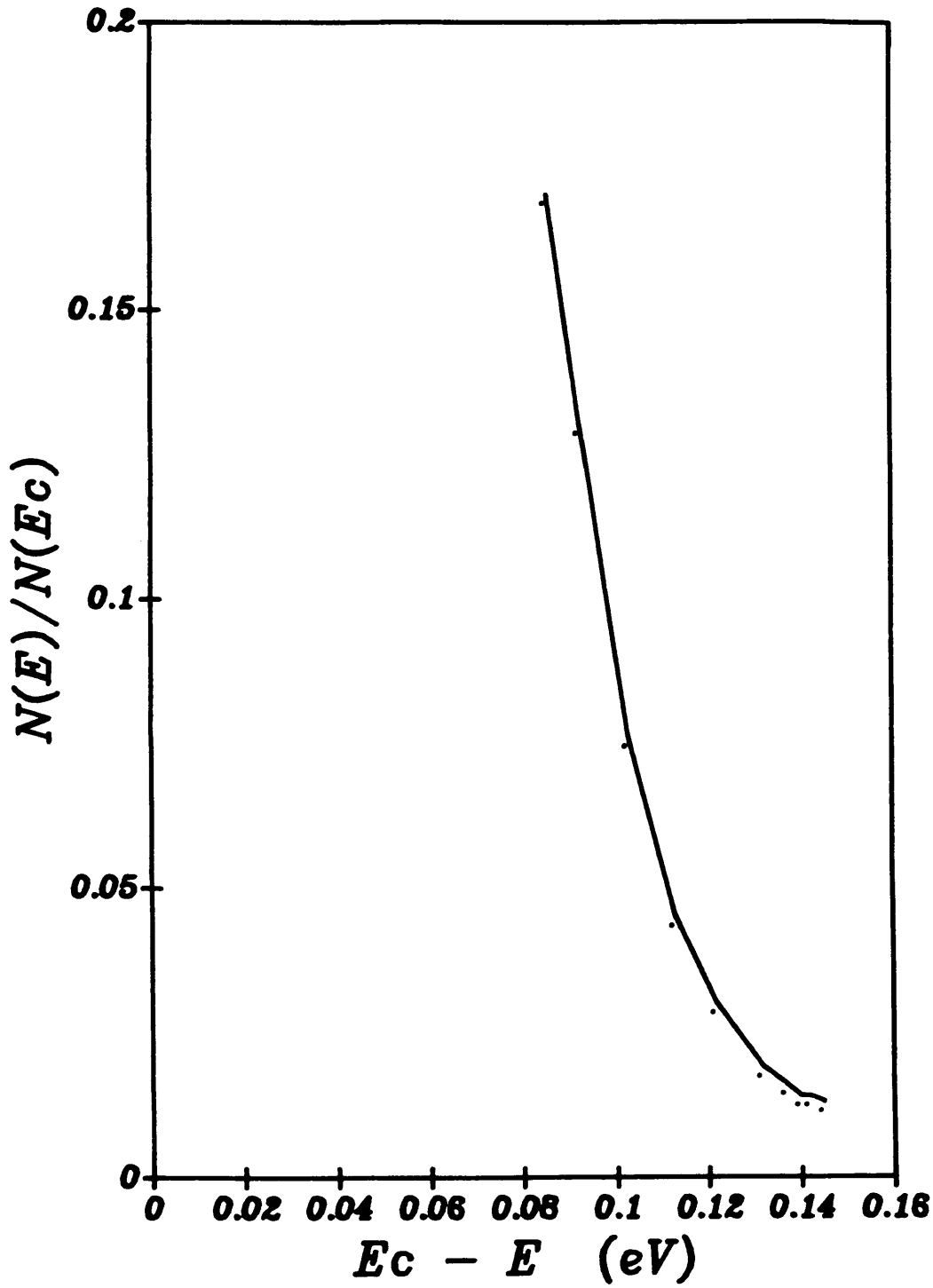

Figure 5.4 Results from the low temperature high field regime for a-Si:H.

a) using equation 4.1

b) using equation 4.3

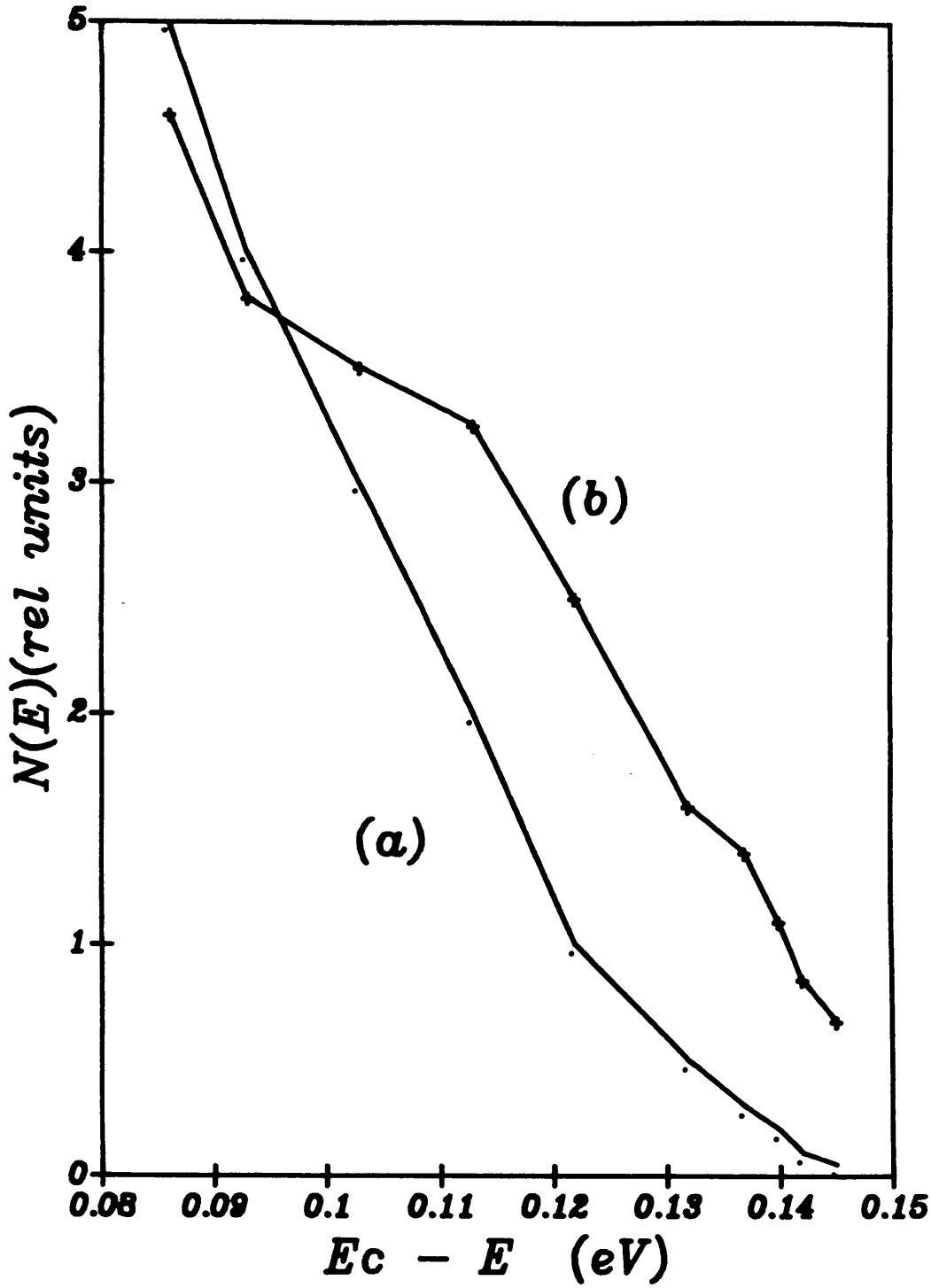

It is noted at this point that the mobility activation energy increases in the low field region as the field is reduced, but only changes slightly once a value of $\simeq$ 0.14eV is reached. This is indicative of an abrupt change either in the density of states or in the nature of those states.

The above authors also present an analysis of the low-temperature high field regime. Both equation 4.1 and equation 4.3 are used in the analysis. The results obtained in both cases can be seen in figure 5.4. Use of equation 4.1 predicts a curving density of states that falls to a low value at around 0.15eV. However, use of equation 4.3 predicts that the density of states is linear over the entire accessible energy range (0.08-0.15eV). This linear tail still falls to a very small value at 0.15eV.

Further details presented include a comparison of the α_1 and α_2 values for the pre and post transit regimes for the experimental data with those calculated from computer simulations. This comparison again shows that the density of states is exhibiting a linear dependence on energy over the accessible energy range.

A similar set of data for the hole transits is presented in the second paper. Information is extracted from this data on the shape and density of the valence band tail. The methods of analysis employed are the same as those described above. The authors conclude that the shape of the valence band tail is well described by a distribution of the form :-

$$N(E) = N_v \exp(-(E-E_v)^2/\Delta^2) \qquad (5.2)$$

As can be seen from the above review there is still disagreement within the literature as to the shape of the density of states in amorphous silicon. Many of the measured differences will come from variations in material quality, which is dependent on where it was manufactured. However, the differences between samples of device quality material produced in different sites seems to be getting much less. This leads to a need for a method of accurately determining the DOS within this material. It is hoped that the work presented in this thesis goes some way toward filling this need.

6 Computer Simulation Methods.

6.1 Introduction.

All of the computer simulations reported herein were performed using either a Digital Equipment Corporation (DEC) System 20 main frame computer or a DEC VAX 8530 both situated at Dundee College of Technology. The fits of curves to generated data were accomplished using the National Institutes of Health on-line modelling laboratory (MLAB). Two programmes were also written by the author to produce the graphical output presented. These used the Culham Laboratories' Ghost graphics package and the GINO-F graphics package to drive a Calcomp plotter.

6.2 Methods.

It is hoped that the simulations herein described may be able to distingush between model densities currently proposed for a-Si. To further this end two proposed distributions (linear tail of depth 0.15 eV and exponential tail of characteristic temperature 300K) will be studied in depth. It should, however,be noted that neither of the simulation methods used is actually limited to using these distribution and both can in fact use any arbitary distribution that may be required.

Details of the programmes used to simulate various aspects of the time of flight experiment will now be given. Two methods of simulation were used:-

1. The Monte Carlo method

2. The finite difference method.

Of the two techniques the Monte Carlo method was initially preferred because it involves using fewer approximations.

6.2.1 Monte Carlo Methods.

The technique of Monte Carlo simulation uses computer generated pseudo-random numbers to model the processes present in a real sample. In the multiple trapping model a carrier is initially in the extended states and after a time related to the free carrier trapping time constant it is trapped into a localised state. The depth at which it is trapped will depend on the distribution of available trapping states. The carrier will then spend a certain amount of time immobilised in the trapping state, after which it will be released back into the extended states. The time spent immobilised will depend on the energy depth of the state. The process is repeated until the carrier has crossed the sample (see figure 6.1). In a real system each of the above stages, initial trapping, localisation at some energy and release to the extended states will vary randomly about some average value.

The Monte Carlo simulation programmes used worked by taking each carrier in turn. The free carrier trapping time was a random variable with a probability distribution appropriate to the trapping process. The energy depth at which the carrier was trapped was found

Figure 6.1 Schematic diagram showing the Monte Carlo simulation process

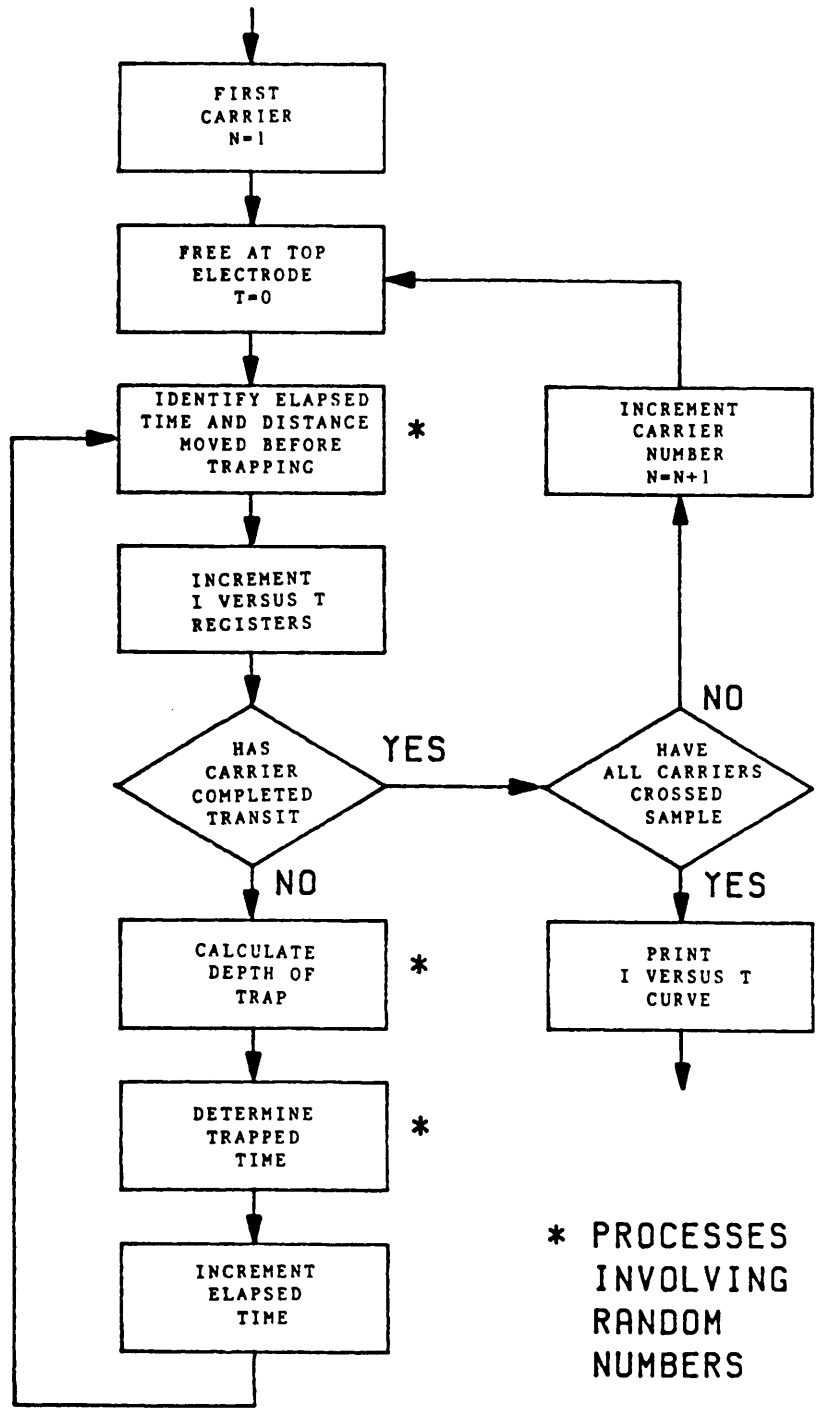

by using a random number in conjunction with a generating function for the distribution being studied. Finally a random number was used to generate an appropriate statistical variation of the release time about its mean value.

6.2.1.1 The D.O.S. Generating Function.

The probability that a carrier will be trapped at a certain energy depth is proportional to the density of states at that depth. In order to take this effect into account a density of states generating function is required which will give the probability that a carrier will be trapped at a certain depth. The generating function needed to form the energy distribution being studied was found using the inverse transform method [51,52]. This method is as follows:-

If the distribution to be sampled has a probability density function f(x) then the cumulative distribution function F(x) is

$$F(x) = \int_0^x f(x)dx \qquad (6.1)$$

A random sample of this distribution may be taken by setting

$$X = F(x)^{-1}(U) \qquad (6.2)$$

where X = random sample of distribution

U = a random function uniformly distributed between 0 and 1.

Using this method the generating function for a linear tail was found to be :-

$$E = 1 - \sqrt{(1-Q)} \qquad (6.3)$$

and for an exponential tail was

$$E = \log_e(Q). \qquad (6.4)$$

Where E = the energy depth of the trapping state.

Q = a random number such that $0 \leq Q \leq 1$.

6.2.1.2 Continuity of the D.O.S..

The dwell time of a carrier trapped at energy E is given by :-

$$t_{rel} = -\tau_o \exp[(E_c - E)/kT] \ln(Q) \qquad (6.5)$$

where t_{rel} = the release time for the trap.

Q = a further random number.

τ_o = constant

In order that the localised states were continuous with the extended states [36] it was necessary to calculate τ_o for each distribution. The general relationship is given by :-

$$\tau_o = t_{free}\left[\int_{E_t}^{E_c} \frac{N(E)dE}{N(E_c)kT}\right] \qquad (6.6)$$

where t_{free} = free carrier trapping time

$N(E)$ = density of states at E

$N(E_c)$ = density of states at E_c

The calculations for each distribution are presented in full in appendix II. The results obtained were:-

$$\frac{1}{\nu} = \frac{2(B+1)}{\tau_{trap} B^2} \qquad (6.7)$$

for the linear tail and

$$\frac{1}{\nu} = \frac{T}{T_c} \qquad (6.8)$$

for the exponential tail. Where :-

$B = kT/\Delta$ (6.9)

Δ = the depth of the linear tail

T = the temperature

T_c = the characteristic temperature of the exponential tail.

Within the simulations the values of Δ was set at 0.15eV and T_c was set at 300K.

6.2.1.3 The Simulation Programmes Used.

Two simulation programmes were developed for each of the distributions studied. The first programme produced the transit pulse associated with the density of states being used as other relevant parameters (temperature and number of trapping events per transit) were varied. This programme also calculated the time ($t_{20\%}$) taken for twenty percent of the carriers to cross the sample. This $t_{20\%}$ was taken as the transit time for the particular conditions employed. The second programme was used to find out the average energy of the deepest state with which a carrier, in the fastest 20% group had interacted during the transit.

Both programmes were run for a variety of temperatures and for different values of the average number of trapping events per transit. The average number of trapping events per transit is a useful way of normalising the effects of variations in thickness and in field. It is given by :-

$$\text{no. of trapping events per transit} \propto w/\epsilon \qquad (6.10)$$

where w = thickness of sample

ϵ = applied field.

Example programmes may be found in appendix III.2.

6.2.1.4 Problems with Monte Carlo Simulation.

The Monte Carlo simulation programmes are very useful and easily adaptable so as to allow many different parameter variations to be studied. However, there are both practical and theoretical problems in their use. On the practical side the programmes require a tremendously long amount of main frame computer time to produce some of the transits, especially the lower temperature results (times of the order of six hours or more cpu time may be required). The transit pulses that are then produced have a marked tendency to be rather noisy. The noise problem could be combated by increasing the number of carriers but problems would then arise with the generation of truly random (rather than pseudo-random) numbers. As the noise is proportional to the square of the number of carriers any increase in this value would have to be very large to significantly reduce the noise. However, any increase in the number of carriers would also increase the run time past an already unsatisfactory value. There would also be problems with the Monte Carlo programmes if the complexity of the model were further increased to include such things as recombination and diffusion. In an attempt to circumvent these problems simulation by the finite difference method was investigated.

6.2.2 Finite Difference Methods.

Transient effects may also be simulated by using a matrix simulation technique as developed by Main [53]. In this case the DOS under consideration is initially sub-divided energetically into a series of strips each of approximately kT width (the arrangement is

Figure 6.2 Schematic showing how the density of states is subdivided both in energy and space.

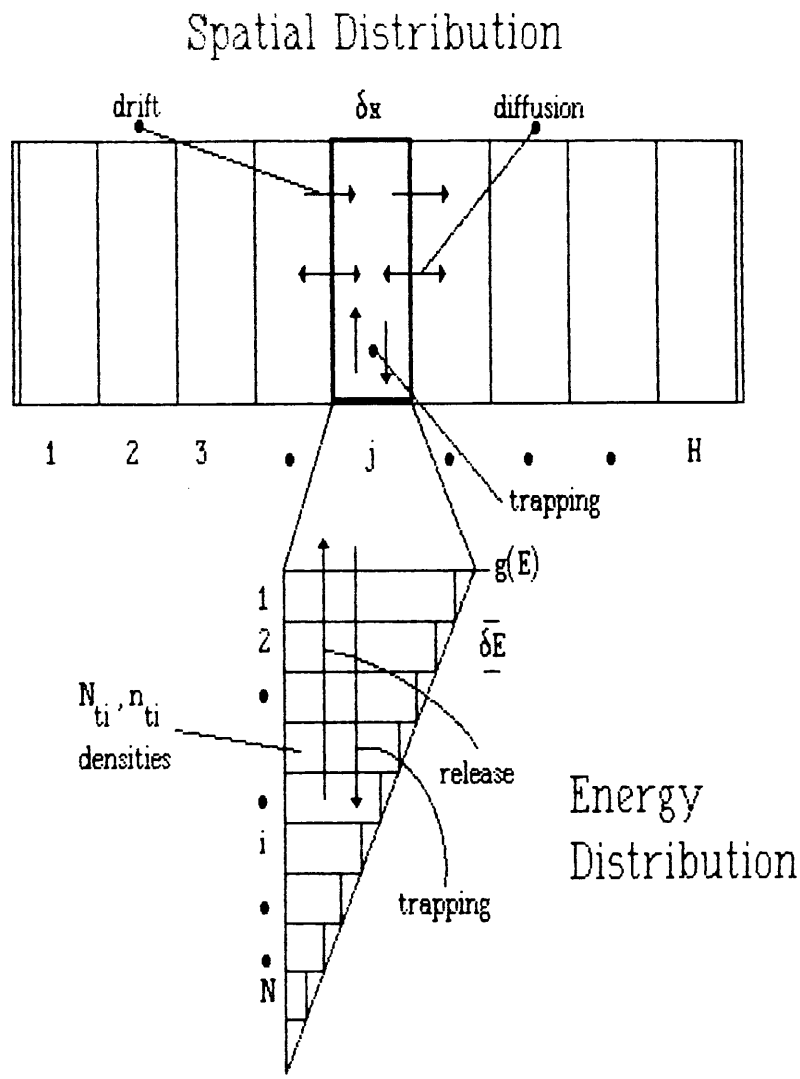

shown schematically in figure 6.2). The sample is also subdivided in space so that carrier motion through it can be studied. The transient is then generated by simultaneous solution of the equations governing the trapping and release of carriers from each of the levels and the drift and diffusion between spatial slices. A programme using this method will run much faster than a Monte Carlo simulation programme and the generated transient will be effectively noise free. However, the method does make use of a certain number of approximations, for instance the D.O.S. is approximated by a number of discrete strips, which makes the final transient less likely to be a true representation of the situation occurring in a real sample. The programme used to solve the equations used an implicit step solution method to obtain the final solution for a set of given initial conditions.

6.2.2.1 The Implicit Solution Method.

The programme developed for this simulation used an implicit solution technique. The solution was developed in the following manner :-

Firstly consider carriers in a sample where there is no drift or diffusion. Let the DOS be subdivided into a number of strips (numbered 1 to NL). The density of free electrons will be determined by the trapping and release within the strip :-

$$dn/dt = -n \sum_{i=1}^{NL} C_{ni}(N_{ti}-n_{ti}) + \sum_{i=1}^{NL} nC_{ni}n_{1i} \qquad (6.11)$$

where n = number of free carriers

N_{ti} = trap density at level i

C_{ni} = electron capture coefficient

n_{ti} = number of carriers trapped at level i

$$n_{1i} = N_c \exp(-(E_c - E_i)/kT)) \qquad (6.12)$$

= emission terms from detailed balance

The rate of change of trapped charge in each strip will be given by :-

$$dn_{ti}/dt = nC_{ni}(N_{ti} - n_{ti}) - n_{ti} C_{ni} n_{1i} \qquad (6.13)$$

Note equations 6.11 and 6.13 are non-linear, however they may be reduced to a linear form if it is assumed that $n_{ti} \ll N_{ti}$.

The drift and diffusion of the charge packet is now considered by spatially dividing the sample into a set of slices. For any one such slice the drift and diffusion contributions to the rate of change of carrier density in the slice are given by the free carrier rate equations :-

$$(\partial n/\partial t)_{drift} = -\epsilon \partial n/\partial x \qquad (6.14)$$

$$(\partial n/\partial t)_{diffusion} = - D\partial^2 n/\partial x^2 \qquad (6.15)$$

where D = diffusion coefficient.

= $\mu kT/e$ via the Einstein relation

The drift and diffusion along the sample can now be approximated by taking finite differences between the slices with :-

$$\partial n_j/\partial x = \frac{1}{2}\left[n_{j+1}-n_{j-1}\right]/\delta x \qquad (6.16)$$

$$\partial^2 n_j/\partial x^2 = (n_{j+1}-2n_j+n_{j-1})/\delta x^2 \qquad (6.17)$$

where j denotes the slice index

The full finite difference equation for the free electrons, formed by including trapping and release in the above is given by :-

$$\frac{\partial n_{ti,j}}{\partial t} = -n_j \sum_{i=1}^{NL} C_{ni} N_{ti} + \sum_{i=1}^{NL} n_{ti,j} n_{1i} C_{ni} - \frac{\mu\epsilon}{\delta x}\frac{1}{2}\left[n_{j+1}-n_{j-1}\right] + \frac{\mu kT}{e\delta x^2}\left[n_{j+1}-2n_j+n_{j-1}\right] \qquad (6.18)$$

The variation in the trapped charge in the i^{th} energy level for any slice j, $n_{ti,j}$, is then given by :-

$$\frac{\partial n_{ti,j}}{\partial t} = n_j C_{ni} N_{ti} - n_{ti,j} n_{1i} C_{ni} \qquad (6.19)$$

A Crank-Nicolson implicit method has proved to be suitable for the solution of the above equations. Explicit methods have not been successful, since the equation system is extremely 'stiff', a

condition which places severe constraints on the size of the time step required for a stable solution.

The equation system is of size (NL+1)*HT=N, where NL+1 is the number of trapping levels plus the conduction band, and HT is the total number of slices. The system may be written in vector form as :-

$$\underset{\sim}{\dot{n}} = \partial \underset{\sim}{n}/\partial t = \underset{\sim}{f}(\underset{\sim}{n}, t) \qquad (6.20)$$

with N*N Jacobian $\underset{\sim}{J} = \partial \underset{\sim}{f}/\partial \underset{\sim}{n}$

$$\text{i.e. } J_{i,j} = \partial f_i/\partial n_j \qquad (6.21)$$

The Crank-Nicolson formula used to compute the values of the variables after a time-step $\Delta t = t_{k+1} - t_k$ is :-

$$\underset{\sim}{n}_{k+1} = \underset{\sim}{n}_k + 1/2(\underset{\sim}{f}_{k+1} + \underset{\sim}{f}_k)\Delta t \qquad (6.22)$$

The second term on the right hand side represents the mean of the derivative functions, $\underset{\sim}{f}$, using pre- and post-step variable values. Since post-step (i.e. k+1) values are unknown, a Newton iteration is employed viz :-

$$(\underset{\sim}{I} - \underset{\sim}{J}\Delta t)^s_{k+1} \underset{\sim}{\Delta n} = 1/2(\underset{\sim}{f}^s_{k+1} + \underset{\sim}{f}_k)\Delta t + \underset{\sim}{n}_k - \underset{\sim}{n}^s_{k+1} \qquad (6.23)$$

where $\underset{\sim}{I}$ is the N*N unit matrix, s represents the iteration index and

Δn is solved for to give :-

$$\underset{\sim}{n}_{k+1}^{s+1} = \underset{\sim}{n}_{k+1} + \underset{\sim}{\Delta n} \qquad (6.24)$$

The process is repeated until the 'correction' term, Δn, reaches some specified small value, and then the next time-step calculations are initiated.

In the above solution a Jacobian matrix containing the system parameters has to be set up. This matrix is both symmetrical and sparse. This means that the computer memory and run-time required to solve for the free electron density is minimal, i.e. the programmes run much faster than the similar Monte Carlo programmes.

7 Computer Simulation Results.

7.1 Transit Pulses.

The transit pulses obtained from the computer simulations are presented below. The data are shown in a format similar to that first used by Marshall and Allen. The transit pulses are superimposed on one another thus allowing the departure from the extraction free transient to be readily identified.

7.2 The Linear DOS.

Transit pulses for the linear tail were obtained over the temperature range 150K to 450K. The number of trapping events per transit was varied from 10 to 1000, this corresponds to field or thickness variations of a factor of 100. An example of the transit pulses obtained using the Monte Carlo method is presented in figure 7.1 and an example of the pulses obtained using the finite difference method is shown in figure 7.2. The temperature dependence of the mobility for the linear tail is shown in figure 7.3.

It should be noted that, although the finite difference method involves more assumptions than does the Monte Carlo method, there are no significant differences in the pulse shapes. The noise present on the pulses generated by the Monte Carlo is due to the small number of carriers (10000) that were used in the simulation. This relatively small number of carriers was used because of the very large amounts of computer time required to run the programmes.

Figure 7.1 An example of the transit pulses obtained for the linear DOS using the Monte Carlo simulation method. ● = 10, ■ = 30, × = 100, ◆ = 300 and + = 1000 trapping events per transit.

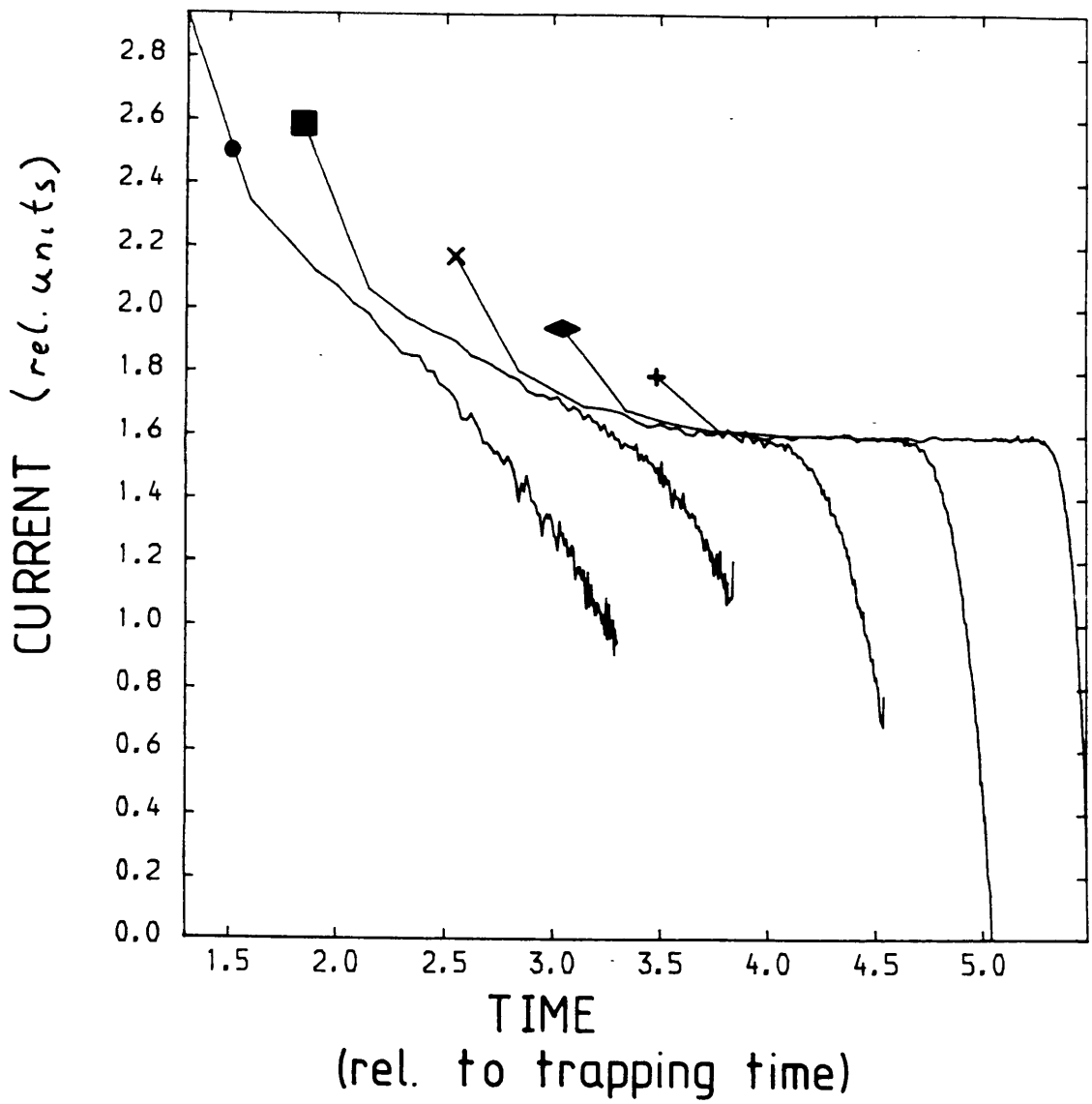

Figure 7.2 An example of the transit pulses obtained for the linear DOS using the finite difference simulation method. ● = 10, ■ = 30, × = 100, ◆ = 300 and + = 1000 trapping events per transit.

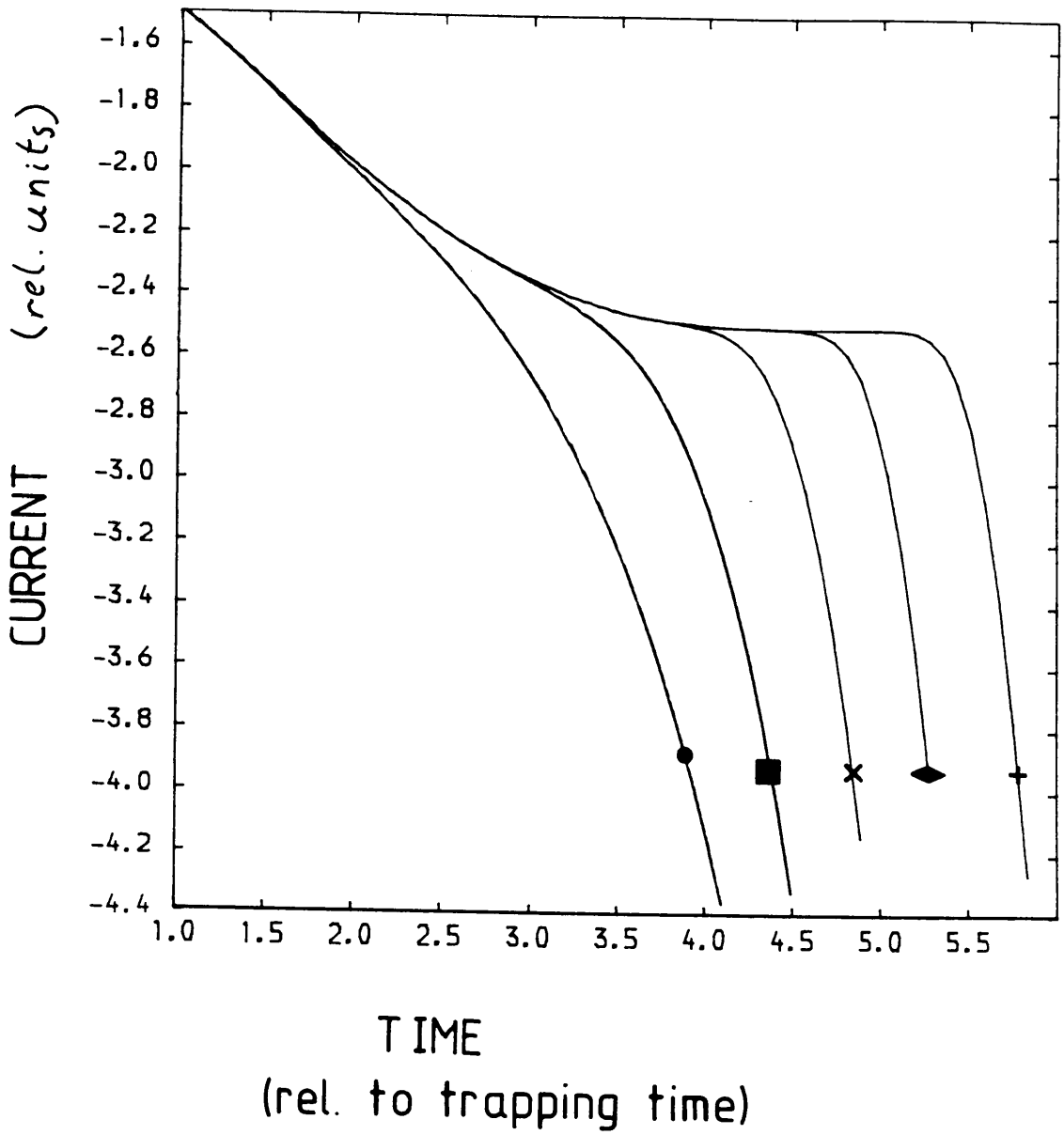

Figure 7.3 Mobility versus reciprocal temperature for linear tail. ■ - 10, o - 12, X- 15, ◇- 20, + = 25, ● = 30, □ = 60, O = 100, ◊ = 300 and ⊘ = 1000 trapping events per transit.

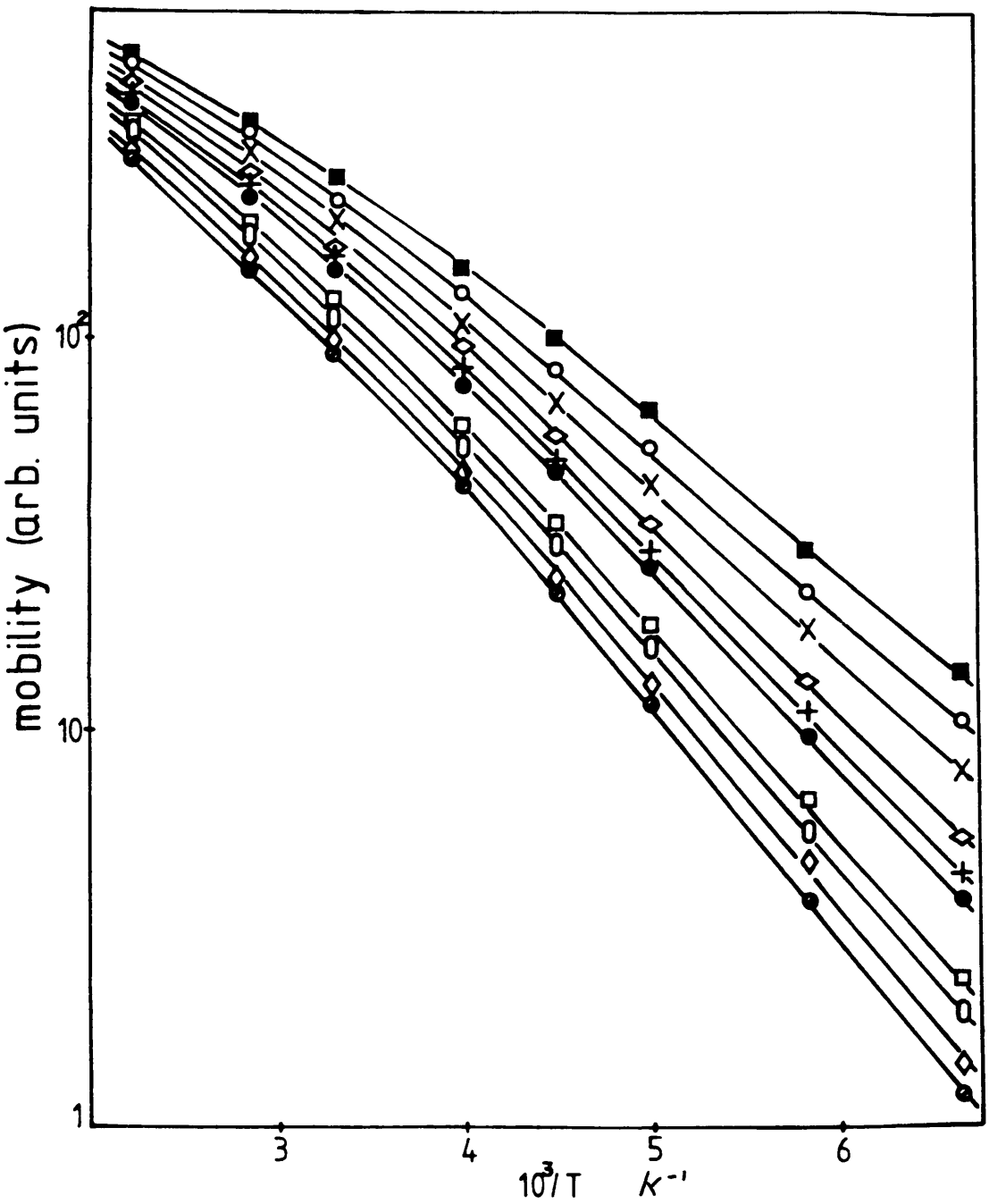

Information on the energy depth of the mobility dominating states was found in two ways. These states will be the deepest encountered by a carrier that have released in the time $t_{20\%}$. For an anomalously dispersive transient these will be the states that have been visited once on average. The 'average deepest trapping' level encountered during the transit was calculated from the activation energy of the mobility. This result was then compared with that predicted by the integral method and with the actual deepest level encountered as found directly from the Monte Carlo programmes (see table 1).

Table 1

Number of trapping events per transit.	Mobility activation energy. Monte Carlo method. eV.	Mobility activation energy. Finite difference method. eV.
10	0.075	0.081
30	0.095	0.100
100	0.105	0.107
300	0.110	0.112
1000	0.112	0.113

Number of trapping events per transit.	Actual deepest level encountered. Monte Carlo method. eV.	Level predicted by integral method eV.
10	0.086	0.095
30	0.114	0.118
100	0.131	0.132
300	0.140	0.140
1000	0.144	0.144

The DOS calculated from the above results for the mobility activation energy using the TROK (using equation 3.10) method is shown in figure 7.4. The form of the DOS calculated is an exponential tail

Figure 7.4 The form of the DOS calculated for the linear distribution using the TROK method.

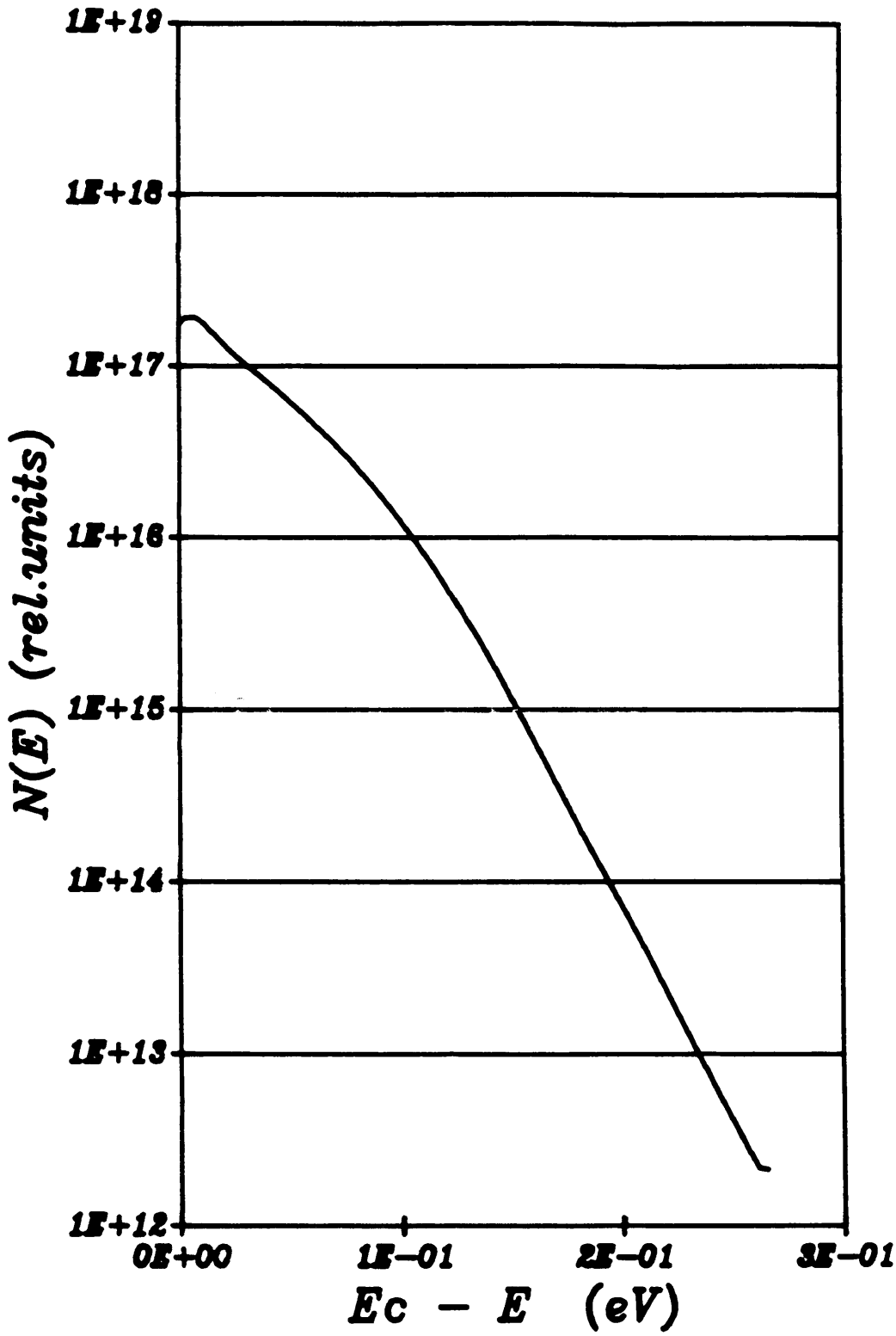

Figure 7.5 The form of the DOS calculated for the linear distribution using the MA method.

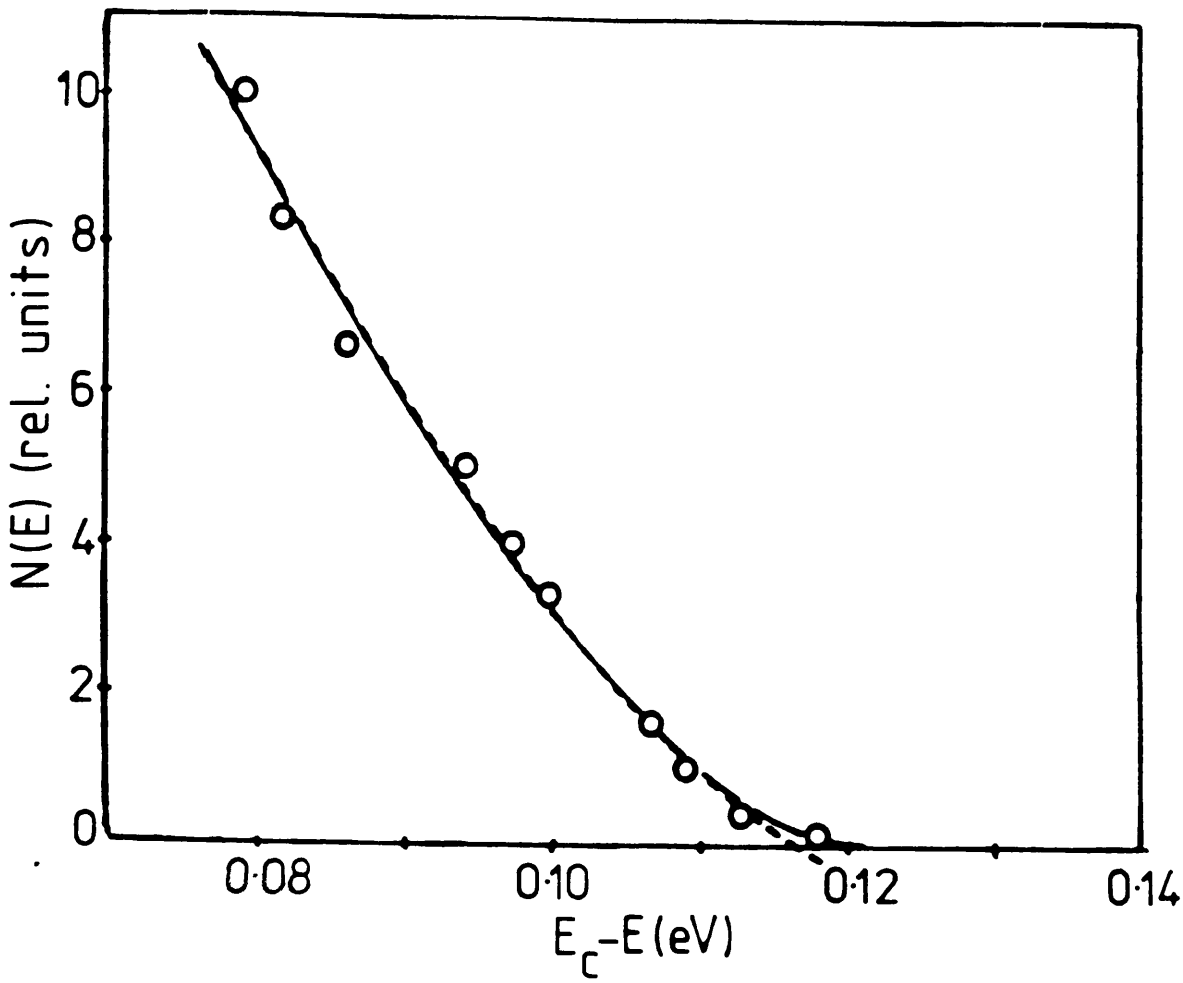

with a characteristic temperature of 312K (over the range 0.08-0.12eV)

Figure 7.5 shows the form of the DOS found using the Marshall and Allen (MA) method of analysis (equation 3.2). The shape attributed to the DOS by the MA method is found to be best fitted, using MLAB, by a parabola. Other functional forms for this fit were tried but the best result was obtained by using the parabolic form. The form of the parabola is :-

$$N_{rel}(E) = 32.4 \quad E^2 + 8.7 \quad E + 0.5 \qquad (7.1)$$

As the calculation of the DOS using the Marshall Berkin and Main (MBM) method is basically to take the differential of the MA result it can be seen that a linear form will be obtained in this case. The actual calculated result (using equation 4.3) is shown in figure 7.6. The equation of this line is :-

$$dN_{rel}(E)/dE = 64.8 \; E - 8.7 \qquad (7.2)$$

The solution of this equation puts the cut-off point of the linear tail at 0.135 eV (from N(E) = 0 at E = 8.72/64.82).

If the integral method is used with the results for the actual deepest level encountered instead of with the values for the mobility activation energy then the equation of the calculated line becomes :-

$$dN(E)_{rel}/dE = 46.4 \; E - 7 \qquad (7.3)$$

Which in turn gives a cut-off point for the DOS at 0.151 eV. It

Figure 7.6 The form of the DOS calculated for the linear distribution using the integral method.

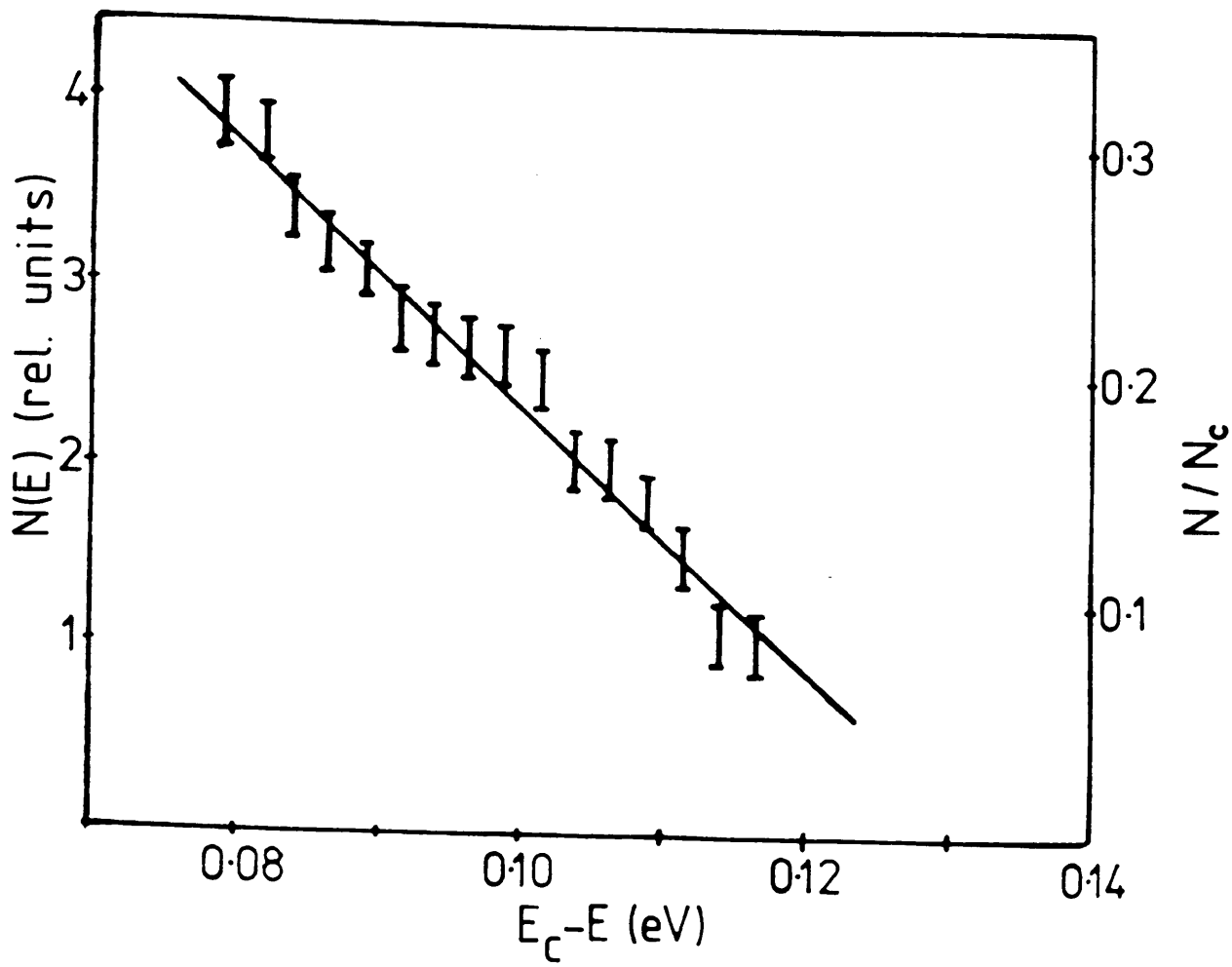

should be noted that it is not possible to obtain information on the actual deepest level encountered experimentally so the above is only useful from a theoretical veiwpoint.

The gradient of the linear tail can also be calculated. The calculated value is $N_c/(0.17 \pm 0.03)$, which is a good fit to the actual value of $N_c/0.15$.

Using values for the mobility activation energy generated by the finite difference method the cut-off point is found to be at 0.13 eV. It should be noted that it is not possible to obtain values for the actual deepest level encountered using the finite difference method.

7.3 The Exponential DOS.

Data on the transit pulses produced by an amorphous material possessing an exponential distribution of tail states (T_c = 300K) obtained using the same variations in temperature and number of trapping events per transit as was used for the linear distribution. An example of the transit pulses produced using the Monte Carlo simulation method is shown in figure 7.7 and an example of the pulses produced by the finite difference method is shown in figure 7.8. The temperature dependence of the mobility is shown in figure 7.9.

As for the linear, case the 'average deepest trapping level' encountered was estimated from the mobility activation energy. The comparison of this result with the actual deepest level encountered and the level predicted by the integral method is shown in Table 2.

Figure 7.7 An example of the transit pulses obtained for the exponential DOS using the Monte Carlo simulation method. ● = 10, ■ = 30, × = 100, ◆ = 300 and + = 1000 trapping events per transit.

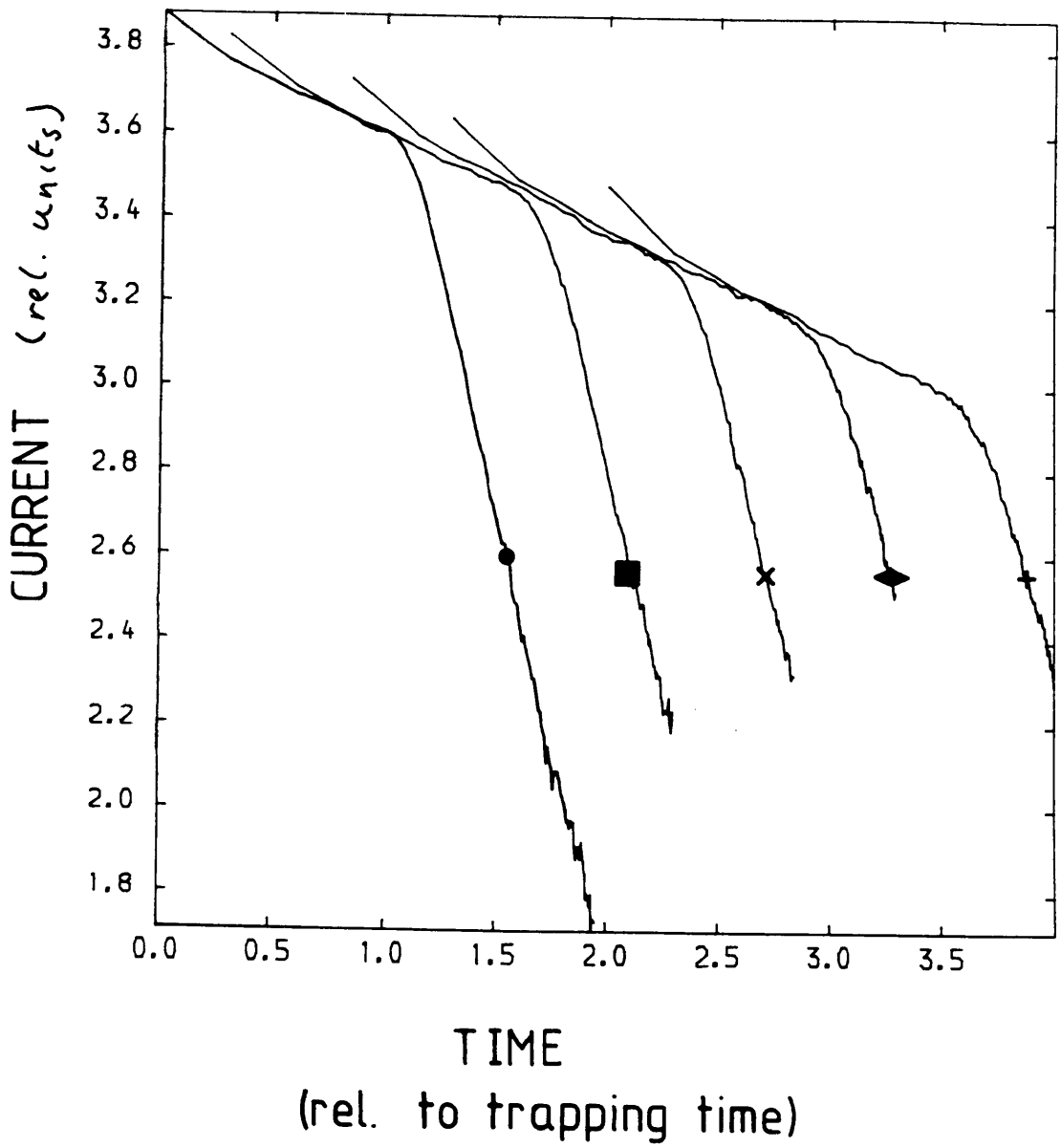

Figure 7.8 An example of the transit pulses obtained for the exponential DOS using the finite difference simulation method. ● = 10, ■ = 30, × = 100, ◆ = 300 and + = 1000 trapping events per transit.

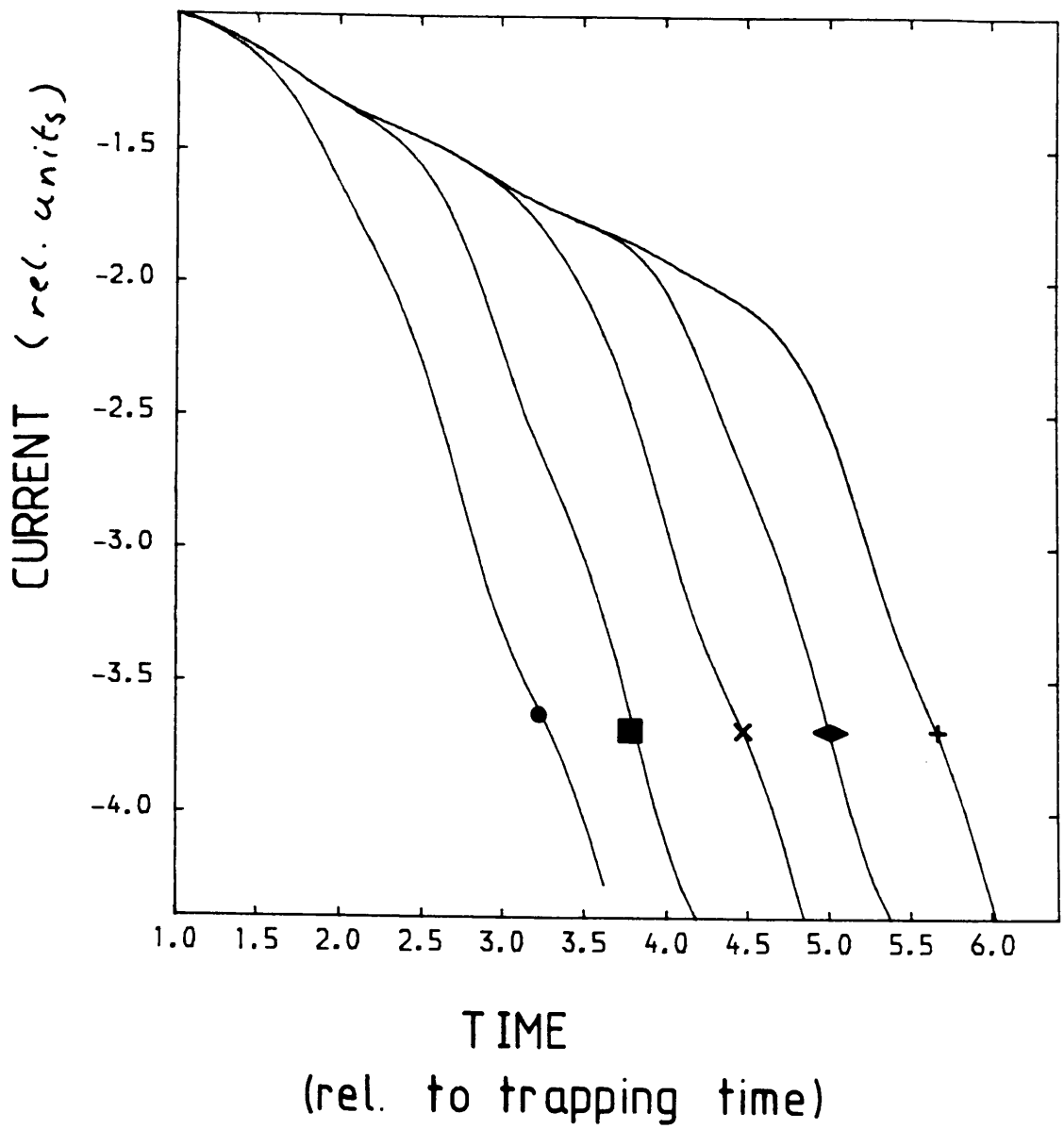

Figure 7.9 Mobility versus reciprocal temperature for the exponential distribution. ■= 10, o = 12, X = 15, ◇- 20, +- 25, ● - 30, □ - 60, O- 100, ◊ = 300 and ⊘ = 1000 trapping events per transit.

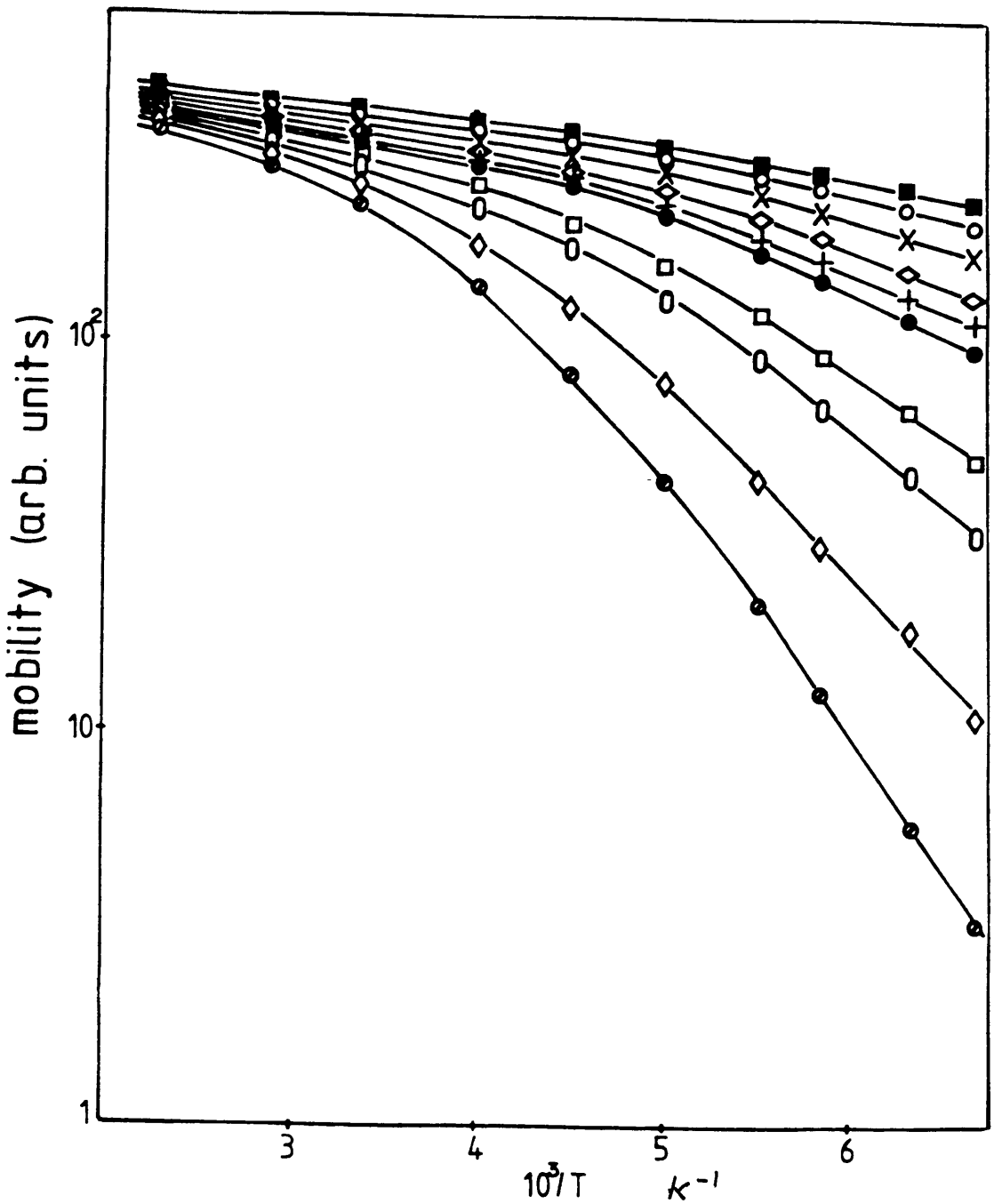

Table 2

Number of trapping events per transit.	Mobility activation energy. Monte Carlo method. eV.	Mobility activation energy. Finite difference method. eV.
10	0.029	0.0344
30	0.061	0.0553
100	0.094	0.0802
300	0.126	0.1042
1000	0.158	0.1316

Number of trapping events per transit.	Actual deepest level encountered Monte Carlo method. eV.	Level predicted by integral method. eV
10	0.042	0.056
30	0.073	0.085
100	0.102	0.115
300	0.129	0.142
1000	0.161	0.172

The DOS calculated by the TROK method and by the MA method are shown in figures 7.10 and 7.11 respectively. As the integral method takes the differential of the MA method, the DOS calculated using it would be very similar to figure 7.11 and would have an identical characteristic temperature (T_c = 331K), but a different pre-exponential factor.

Figure 7.10 The form of the DOS calculated for the exponential distribution using the TROK method.

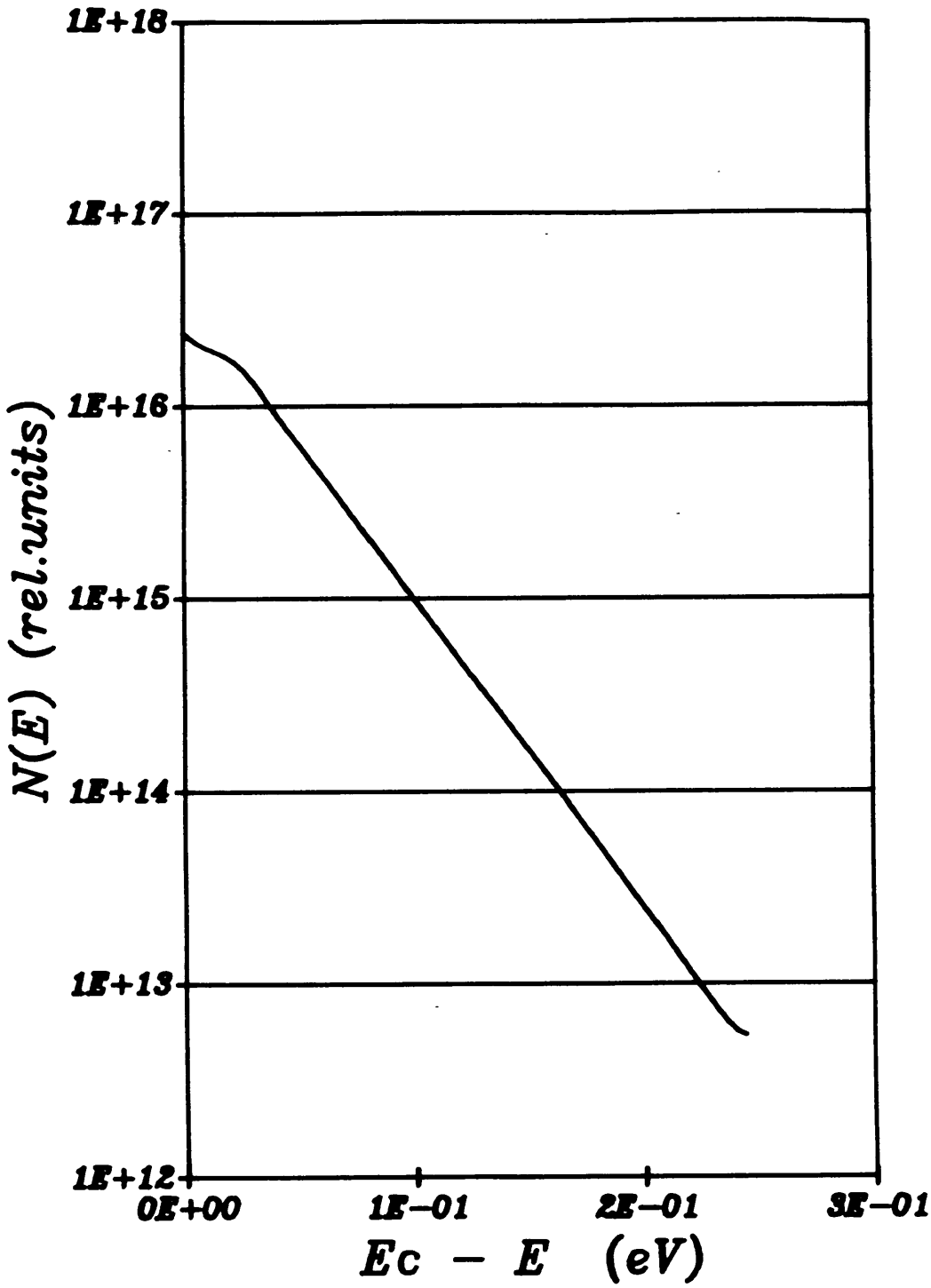

Figure 7.11 The form of the DOS calculated from simulation for the exponential distribution using the MA method.

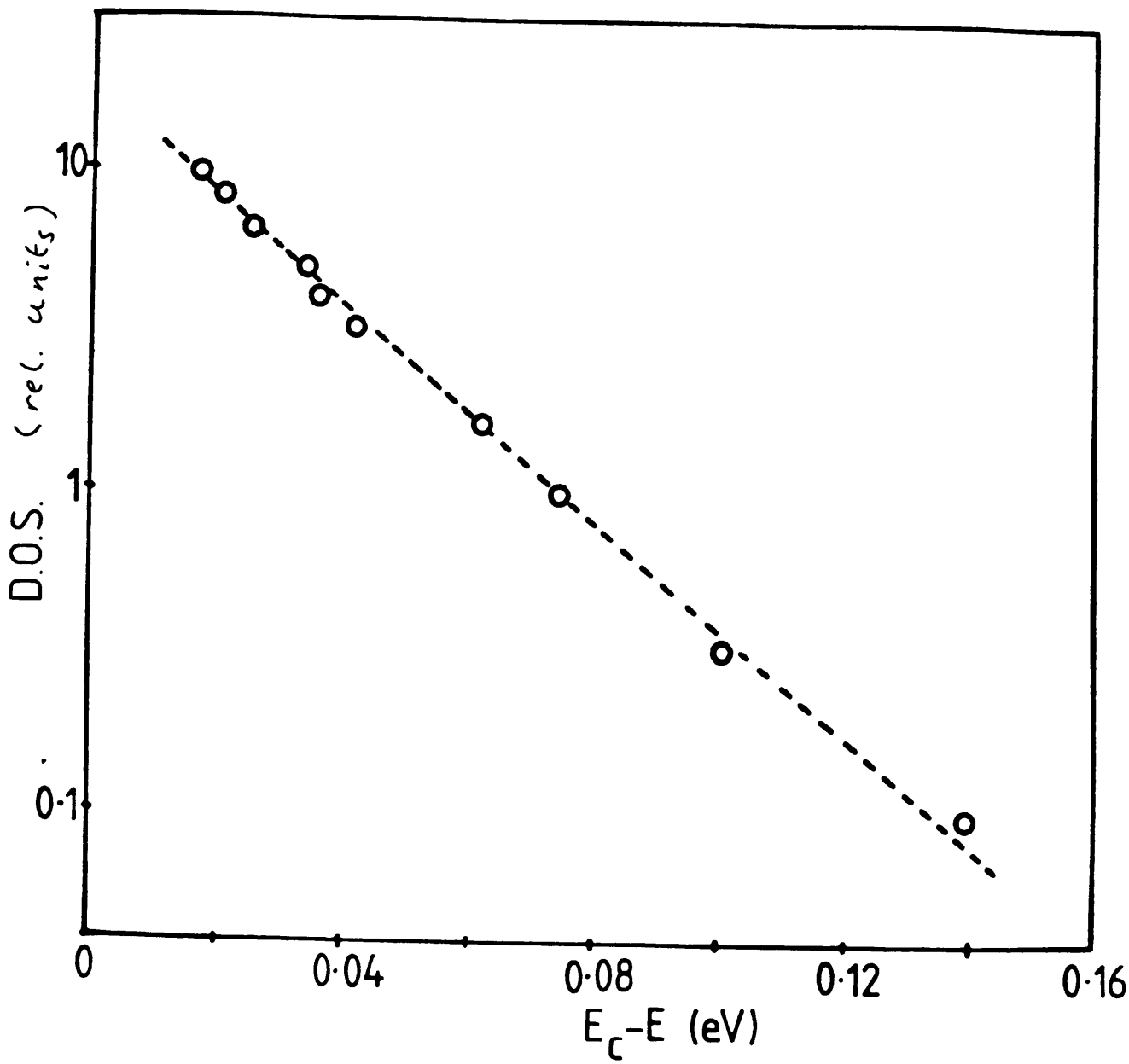

8 Experimental Methods.

8.1 Sample Details.

The measurements herein described were performed on a sample of amorphous silicon that was kindly provided by the Dundee University Amorphous Materials Group. The sample studied (a-Si (p^+-i-n^+)335) is a p^+-i-n^+ junction structure which has a bottom electrode of aluminium, a top electrode of gold, and is 5.1μm thick. The sample structure is shown in figure 8.1. Deposition conditions for the sample were :-

Substrate temperature	= 295°C
RF frequency	= 40 MHz
Deposition pressure	= 0.1 torr
Power	= 9 W

8.2 Experimental Arrangement.

The sample was mounted in an Oxford Instruments DN704 liquid nitrogen cryostat. Temperature control was provided by an Oxford Instruments digital temperature controller DTC2. A charge packet was created in the sample via illumination through the side window of the cryostat. Laser illumination was provided by a LSI Laser Science Inc. VSL/337 pulsed dye laser unit. This laser unit is a two stage system, the first stage of which produces UV pulses, which are then converted into pulses of the required wavelength by a dye stage. The dye used

Figure 8.1 The sample structure.

Sample Details.

a-Si (p^+-i-n^+) 335
d = 5.1 μm
Frequency = 40MHz
Power = 9w
T = 295 °C
Pressure = 0.1 torr

Sample Structure.

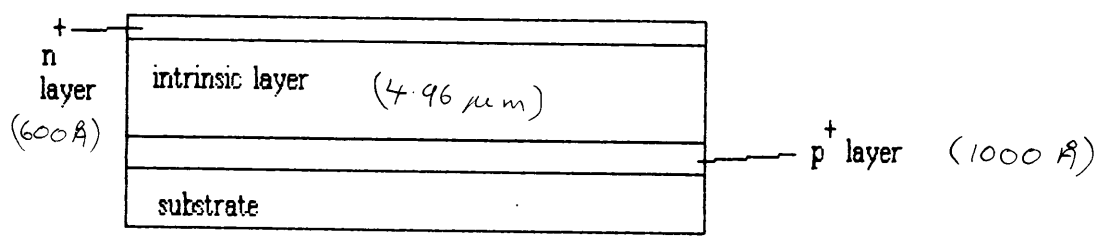

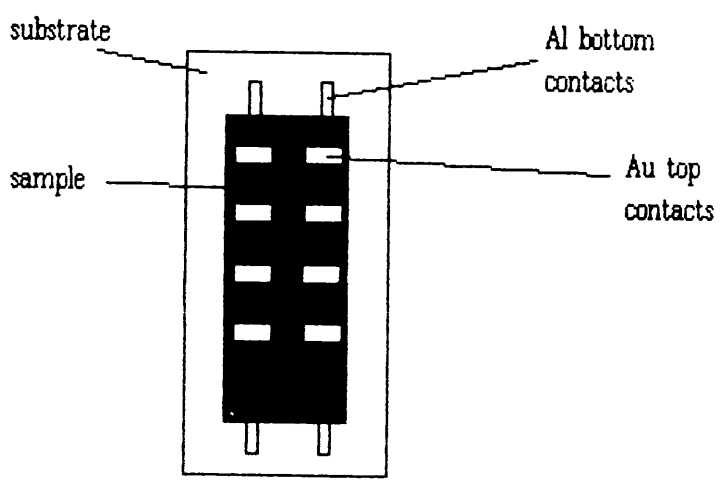

Figure 8.2 Experimental arrangement used in the 'Time of flight' experiment

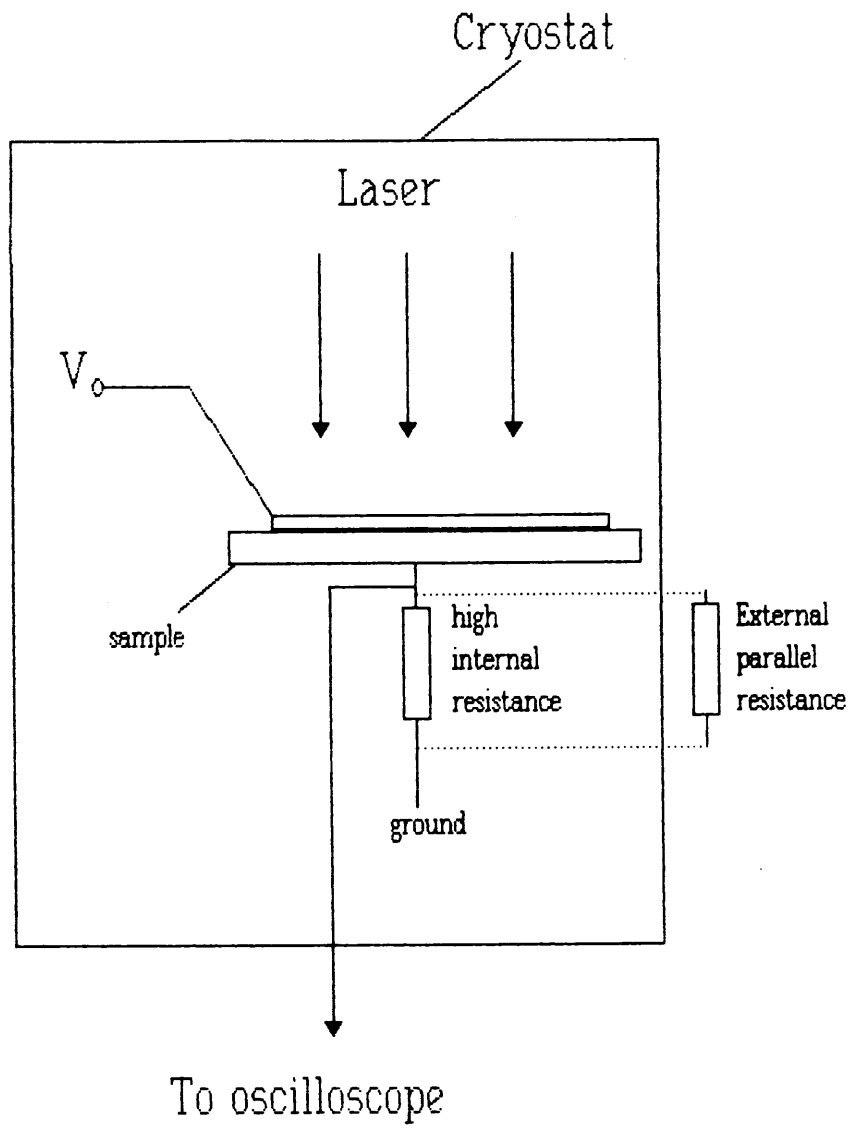

in this experiment was Rhodamin 6G which produces a final pulse of wavelength 580μm and of measured width $\leq$ 5ns. A pulsed field was set up across the sample using an Advance Instruments pulse generator PG 52, which also triggered the laser. An opto-isolator was used to isolate the laser unit from the rest of the measurement system, this being necessary to prevent 'ringing' on the measured signal. Measurement of the transient current signal was accomplished by sampling the voltage developed across a resistor mounted between the sample and ground (see figure 8.2). Since the signal voltage was frequently very low amplification was needed. The amplifiers used were type 5539 ultra fast operational amplifiers with <10 ns rise time at gain of 20. Both the amplifiers and the opto-isolator were constructed in house by the author. After amplification (if needed) the transient pulse was captured on a Philips PM 3311 digital storage oscilloscope. This oscilloscope has a time resolution of 8 nano seconds for non repetitive signals. The oscilloscope was triggered from the laser pulse via a fast photodiode. Data were transfered from the oscilloscope, via an IEEE 488 interface, into a Gemini Microcomputer. All of the software used by the Gemini was written by the author in Microsoft FORTRAN 80. The control software allowed for :-

averaging of multiple pulses
calculation of the integrated charge
a check that the CV limitation had not been exceeded
storage and retrieval of pulses
logarithmic/linear displays of the pulse on the monitor
logarithmic/linear plots of the pulse on paper.

Figure 8.3 Schematic of the experimental system used.

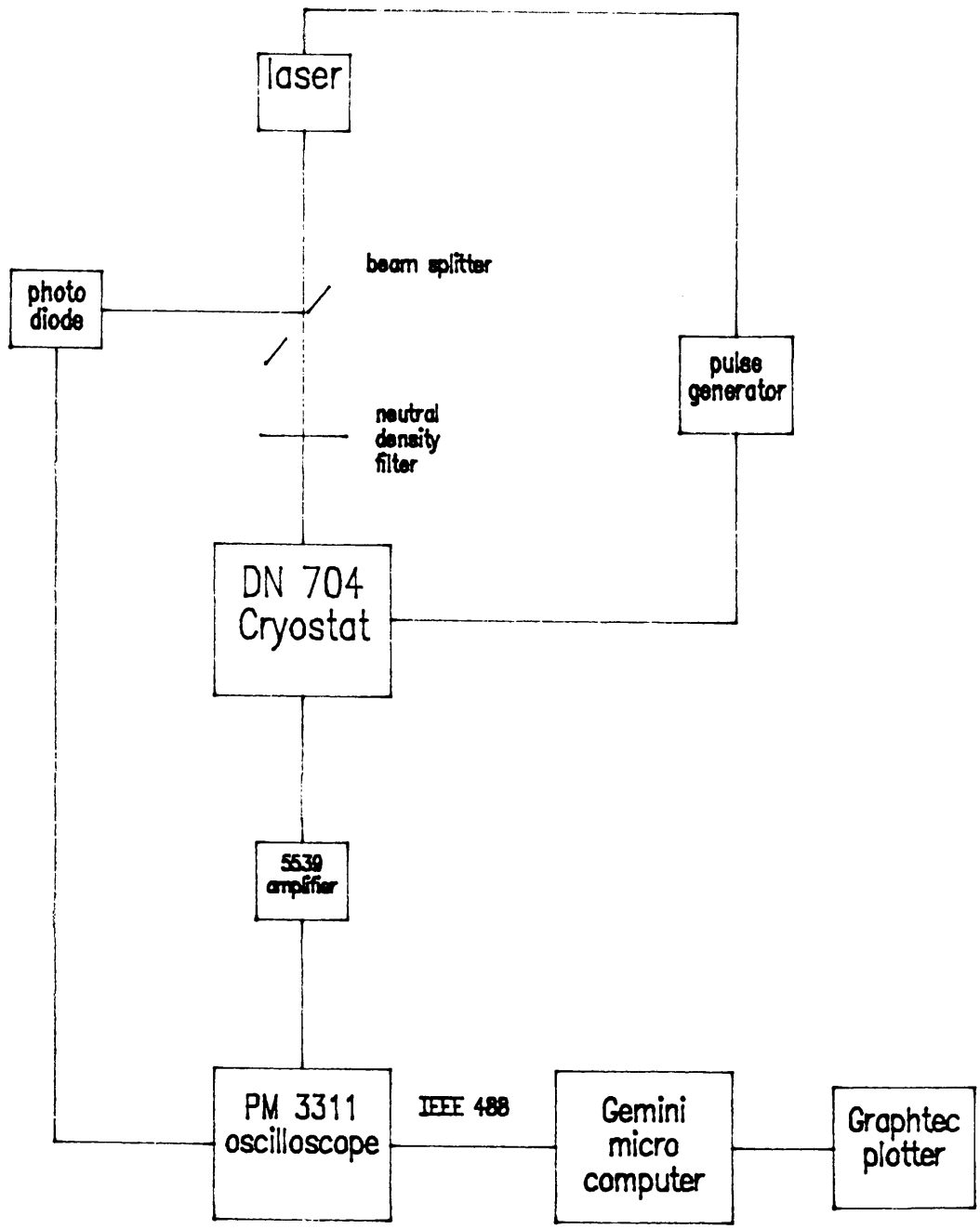

The final output was drawn on a graphtec MP 1000 plotter. Final computional analysis was performed on both a Dec-Vax 8530 main frame computer system and on an Amstrad PC1512 personal computer fitted with 20 Mbyte hard card and 8087 co-processor. The full experimental layout is shown in figure 8.3.

8.3 Experimental Procedures.

Experimental procedures were as follows. Firstly as the sample was not in a light tight enclosure a black out was established. This was necessary as it was found that any background illumination could have a marked effect on the recorded transient, especially at low (<200K) temperatures.

Measurements were taken over the temperature range 106 to 295K. Once the sample temperature was stable at the required value a series of readings for different fields was taken. Readings were taken whilst a pulsed reversed bias field (0.49 to 49 $kVcm^{-1}$) was applied. A pulsed field was used so as to prevent all of the field being dropped across the electrodes and the junctions as would have been the case if a steady field had been employed. This pulse was always set to be of slightly longer duration than the transit time. The laser was triggered after a short delay (typically $\simeq$ 80 μs) which allowed for the rise time of the field pulse across the sample. This event was detected by the photodiode which in turn triggered the oscilloscope. The oscilloscope possesses a pre-trigger facility whereby the input immediately prior to the trigger pulse can be observed. This was used to examine the start of the transit pulse and

thereby allow a base line to be determined.

As soon as the oscilloscope had been triggered it signaled the computer system which then removed the acquired data. The scope was then set to acquire a further sample so that signal averaging procedures could be used. The computer system used did not have any facility whereby it could trigger the pulse generator, so to allow automated capture of a large number of results the pulse generator was left to free run with a very low repetition rate (of the order of one pulse every ten seconds or more). A low repetion rate for pulse collection was used so as to allow any trapped charge still in the sample from the previous excitation pulse time to escape.

A sufficient number of transit pulses (up to 200 depending on prevailing conditions)were taken to allow noise reduction by signal averaging techniques. This procedure is especially significant at low temperatures where the pulses have a very low amplitude and so tend to be swamped by noise. Once a reasonable transit pulse had been assembled, the data were stored on floppy disc and the pulse was plotted on logarithmic axes. The plot also contains all of the data (temperature field etc) relevant to the measurement (an example of the output produced can be seen in figure 8.4).

It should be noted that the measurement system automatically checked the amount of collected charge, by numerical integration of the current pulse, so as to ensure that the carrier packet was never sufficiently large that it would cause a significant perturbation of the applied field. The criterion used for this check was that the

Figure 8.4 An example of the output produced by the computerized 'Time of Flight' measurement system.

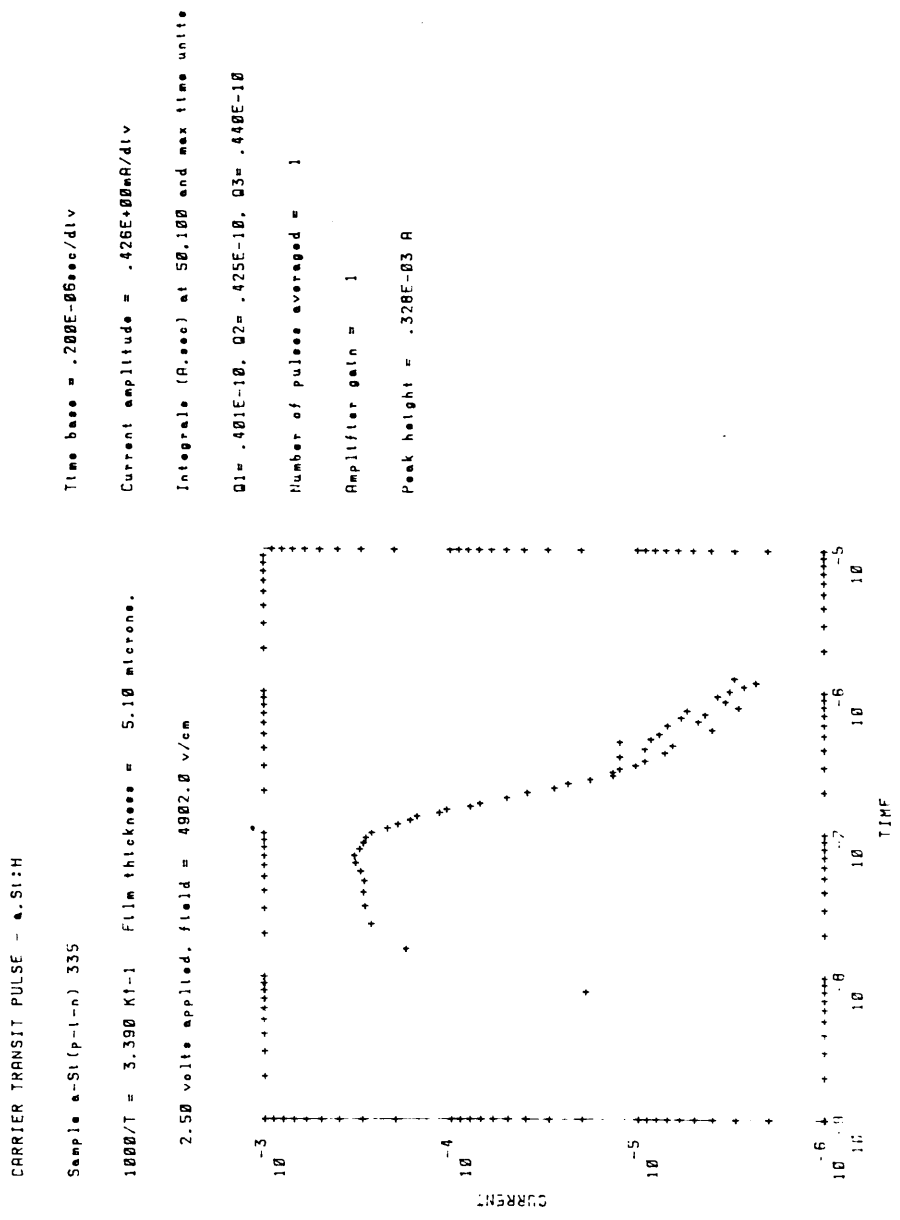

Figure 8.5 An example showing several pulses combined to form one composite pulses so as to allow the determination of the transit time. Measurements taken at 180K, fields are ● = 9.8, ■ = 19.6, × = 29.4, ◆ = 39.2 and + 49.0 $kVcm^{-1}$.

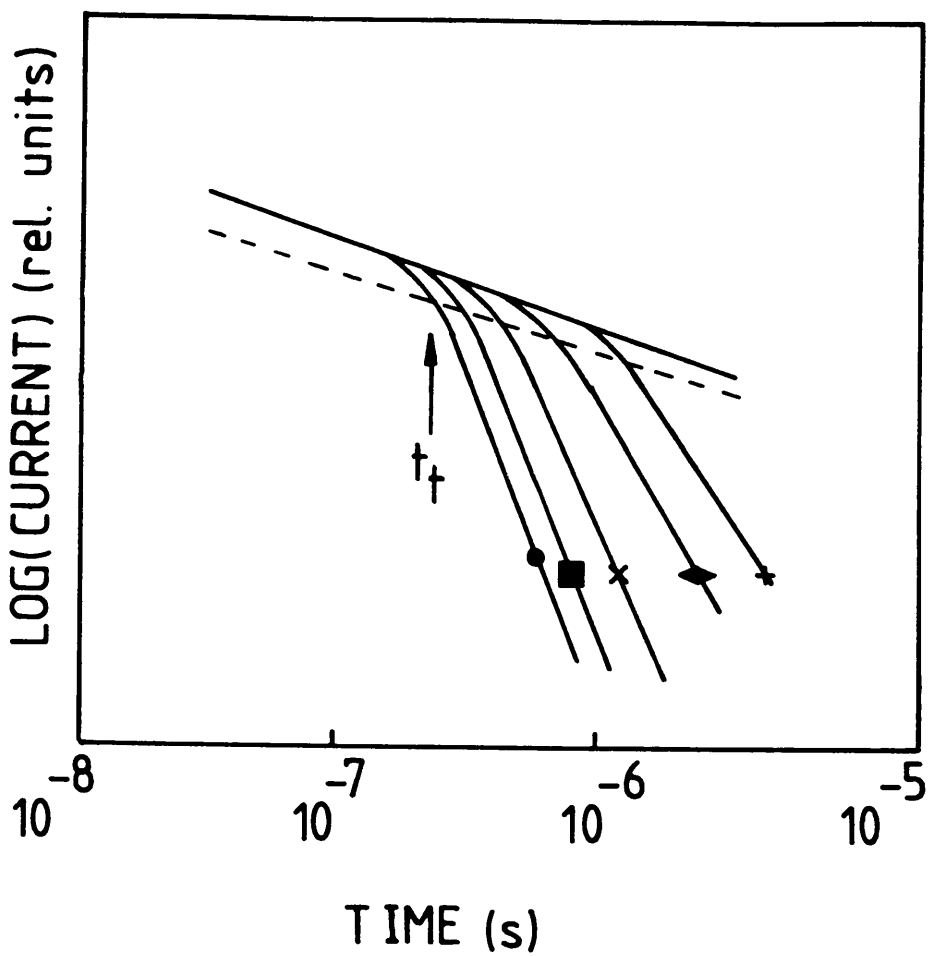

integrated charge should never exceed 20% of the CV product for the sample. The amount of charge created in the sample was controlled by mounting one or more neutral density filters between the sample and the laser.

Once all of the data for a certain temperature had been collected a composite pulse of the type orginally used by Marshall and Allen was constructed by hand. This composite pulse shows the extraction free transit with each of the individual pulses 'peeling' away from it (an example is shown in figure 8.5). From this composite plot the transit time of the fastest 20% of the carriers for each pulse was identified. In line with the critrion used by Marshall Street and Thompson [1], this time, $t_{20\%}$, was defined to be the point at which the pulse had fallen to 80% of its extraction free value. It should be noted that the use of the 20% through point will lead to shorter values for the transit time and hence higher mobilities than would the more usual 50% through point.

9 Experimental Results.

In accordance with the analytical method outlined by Marshall, Berkin and Main [46] all of the transit times herein quoted are the time for twenty percent of the carriers to cross the sample. This will result in the transit times appearing shorter than the 'fifty percent' results often quoted. For the same reason the calculated drift mobility may also be slightly larger than that obtained in other studies.

9.1 Measurements Taken.

Details of the sample used are given in the preceeding chapter. Transient curves were recorded over the temperature range 106K - 295K. At each temperature chosen the field was varied between 0.49-49.0 $kVcm^{-2}$, where possible. It proved impossible to obtain readings for the lower fields at lower temperatures because the signal amplitude becomes so small that it is not possible to distingush it from the noise. Results for higher fields at higher temperatures also could not be obtained as the transit was complete in a time that was shorter than that resolveable by the equipment used.. A complete list of the results obtained is shown in table 1. Examples of the type of results obtained experimentally are shown in figures 9.1 and 9.2.

Figure 9.1 A sample of the transit pulses obtained at high temperatures.

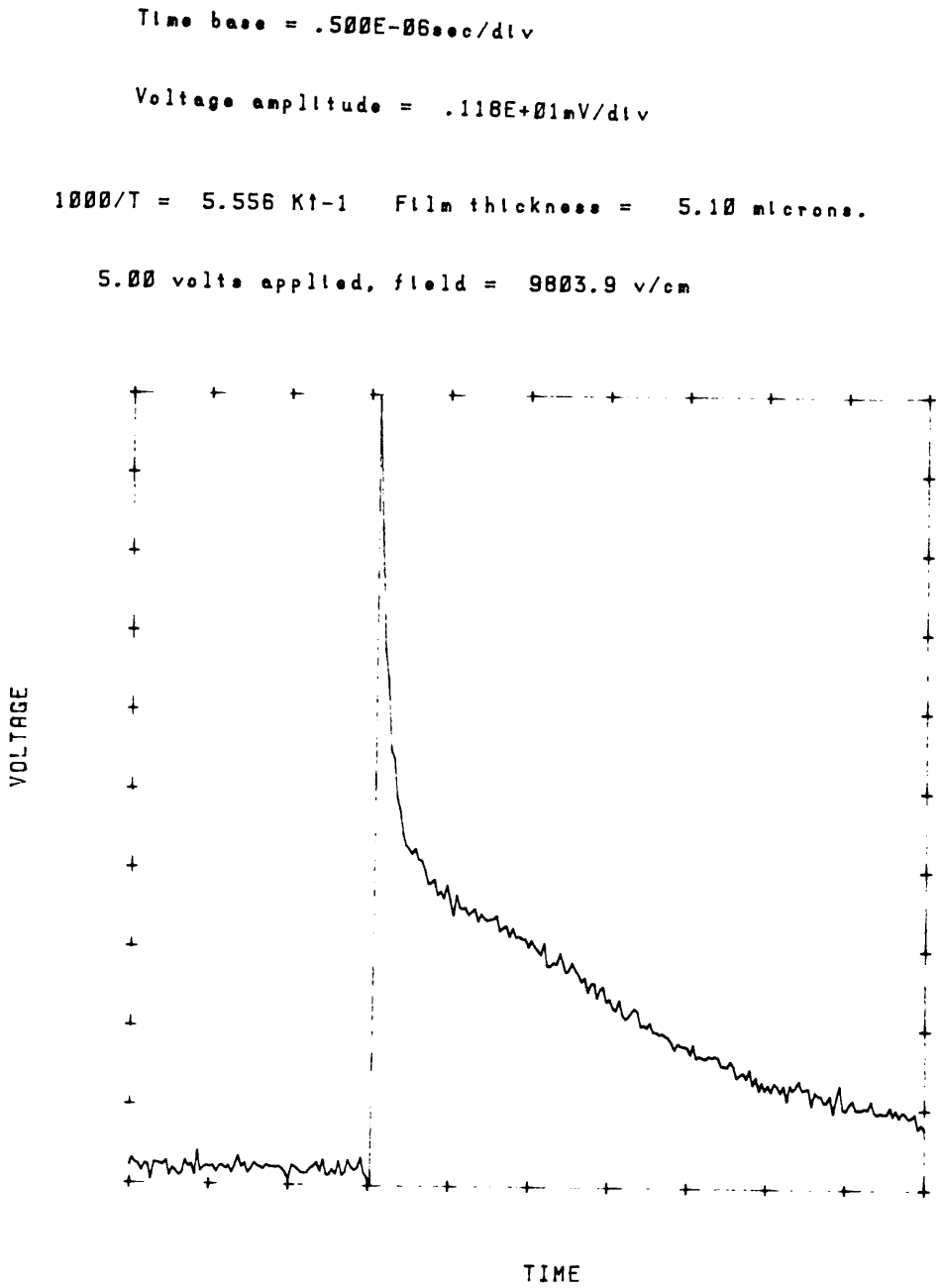

Figure 9.2 A sample of the transit pulses obtained at low temperatures.

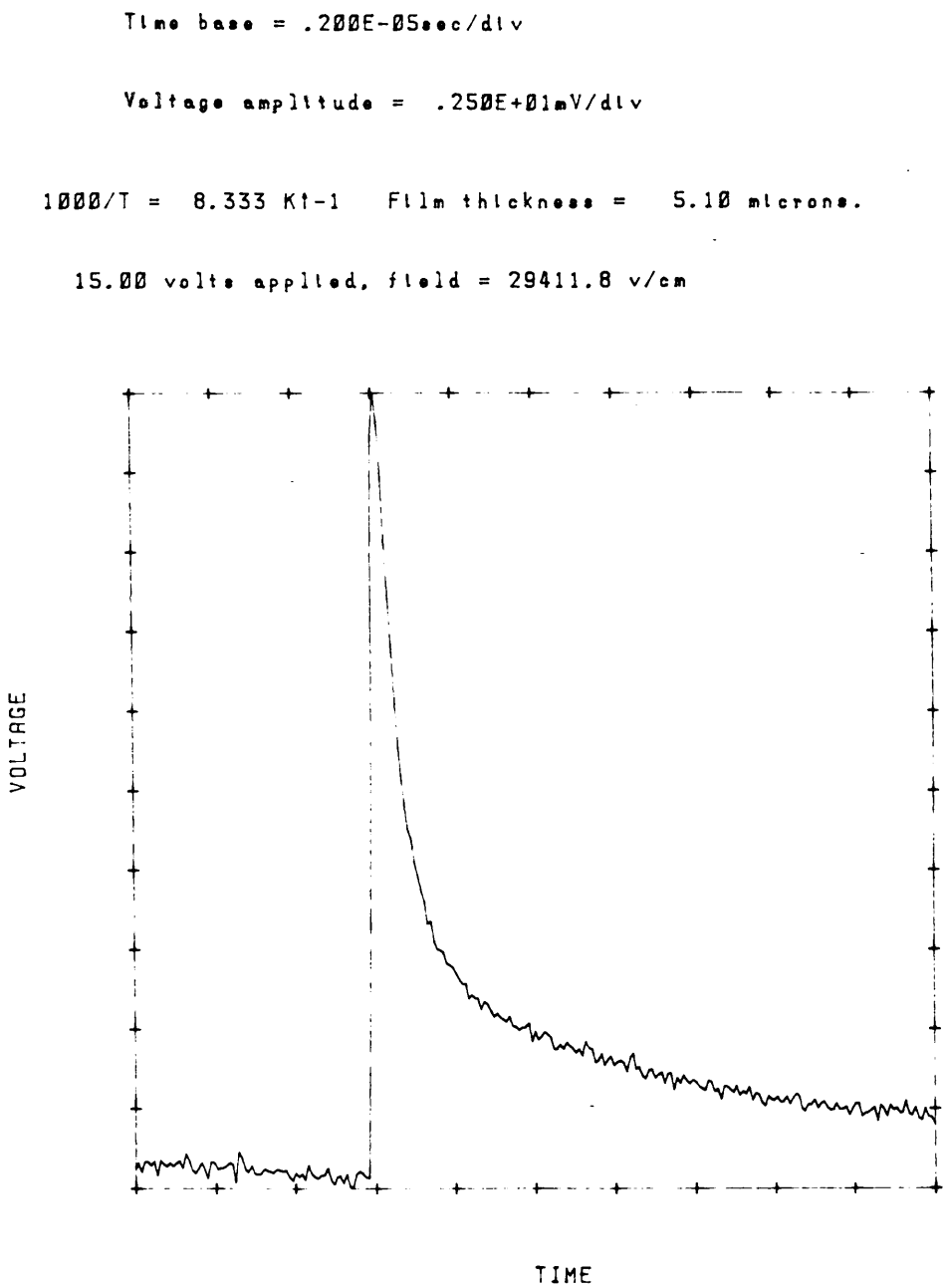

Table 1

20% transit times for a-Si:H at the temperatures and fields shown.

Temp (K)	106	120	132	145	157	180	250	295
Field $kVcm^{-1}$								
0.49	*	*	*	*	3.1e-4	4.6e-5	8.1e-7	4.2e-7
0.98	*	*	*	5.3e-4	2.4e-4	2.1e-5	6.3e-7	3.5e-7
1.96	*	*	*	2.8e-4	7.1e-5	1.2e-5	4.3e-7	2.3e-7
2.94	*	*	4.6e-4	1.7e-4	4.5e-5	7.0e-6	3.4e-7	1.6e-7
4.90	*	7.2e-4	2.4e-4	*	2.3e-5	3.0e-6	2.8e-7	1.1e-7
9.80	1.1e-3	3.5e-4	1.1e-4	1.9e-5	7.6e-6	8.9e-7	*	*
19.6	4.7e-4	1.1e-4	2.7e-5	7.3e-6	2.5e-6	5.1e-7	*	*
29.4	2.8e-4	4.0e-5	1.0e-5	3.3e-6	1.3e-6	3.3e-7	*	*
39.2	1.8e-4	3.0e-5	6.0e-6	2.0e-6	7.8e-7	2.3e-7	*	*
49.0	1.2e-4	1.6e-6	4.0e-6	1.2e-6	4.6e-7	1.8e-7	*	*

Table 2

20% transit time activation energies for the indicated fields.

Field $kVcm^{-1}$	Activation Energy eV
49.0	0.1478
39.2	0.1508
29.4	0.1519
19.6	0.1542
9.80	0.1598
4.90	0.1615
2.94	0.1784
1.96	0.1927
0.98	0.2060
0.49	0.2175

Figure 9.3 Transit time versus reciprocal temperature at fields of • = 49.0, + = 39.2, ✱ = 29.4, O = 19.6, × = 9.8, — = 4.9, · = 2.94, + = 1.96, ✱ = 0.98 and O = 0.49 $kVcm^{-1}$.

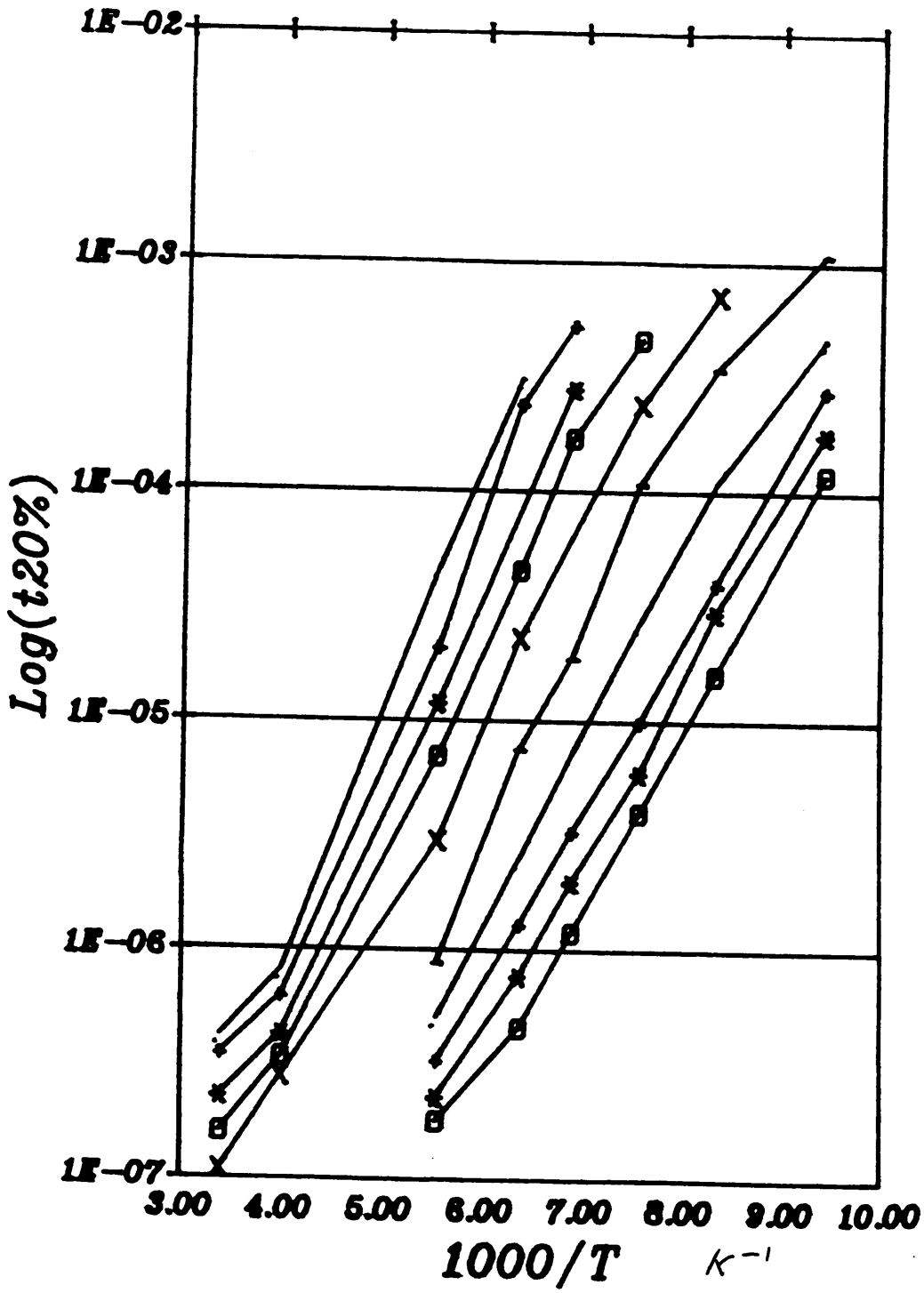

Figure 9.4 Carrier mobility versus reciprocal temperature at fields of • = 49.0, + = 39.2, ✱ = 29.4, O = 19.6, × = 9.8, – – = 4.9, ·– = 2.94, + = 1.96, ✱ = 0.98 and O = 0.49 $kVcm^{-2}$.

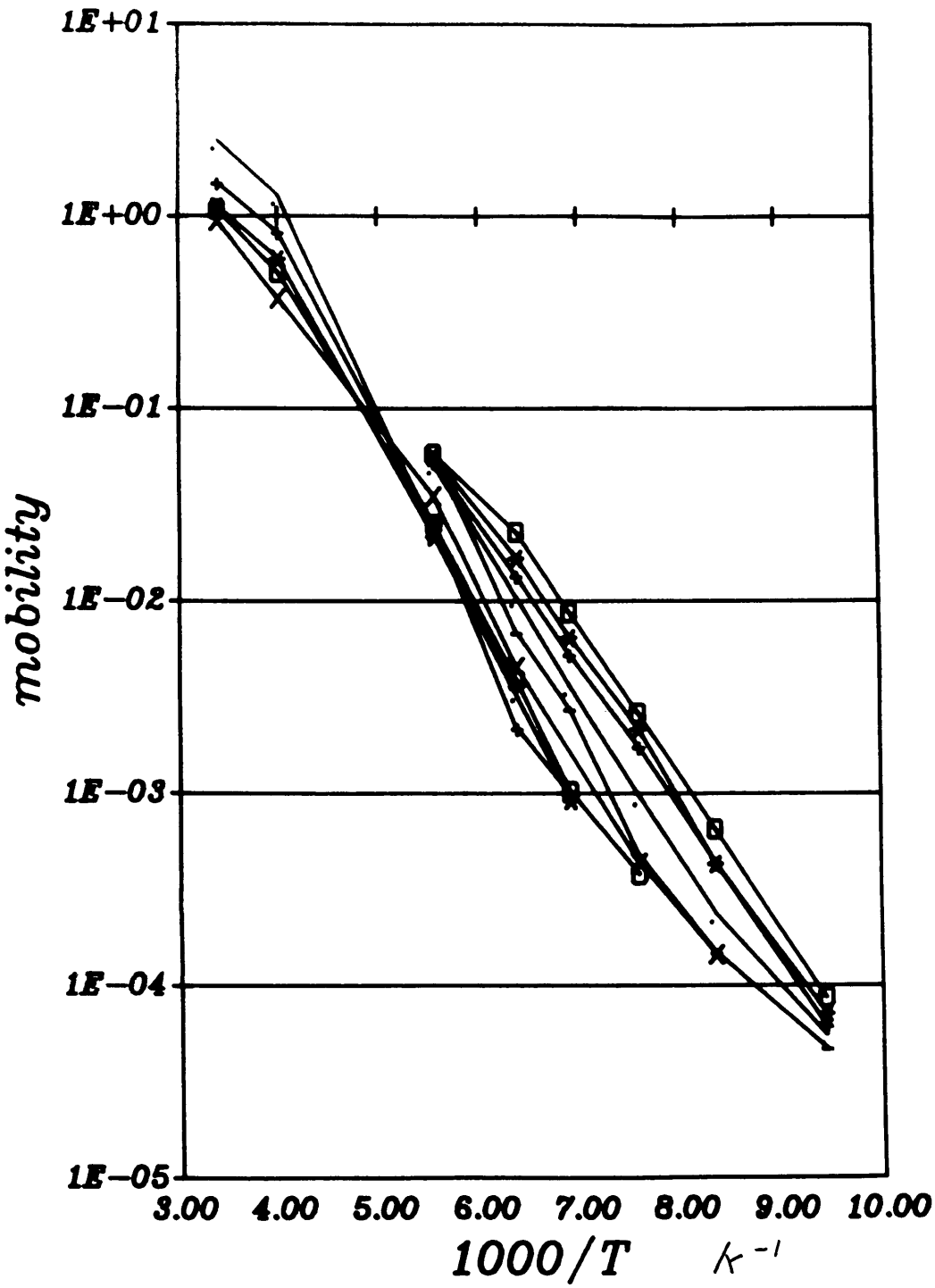

Figures 9.3 and 9.4 show respectively the transit times and calculated mobilities at several constant applied fields versus reciprocal temperature. It is noted that the low field mobility results behave in an unexpected manner, crossing over results for other fields. It is believed that this is due to the presence of depletion layers and hence built in fields at the p^+-i and i-n^+ interfaces. This will be considered in more detail later.

The lower temperature results were used to calculate the mobility activation energy for each of the applied fields. This value was found from the low temperature results because, as the temperature increases, the curves tend to deviate from a well defined activated form toward a constant value, which is presumably the extended state mobility. The values determined for the mobility activation energy are given in table 2.

9.2 Analysis of Results.

Figure 9.5 shows a plot of the applied field versus the calculated activation energy. The curve shown is a free-hand best fit to the data points. The low field results shown on this curve are affected by the presence of a built in field. If, for the moment, the low field results (fields below 4.9 $kVcm^{-1}$) are ignored then the data can be re-plotted as in figure 9.6. The two curves shown on this figure are a best-fit polynomial (degree 2) and a best-fit exponential. As can be seen the polynomial is a slightly better fit than the exponential. The details of this polynomial are as follows (assuming $N_c = 10^{21}\ cm^{-3}$):-

Figure 9.5 Applied field versus activation energy.

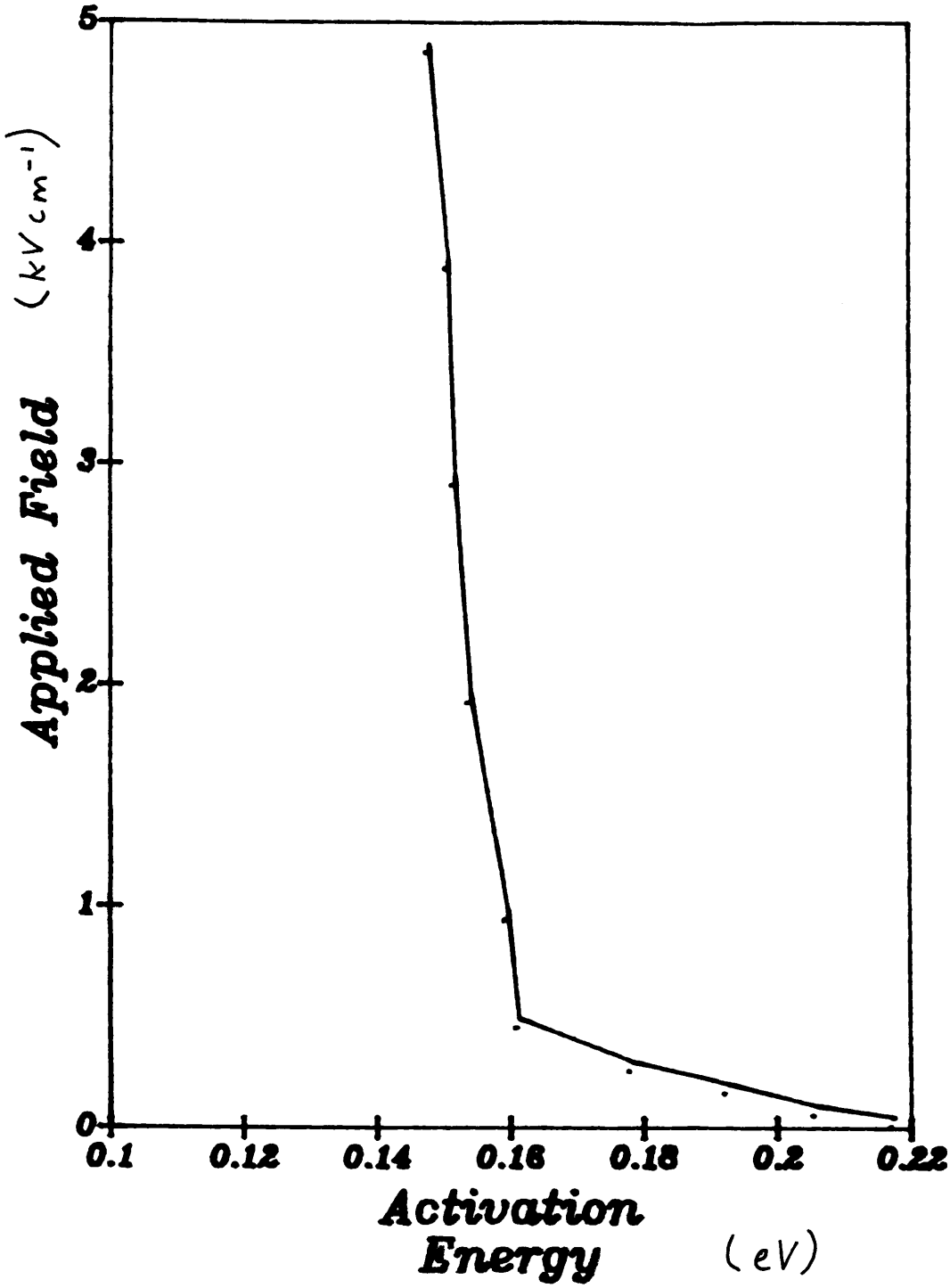

Figure 9.6 Applied field versus activation energy excluding the low field results. Also shown are the best exponential and the best polynomial fits to the data.

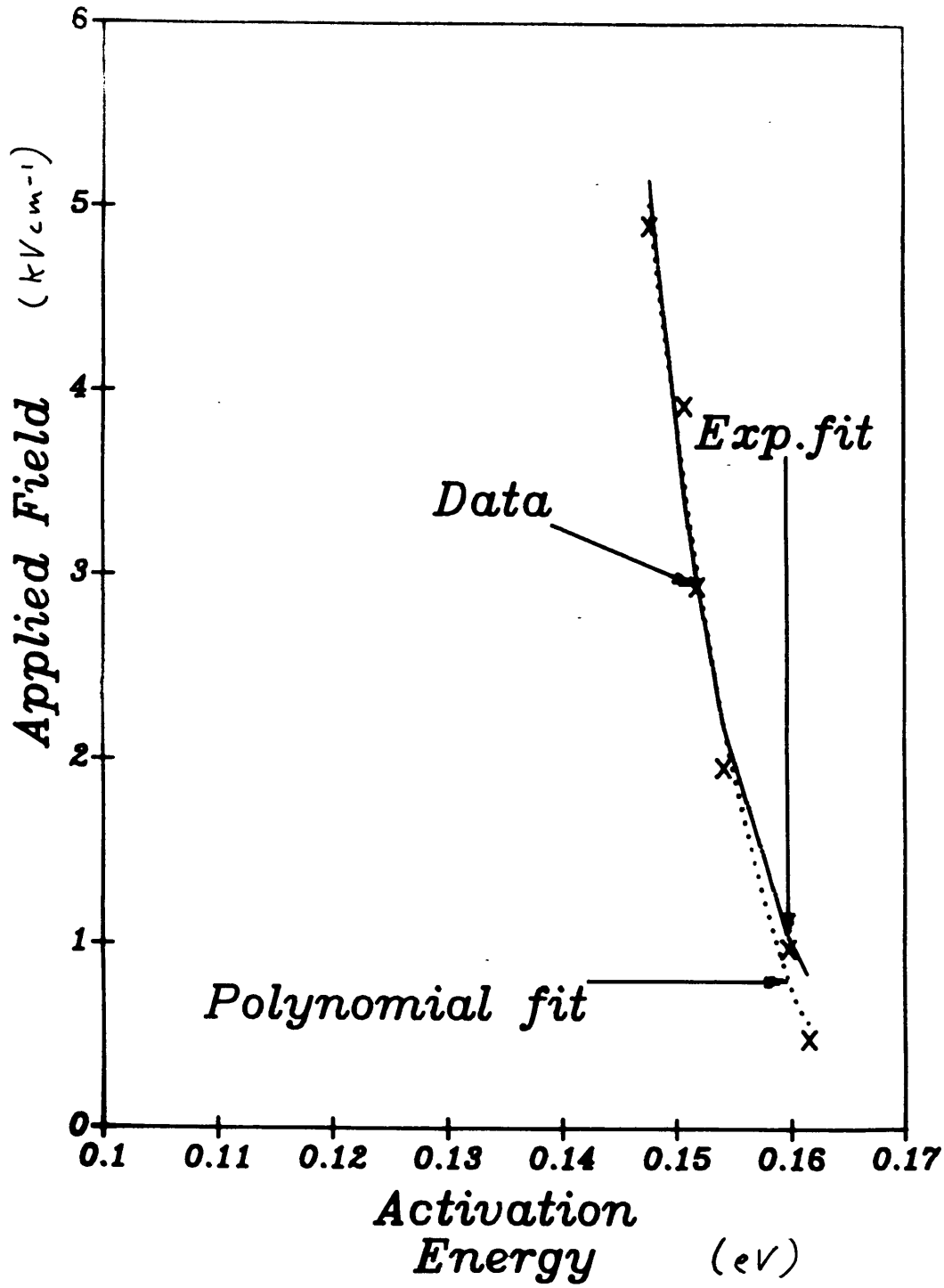

$$N_{rel}(E) = 158639 \quad E^2 - 52306 \quad E + 4315 \qquad (9.1)$$

This gives rise to a functional description for the density of states (from equation 4.6) of :-

$$N_{rel}(E) = 317278 \quad E - 52306 \qquad (9.2)$$

This form for the DOS is shown in figure 9.7. The cut-off point for this distribution is at 0.165 eV.

The details of the exponential fit to the data are :-

$$N_{rel}(E) = 5.2x10^{9}\exp\left[\frac{-E}{kT_c}\right] \qquad (9.3)$$

where T_c = characteristic temperature = 93K.

This gives a density of states function described by :-

$$N_{rel}(E) = 6.45x10^{11}\exp\left[\frac{-E}{kT_c}\right] \qquad (9.4)$$

Figure 9.8 shows this exponential distribution. It is noted that the calculated value for T_c may be inconsistent with the occurence of the observed anomalous dispersive transport at temperatures below $\simeq$ 150K. This anomaly is discussed in detail in chapter 10.

The presence within the p^+-i-n^+ diode structure of depletion

Figure 9.7 A linear density of states distribution function.

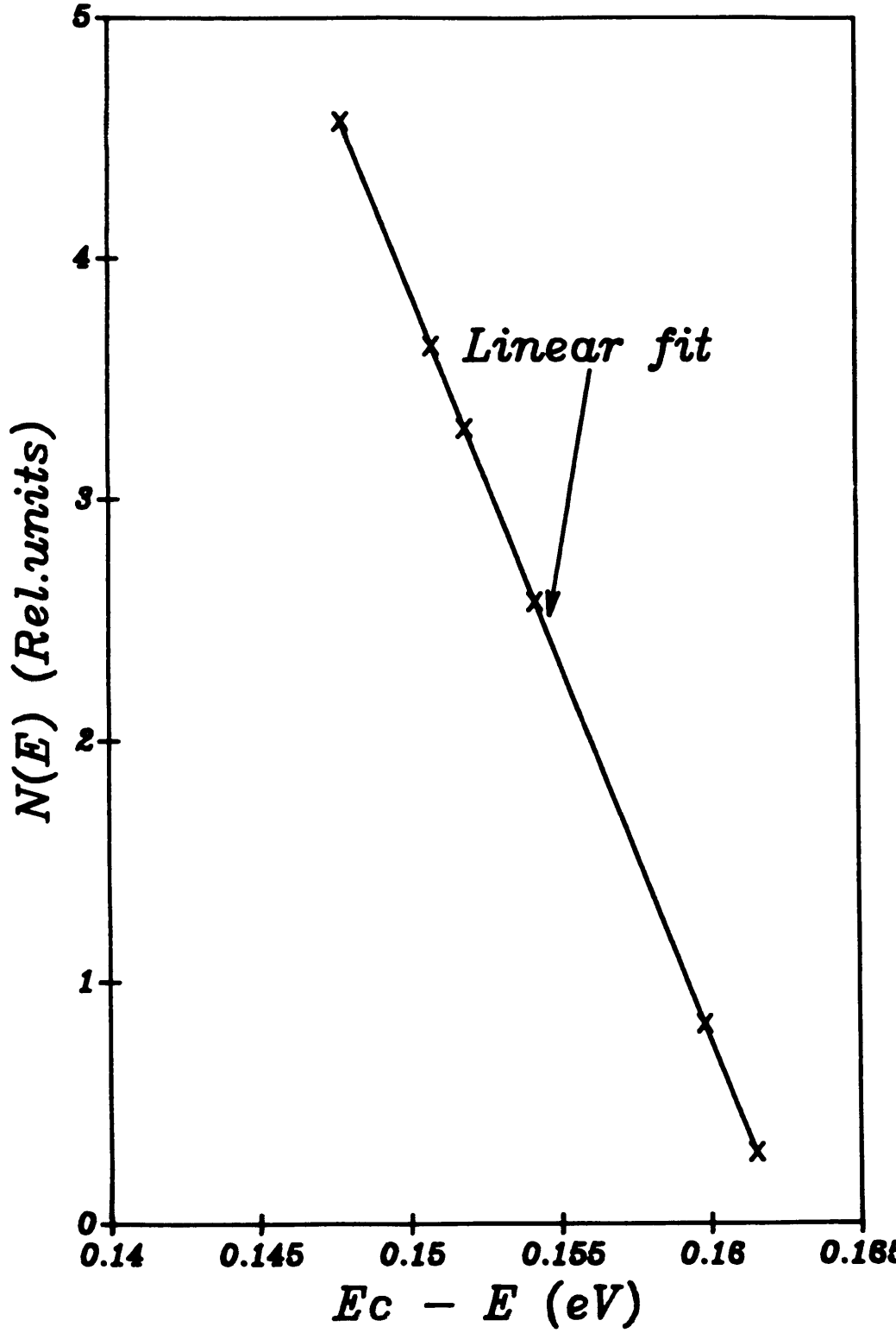

Figure 9.8 An exponential density of states distribution function.

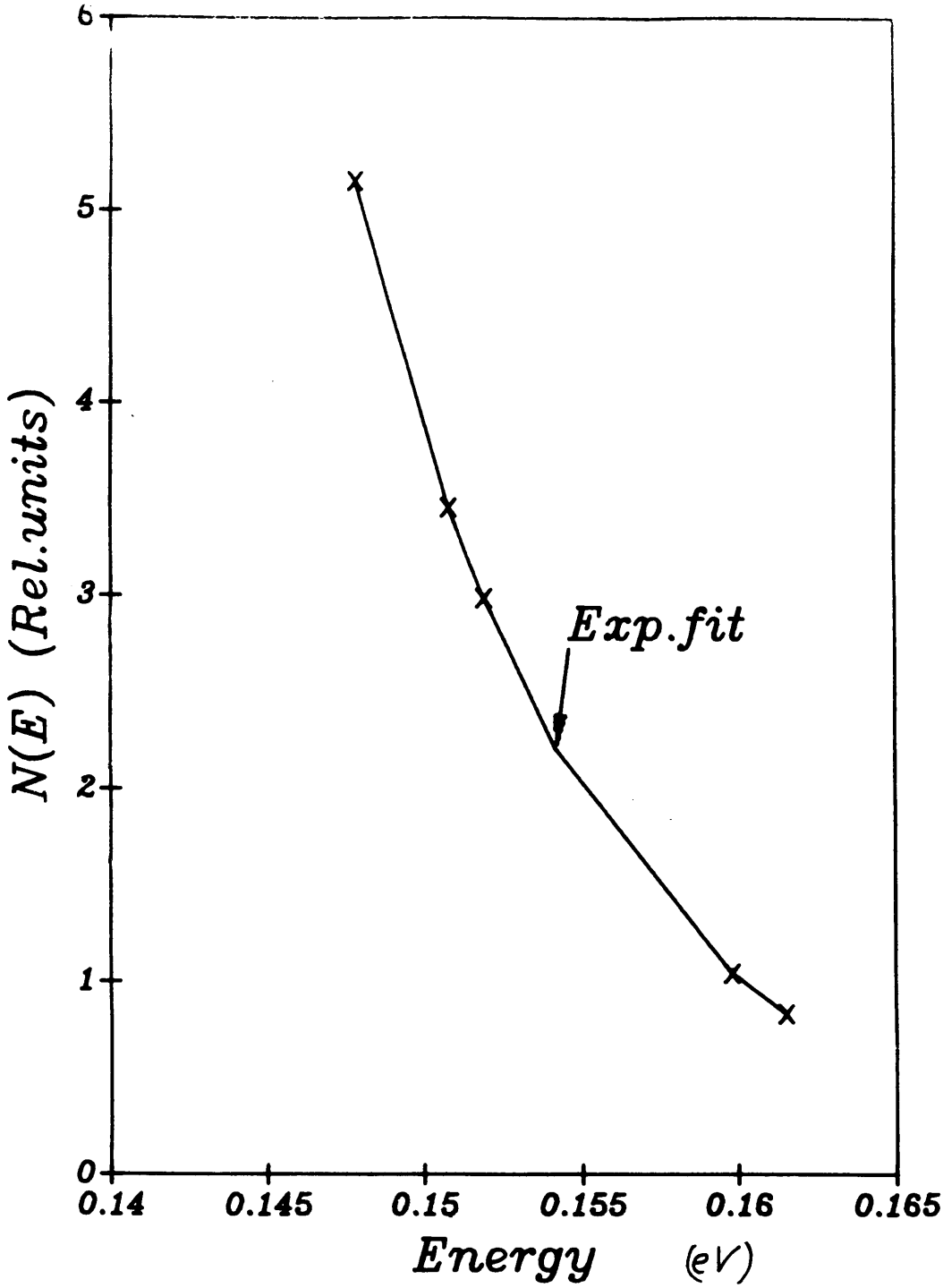

layers causes major problems with the analysis of the results. Typically the depletion layer thicknesses in a p^+-i-n^+ junction is expected to be of the order of 1μm in the i region and the contact potential to be up to 0.5 volt. Therefore it is not possible to simply correct for these built in fields by adding them to the applied field [48] as they will not be uniform over the entire thickness (5.1μm) of the sample. Schottky barrier structures used in earlier studies possess lower contact potentials and built in fields and so the perturbation of the applied field is reduced. Unfortunately such a sample was not available for study so the diode structure had to be used.

The possible effects caused by the presence of a built in field can be assessed via computer simulation using the finite difference method. Figure 9.9 shows simulated transients both with and without built-in fields. The simulation of the sample with the built in field used a value of 0.35 v built in voltage at each junction and a value of 1.0 μm of the depletion layer width. These values are expected to be typical of this type of interface. This clearly shows that the presence of these depletion layers within the sample will alter the transit pulse shapes markedly. Mobility versus reciprocal temperature curves for these simulated data are shown in figure 9.10. These figures clearly show that the presence of the built in fields at the junction interfaces can lead to a cross over of the mobility curves as was observed experimentally.

Figure 9.9 Simulated transits for a linear distribution of trapping states. ● - 500, ■ - 1000, × - 2000, ◆ - 3000 and + - 5000 Vcm^{-1}.

a) without built in fields

b) with built in fields.

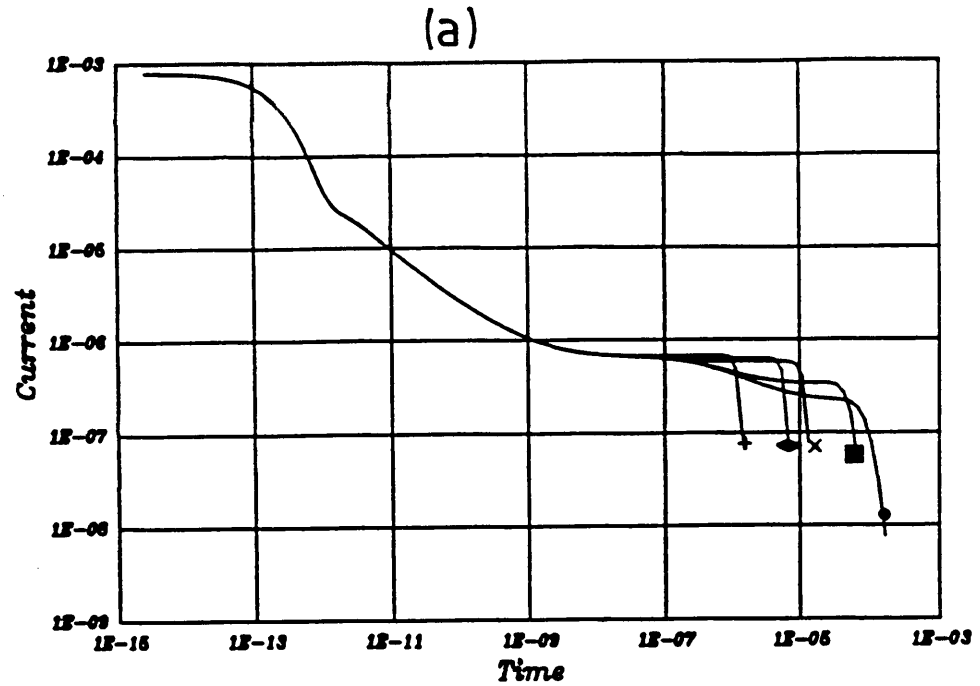

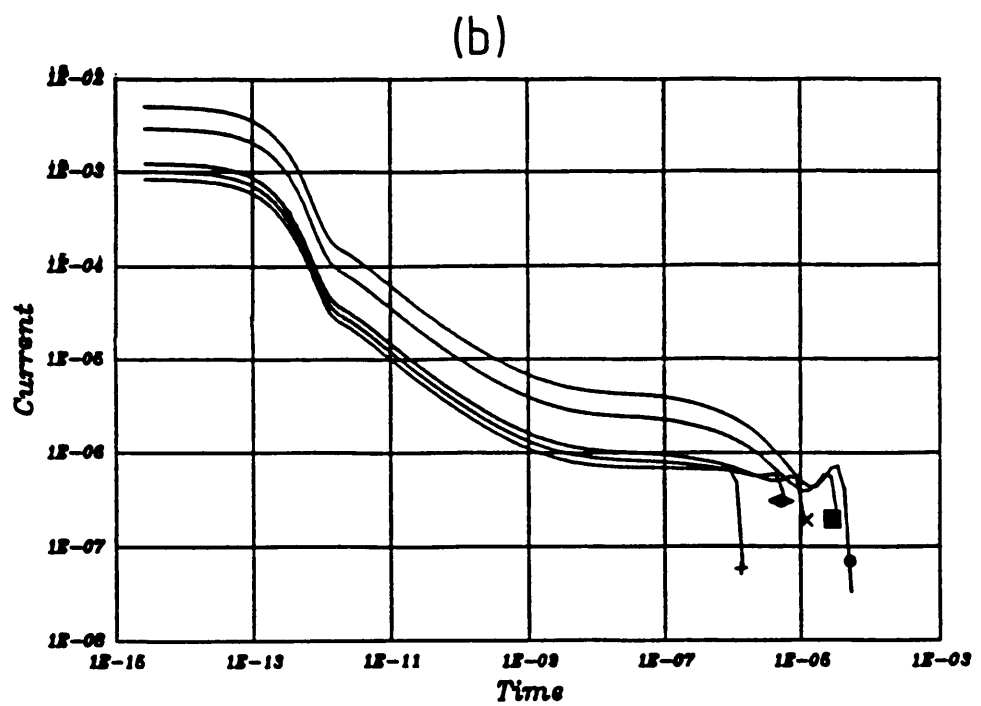

Figure 9.10 Mobility versus reciprocal temperature for the simulated pulses. This shows that the inclusion of built in fields can lead to the mobility curves crossing one another. + = 500, ◆ = 1000, × = 2000, ■ = 3000 and ● = 5000 Vcm^{-1}.

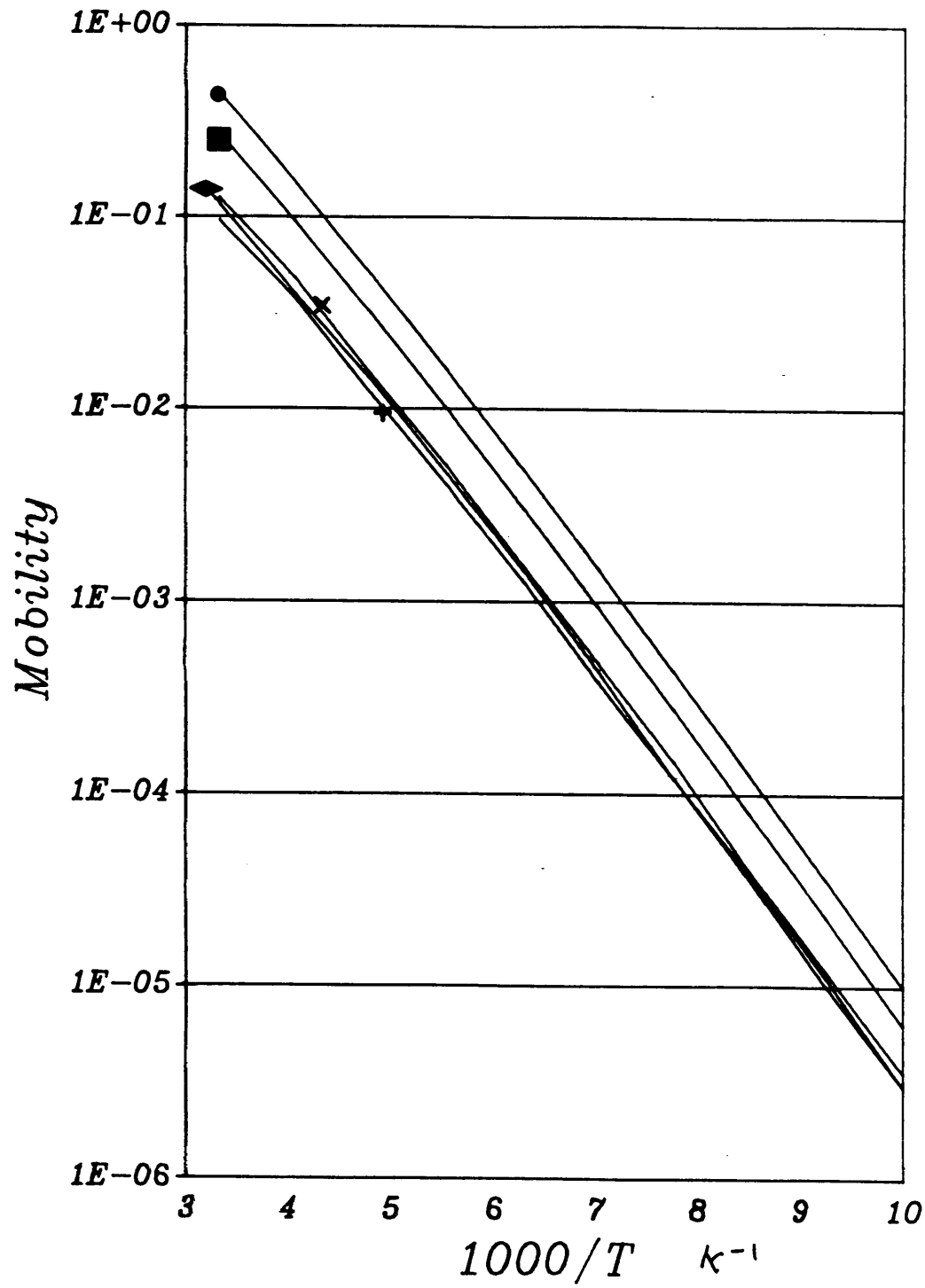

10 Discussion of Results.

10.1 Comparison of Simulation Methods.

Two methods of computer simulation have been used to simulate the response expected from an amorphous semiconductor possessing either a linear or exponential distribution of tail states. The Monte Carlo method of simulation uses very few assumptions about physical mechanisms and so the result obtained from it is more likely to be a realistic representation of the actual physical system. However, the Monte Carlo programmes require extremely large amounts of computer time and the resulting transient is still very noisy. As the noise on the pulse only varies as the square root of the number of carriers (proportional to run time), it is not possible to improve the noise by any significant amount without having run times that are measured in days.

Use of the finite difference method leads to the production of a transit pulse which is effectively the same as that produced by the Monte Carlo method. This shows that in spite of the approximations made in the creation of this programme, it is still sufficiently accurate in simulating transit pulses (see chapter 7). Further developments of these programmes have been made to include such phenomena as diffusion and contact potentials, which would be more difficult to include in a Monte Carlo simulation. The finite difference programmes run in a much shorter time and the transient is effectively noiseless. The major limitation on the use of the finite difference programmes is that the solutions begin to lose stability in

certain situations, such as at high applied fields. While this problem can often be overcome simply by using shorter timesteps, proper stability criteria have yet to be developed and incorporated. However it is precisely at this point that the Monte Carlo simulations perform most efficiently. It is suggested from these observations that it is better to employ the finite difference method for the production of computer simulated transit pulses in most cases, but that the results obtained should be compared with Monte Carlo simulations. This is to ensure that any errors caused by the approximations used have not significantly effected the calculated transient.

10.2 Different Methods of Analysis.

10.2.1 TROK Analysis.

It can be seen from the results shown in figures 7.4 and 7.10 that the TROK [37] method of analysis gives an exponential distribution of states even when a linear distribution is being analysed. It is interesting to note that the analysis of the 0.15 eV linear tail by the TROK method resulted in the prediction of an exponential tail of characteristic energy $\simeq$ 300K. There has been much discussion in the literature recently as to the best description of the DOS revealed by TOF measurements, proposed models include a linear tail (0.15eV deep over the range 0.08eV to 0.15 eV), an exponential (T_c=300K) or even a double exponential (T_{c1}= 390K and T_{c2}= 210K)[48].

These results may go some way toward explaining this disagreement. For instance, if a material possesses a linear DOS of

depth 0.15 eV, an analysis of it using the TROK method would predict that it had an exponential DOS of characteristic energy ≃ 300K.

Further errors can occur when using the TROK method of analysis if the requirement that the transport be anomalous is not strictly adhered to. This problem was highlighted in a recent paper by Silver Snow and Adler [54], in which a value of the free mobility of 1100 $cm^2V^{-1}s^{-1}$ was derived. This value was calculated when the TROK thermalisation energy concept was applied to a conventionally dispersive transit pulse, for which the transit time was $1x10^{-7}$sec. This time gave a value of 0.29 eV for the thermalisation energy, the energy at which the carrier occupancy peaks in the TROK formalisation. Using this value for E_{th} together with the measured drift mobility produced an increased value of the free carrier mobility. However, as was pointed out by Marshall, LeComber and Spear [55], the thermalisation energy concept is only valid for anomalously dispersive transients. The experiment results presented by Adler, Silver and Snow clearly show non-dispersive transport over a wide range of temperature. These transients all possessed activation energies ≃ 0.17eV, ie the carriers were only in contact with the states at this depth. There was, in fact no evidence of deep trapping to 0.29eV depth. It has been suggested by Marshall et al that this may be due to either a low density of states or a reduction in the capture cross section, below 0.17eV depth. In these circumstance the TROK thermalisation concept would not be valid. In fact Marshall, LeComber and Spear showed that the thermalisation would be complete after after a time of < 1 ns, which leads to a calculated value of $E_{th} < 0.17$ eV. Using this value the more generally accepted value of $\mu_o \simeq 10 - 20$ $cm^2V^{-1}s^{-1}$ can be determined.

10.2.2 MA Analysis.

The Marshall Allen technique quite adequately predicts the shape of the exponential distribution and does not produce an exponential distribution when used with the linear tail, so this technique can be used to distinguish between the two types of distribution. However, the energy dependence predicted by this method is not accurate in all cases. Thus although it may be used to differentiate between different types of distribution it cannot be used to to quantitatively evaluate the form of the distribution.

10.2.3 Integral Technique.

The integral technique accurately reproduces both of the test distributions used in the simulations. It may therefore be used as a tool for probing the density of states in a real material. The slight discrepancy between the predicted cut-off point of the linear distribution and the actual cut-off point used in the simulations is probably due to the fact that when the carriers have thermalised to the bottom of the model distribution they will still remain distributed about the lower kT of the band tail. Hence the mobility activation energy will show carriers being activated from above the cut-off point, thus causing a slight distortion of the final result.

10.3 Experimental Results.

The calculation of the functional form of the density of states within the sample used was very complicated due to the presence of

10.3 Experimental Results.

The identification of the functional form of the density of states within the sample used was complicated by the presence of depletion layers at the junction interfaces. However by using only the higher field values, which are less perturbed by the presence of the built in fields, it has proved possible to get a resonably good DOS fit to the experimental data. This could alternatively be interpreted as a linear distribution function or an exponential distribution function over the range of energies probed. Of the two, the linear distribution is a slightly better fit but it is not overwhelmingly better than the exponential over the range of energies probed. The exponential DOS fit could be rejected for other reasons however, as discussed below.

10.3.1 Problems with the Exponential Distribution.

Firstly it should be noted that the energy range covered by the easily usable results (0.1478 eV to 0.1615 eV) is not of very great extent. This means that that a number of distributions of different global form could be made to fit reasonably well *over the energy range explored*. This situation is shown in figure 10.1. Part a of this figure shows the linear and exponential distributions plotted over the experimental energy range. Part b shows the same two distributions plotted over an extended energy range. While both distributions are similar (as expected) over the experimental energy range, they diverge markedly outside this range.

Figure 10.1 Linear and exponential fit to the experimental data.

a) over the energy range investigated

b) over an extended energy range.

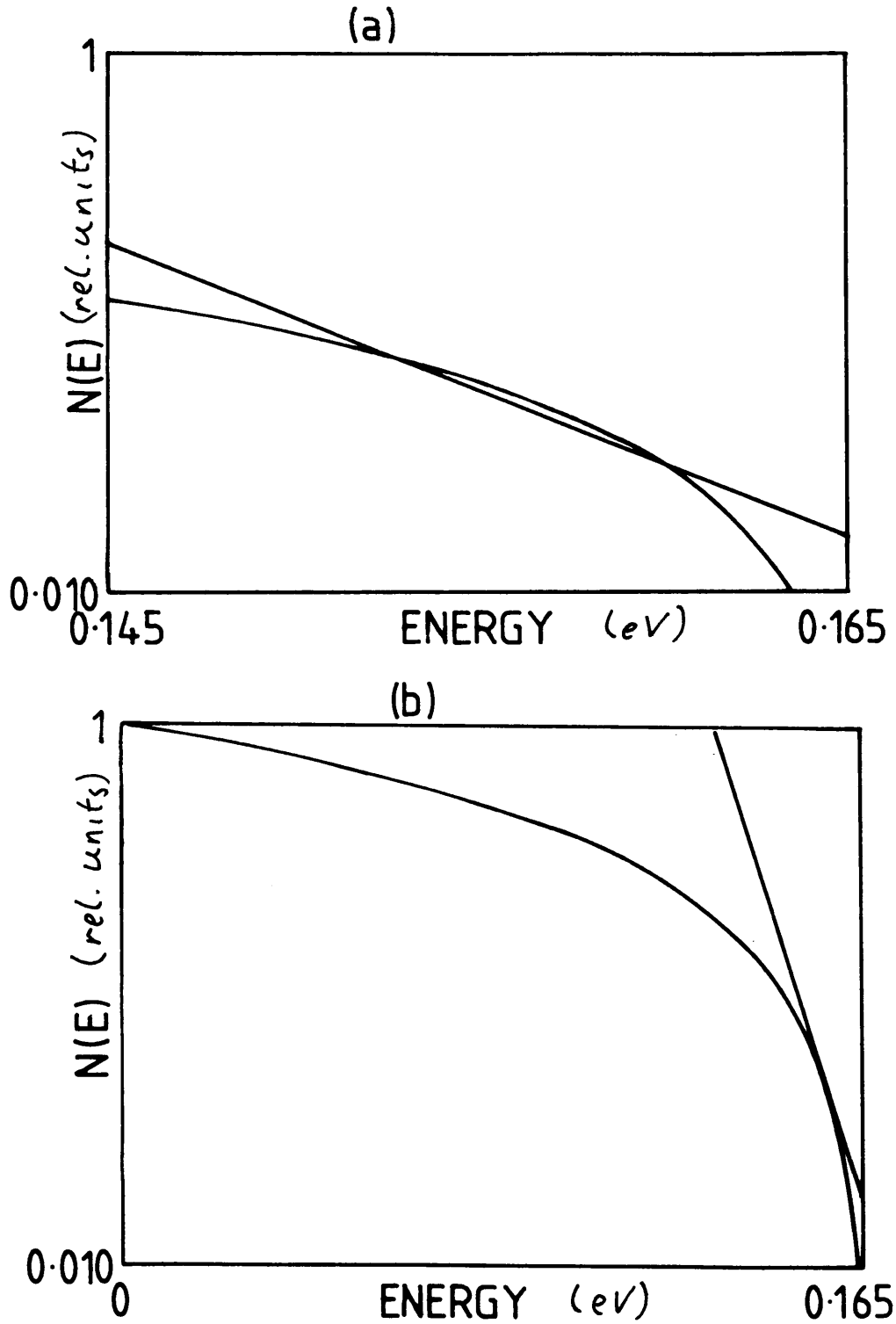

The above shows why two complete different distributions may be predicted from the experimental results obtained. However, it was shown by Tiedje and Rose [37] that anomalous dispersion would only be expected to occur for a sample with an exponential distribution of trapping states if the temperature T is less than the characteristic temperature T_c of the exponential. Therefore for the exponential predicted from the experimental results anomalous dispersion would only be expected to occur for T < 93K. As the lowest temperature reached was only 106K the none of the transient pulses should have been anomalously dispersive if the density of states were exponential. However, anomalous dispersion was clearly observed at temperatures well in excess of 106K. Furthermore if the exponential distribution were to continue upto the band edge the measured value of the drift mobility activation energy would approach zero because the carrier distribution would peak near E_c. In addition the extrapolated $g(E_c)$ would be very large ($>> 10^{21} cm^{-3}$). Given the above factors it is reasonable to assume that the density of states within the experimental sample *cannot have an exponential distribution.*

10.4 Future Investigations.

There is much further work that could be carried out in this field. The most obvious from an experimental point of view would be to repeat the measurements of the 'time of flight' transients using a sample that has a Shottky barrier structure. This would remove most of the distortions caused by built in voltages and also allow a wider energy range to be covered. The computer simulation programmes used could be up graded to include many more physically significant

processes. In fact a version of the finite difference programme which includes diffusion has been developed by Main. This simulation is more closely related to the transients that would be obtained experimentally and as already shown the significance of several effects (eg. back diffusion of charge to the top electrode) that have previously been ignored.

Finally it would be useful to perform a computer simulation of the situation envisaged by Monroe [32], wherein the transport mechanism consist of charge trapping followed hopping at a define *transport energy* rather than trap limited band. Such a simulation could be compared wiht experimental data to see if this model is in fact a better description of the charge transport mechanism in amorphous semiconductors.Layouts for such a programme have been discussed but the actual implementation of it has proved to be rather difficult. The main difficulty encountered has been the creation of a large enough random site distribution, without a very large distrbution the energy depth of any tail is far to small to be useful. However the number of sites cannot just simply be increased as both their position and the position of their nearest neighbours need to be stored, so both storage and run time requirements rapidly increase beyond the resources available.

11 Conclusions.

11.1 Simulation Methods.

It has been shown that it is possible to produce accurate computer simulations of the transit pulses that would be expected from amorphous materials possessing a particular density of states. Furthermore by comparison of the results obtained from the two different simulation methods used it is possible to state that the recently developed finite difference method gives results which are just as good has the older established Monte Carlo simulation method. Given that this is so then it becomes advantageous to use the finite difference method in most foreseeable situations. The finite difference method produces results using much less computer time than would be required for similar Monte Carlo simulations. The transit pulses produced using the finite difference method simulations also do not exhibit the sometimes extreme amount of noise usually associated with Monte Carlo simulations. It is also much easier to use the finite difference programs to obtain information other than just the transit pulse. In fact, it is possible to get the same program to show quantities such as the charge collection, the mobility Arrhenius plot, the electron distribution at any given time and many other quantities. In addition this programme allows for many of the physical quantities of the sample (attempt to escape frequency, built in voltages etc) to be individually specified and varied.

11.2 Analysis Methods.

Three different methods of determining the density of states distribution from simulated 'time of flight' transit pulses were tested. Of the three the integral technique developed and assessed in this work gave the most accurate construction of the actual density of states used in the simulation. The Marshall-Allen analysis method will distinguish between the different density of states distributions but the distribution that it predicts is severely distorted from that used in the simulation. The TROK analysis method is very accurate if it is used to examine an exponential distribution, but it implicitly assumes that all densities are of exponential type. Therefore if it is used to examine transit pulses resulting from a linear tail distribution these are interpreted in terms of an exponential distribution. Other clues as to the true nature of the trapping state distribution are often present in experimental data and a 'blind' application of the TROK based analysis, with its implicit assumptions , does not take these into account and can produce misleading results. The integral method developed and tested in this work is essentially 'model independent' and should return an accurate representation of any arbitary density of states distribution, but it does require much more data. The method effectively does take into account all of the experimental 'clues'. This is borne out by the experimental 'time of flight' measurements performed in this work.

A particular example of the misleading results that can arise from the use of the TROK analysis can be seen if a linear tail with a cutoff point at around 0.15ev, as proposed by Marshall, Street and

Thompson [49], is considered. An exponential distribution will be calculated via a TROK type analysis. This will have a characteristic temperature of ≃ 300K, as was obtained for amorphous silicon by both Tiedje and Rose [37] and Orenstien and Kasner [38].

Experimentally it has been shown that, over the limited energy range investigated, the sample of amorphous silicon examined in this work could, by the integral analysis possess either a linear (ΔE = 0.165ev) or exponential (T_c = 100K) distribution of trapping states. However, as an amorphous material which possess an exponential density of states will only show anomalous dispersion at temperatures below T_c and such anomalous transients were observed the exponential distribution was rejected as a viable alternative. It is therefore concluded that it is likely the sample studied possesses a linear distribution of trapping states. This distribution has a cutoff point of 0.165 eV which is similar to that reported elsewhere [49]. Many of the results obtained experimentally unfortunately could not be used in the final analysis of the density of states. This arises because of the the distorting effect of the built in fields within the p^+-i-n^+ sample. A Schottky barrier structure will need to be obtained before further experimental measurements are performed.

References

1 Roberts GG, Apsley N and Munn RW, Physics Reports., Vol. **60**, 59, 1980

2 Nagels P, Topics in Applied Physics Volume **36**., Springer-Verlag, 113, 1979

3 Mott NF, J. Applied Phys., Vol. **16**, 49, 1967

4 Anderson PW, Phys. Rev., Vol. **109**, 1492, 1958

5 Mott NF and Davis EA, Electronic Processes in Non-crystalline Materials., Claredon Press Oxford, 1979

6 Cohen MH, J. Non-Cryst. Solids., Vol. **4**, 391, 1970

7 Miller A and Abrahams S, Phys. Rev., Vol. **120**, 745, 1960

8 Mott NF, J. Non-Cryst. Solids., Vol. **1**, 1, 1968

9 Haynes JR and Shockley W, Phys. Rev., Vol. **75**, 691, 1949

10 Spear WE, J. Non-Cryst. Solids., Vol. **1**, 197, 1969

11 Marshall JM, Rep. Prog. Phys., Vol. **46**, 1235, 1983

12 Marshall JM, In Print 1988

13 Spear WE and Steemers H., Phil. Mag. Letts., Vol. **47**, L77, 1983

14 Pai DM and Scharfe ME, J. Non-Cryst. Solids., Vol. **8-10**, 752, 1972

15 Scharfe ME, Bull. Am. Phys. Soc., Vol. **18**, 454, 1973

16 Scher H and Montroll EW, Phys. Rev. B., Vol. **12**, 2455, 1975

17 Marshall JM and Owen AE, Phys. Stat. Solidi. a., Vol. **12**, 181, 1972

18 Pfister G, Phys. Rev. Lett., Vol. **36**, 271, 76

19 Pfister G and Griffiths CH, Phys. Rev. Lett., Vol. **40**, 659, 1978

20 Kolomiets BT, Lebedev EA and Kazakova LP, Sov. Phys. Semicond., Vol. **12**, 1049, 1978

21 Marshall JM and Sharp AC, J. Non-Cryst. Solids., Vol. **35-36**, 99, 1980

22 Tiedje T, Cebulka JM, Morel D and Arles B, Phys. Rev. Lett., Vol. **46**, 1425, 1981

23 Marshall JM, Phil. Mag., Vol. **36**, 959, 1977

24 Marshall JM, Proc. Int. Conf. on Amorphous and Liquid Semiconductors., Edinburgh:University of Edinburgh (ICL), 541, 1977

25 Silver M and Cohen L, Phys. Rev B., Vol. **15**, 3276, 1977

26 Schmidlin FW, Phys. Rev. B., Vol. **6**, 2362, 1977

27 Schmidlin FW, Bull. Am. Phys. Soc., Vol. **22**, 434, 1977

28 Noolandi J, Phys. Rev. B., Vol. **16**, 4466, 1977

29 Noolandi J, Phys. Rev. B., Vol. **16**, 4474, 1977

30 Pollack M, Phil. Mag., Vol. **36**, 1157, 1977

31 Marshall JM, Phil. Mag. B., Vol. **36**, 335, 1978

32 Monroe D, Phys. Rev. Lett., Vol. **54**, 146, 1985

33 Monroe D, Orenstein J and Kastner MA, J. Phys., Vol. **42**, C4-559, 1981

34 Kristensen K and Hvam JM, Solid State Commun., Vol. **50**, 845, 1984

35 Shapiro FR and Adler D, J. Non-Cryst. Solids., Vol. **74**, 189, 1985

36 Marshall JM and Allen D, Phil. Mag. B., Vol. **40**, 71, 1979

37 Tiedje T and Rose A, Solid State Commun., Vol. **37**, 48, 1981

38 Orenstein J and Kastner M, Phys. Rev. Lett., Vol. **23**, 161, 1979

39 Orenstein J, Kastner M and Vaninov V, Phil. Mag. B., Vol. **46**, 23, 1982
40 Marshall JM, Michiel H and Adriaessens, Phil. Mag B., Vol. **47**, 211, 1983
41 Marshall JM and Main C, Phil. Mag. B., Vol. **47**, 471, 1983
42 Marshall JM, Barclay RP, Main C and Dunn C, Phil. Mag. B., Vol. **52**, 997, 1985
43 Michiel H, Marshall JM and Adriaenssens GJ, Phil. Mag. B., Vol. **48**, 187, 1983
44 Marshall JM and Barclay RP, Physics and Chemistry of Disordered Sytems, (New York:Plenum Press), 567, 1985
45 Berkin J, M.Sc. Thesis., Dundee University, Unpublished, 1985
46 Marshall JM, Berkin J and Main C, Phil. Mag. B., Vol. **56**, 641, 1987
47 LeComber PG and Spear WS, Phys Rev Lett., Vol. **25**, 509, 1970
48 Vanderhagen R and Longeaud C, J. Non-Cryst. Solids., Vol. **97-98**, 1059, 1987
49 Marshall JM, Street RA and Thompson MJ, Phil. Mag. B., Vol. **54**, 51, 1986
50 Marshall JM, Street RA, Thompson MJ and Jackson WB, Phil. Mag. B., Vol. **57**, 387, 1988
51 Hammersley JM and Handscomb DC, Monte Carlo Methods., Methuen, 1964
52 Rubinstein RY, Simulation and the Monte Carlo Method., John Wiley and Sons., 1981.
53 Main CM,Private Communications 1985-1988
54 Silver M, Snow E and Aldler D, Solid State Commun., Vol. **51**, 581, 1984
55 Marshall JM, LeComber PG and Spear WE, Solid State Commun., Vol. **54**, 11, 1985

A1 Appendix 1

A1.1 Comparison of TROK and the Integral Technique for an Exponential Tail.

It is interesting to note that, for a material possessing a simple exponential distribution of tail states, both the TROK analysis and the integral technique give the same value for E_{th}. This is not immediately apparent because the TROK method is based on total time elapsed while the integral method uses the time that the carriers are free. The relationship can be shown as follows.

Consider an exponential density of states distribution of the form :

$$N(E) = N(E_c)\exp(-E/kT) \qquad \text{(A1.1)}$$

TROK show that the thermalisation energy for this distribution is given by :-

$$E_{th}^{TROK} = kT\ln(\nu t_t) \qquad \text{(A1.2)}$$

where t_t = total time elapsed.

Substituting the density of states given in equation A1.1 into equation A1.2 and integrating gives the value of the thermalisation energy predicted by the integral technique :-

$$E_{th}^{new} = kT_c \ln(\nu t_{free}) \qquad \text{(A1.3)}$$

To show the equivalence of these two forms it is necessary to link t_t and t_{free}. This is possible for the special case of the featureless exponential tail being considered provided that there is only one significant trapping/release event (true for any highly anomalously dispersive system). This leads to :-

$$t_{free} \simeq \text{trapping time} \qquad \text{(A1.4)}$$

$$t_t \simeq \text{release time} \qquad \text{(A1.5)}$$

For the exponential density of states the free time is given by :-

$$t_{free}^{-1} = v_o \sigma kT_c N(E_c) \exp(-E_{th}/kT_c) \qquad \text{(A1.6)}$$

from the principle of detailed balance

$$v_o \sigma = \nu / N_c \qquad \text{(A1.7)}$$

where $N_c \simeq kTN(E_c)$

so $$t_{free}^{-1} = (\nu T_c / T) \exp(-E_{th}/kT_c) \qquad \text{(A1.8)}$$

then $$t_{free} = (T/T_c) \nu^{-1} \left[\exp(E_{th}/kT_c) \right]^{T/T_c} \qquad \text{(A1.9)}$$

letting $\alpha = T/T_c$

and substituting $t_t = \nu^{-1}\exp(E_{th}/kT_c)$

then $$t_{free} = \alpha\nu^{-(1-\alpha)}t_t^{\alpha} \qquad \text{(A1.10)}$$

substituting this for t_{free} in equation A1.9 gives :-

$$E_{th}^{new} = kT_c \ln\left[(T_c/T)\nu(T/T_c)\nu^{-(1-\alpha)}t_t^{\alpha}\right] \qquad \text{(A1.11)}$$

$$E_{th}^{new} = kT_c \ln[(\nu t_t)^{\alpha}] \qquad \text{(A1.12)}$$

$$E_{th}^{new} = kT\ln(\nu t_t) = E_{th}^{TROK} \qquad \text{(A1.13)}$$

A2 Appendix 2

A2.1 Continuity of the DOS.

If the simulation programmes used are to produce the correct answers then it is necessary to match the tail states to the band states at E_c. This matching is the 'attempt to escape' frequency, ν. The variable Rel in the simulation programmes corresponds to $1/\nu$. This variable is calculated has shown below:-

A2.1.1 The 'Attempt to Escape' Frequency.

The 'attempt to escape' frequency is related to the free carrier trapping time constant in the following manner:-

$$t_{free} = \nu \int [N(E)dE/N(E_c)kT] \qquad \text{(A2.1)}$$

The calculations for the two cases used in this study are presented below:-

A2.1.1.1 The Linear DOS.

The calculation for the linear tail is (referring to figure A2.1)

$$n_{in} = n_{free}/\text{trapping time} \qquad \text{(A2.2)}$$

$$= n_{free}/N(E_c)\delta v_{th}\nu \qquad \text{(A2.3)}$$

Figure A2.1 The density of states distribution for the linear case.

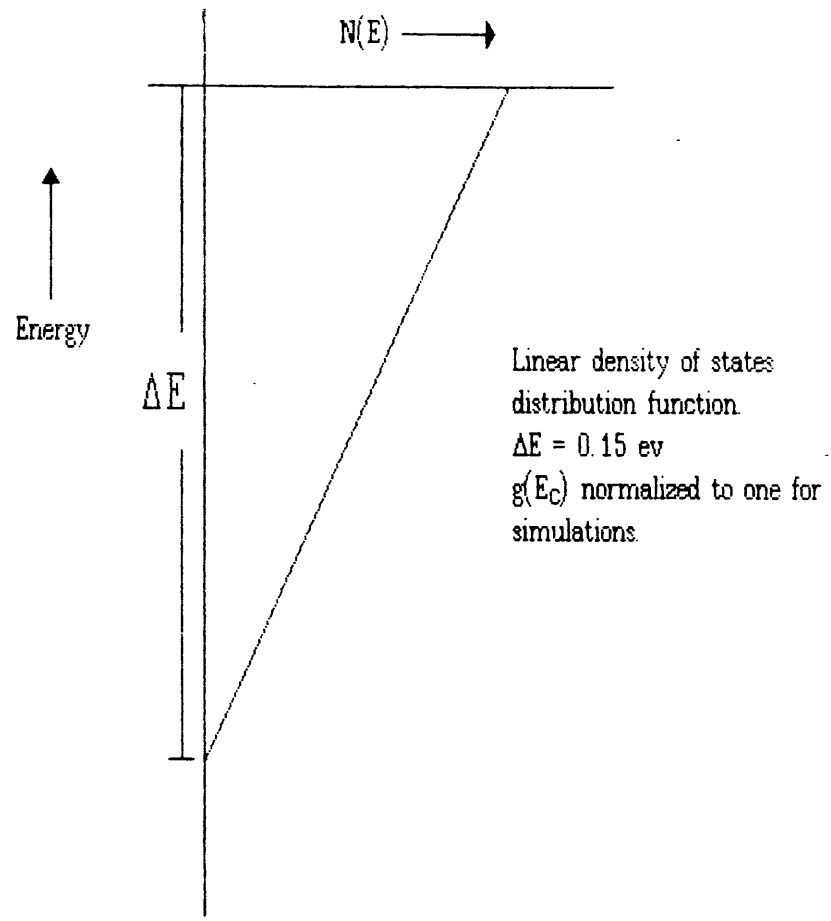

$$n_{out} = n_t \nu \tag{A2.4}$$

where

$$n_{free} = \int_{\Delta}^{\infty} Nf(E)dE \tag{A2.5}$$

$$= f(0)N(E_c)/\Delta \exp(-\Delta/kT)(\Delta kT+kT^2) \tag{A2.6}$$

and $$n_t = N(E_c)\delta f(\Delta) \tag{A2.7}$$

$$= N(E_c)\delta f(0)\exp(-\Delta/kT) \tag{A2.8}$$

so

$$\nu = N(E_c)v_{th}\sigma kT(1+kT/\Delta) \tag{A2.9}$$

now

$$t_{free} = 1/\int N\sigma v_{th}dE \tag{A2.10}$$

$$= 2/N(E_c)\sigma v_{th}\Delta$$

therefore

$$N(E_c)\sigma v_{th} = 2/\Delta t_{free} \tag{A2.11}$$

so

$$= 2kT/t_{free}\Delta(1+kT/\Delta) \tag{A2.12}$$

let $B = kT/\Delta$ then

$$= 2(B+1)/t_{free}B^2 \tag{A2.13}$$

but $REL = 1/\nu$ so

$$REL = t_{free}B^2/2(B+1) \tag{A2.14}$$

A2.1.1.2 The exponential DOS.

The calculation to match the exponential tail to the band is very similar to that for the linear tail. Refer now to figure A2.2. The density of trapping states is described by the equation :-

Figure A2.2 The density of states distribution for the exponential case.

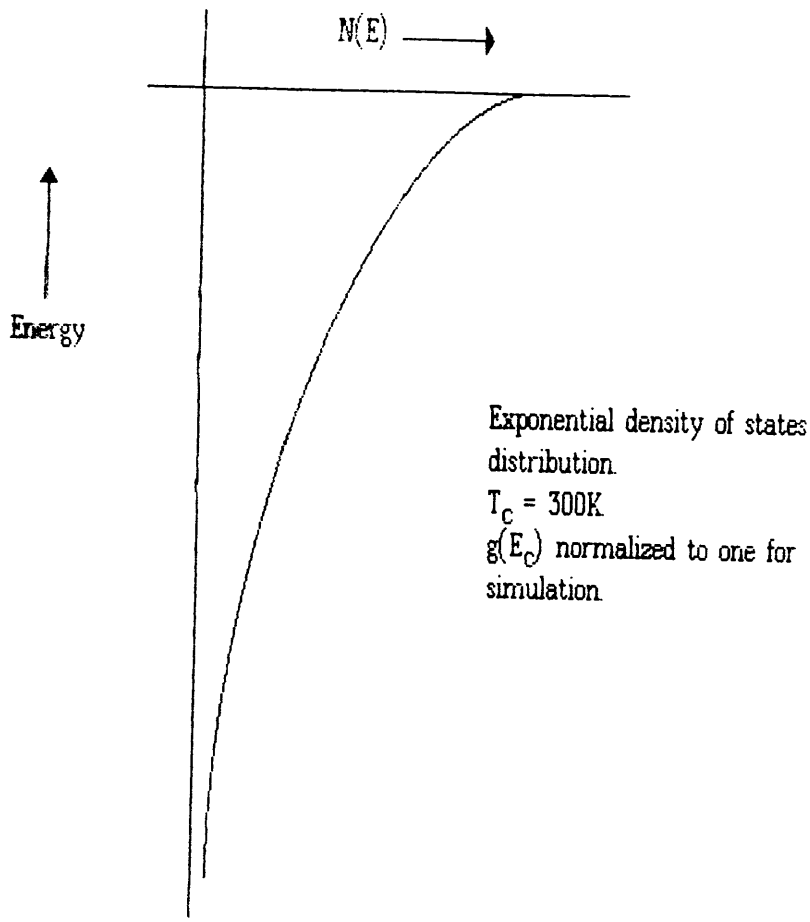

$$N(E) = N(E_c)\exp(-E/E_o) \tag{A2.15}$$

and the total density of trapping states is given by :-

$$\int_0^\infty N(E)dE = [-N(E_c)E_o\exp(-E/E_o)] \tag{A2.16}$$

$$= E_0 N(E_c)$$

The shallowest set of trapping states will have a density of $N(E_c)kT$.

The trapping time τ into the shallowest set of states will be given by :-

$$\tau = E_o t_{free}/kT \tag{A2.17}$$

Now by detailed balance $n_{in} = n_{out}$.

therefore :-

$$n_{free}/\tau = n_t/\tau_{free} \tag{A2.18}$$

so

$$n_{free} kT/E_o \tau_{free} = n_t \nu \tag{A2.19}$$

If $\tau_{free} = 1$ as in the simulation progs then

$$\nu = kTn_{free}/E_o n_t \qquad \text{(A2.20)}$$

Now

$$n_t = N(E_c)f(E_c)kT \qquad \text{(A2.21)}$$

and

$$n_{free} = \int_{E_c}^{\infty} N(E)f(E)dE \qquad \text{(A2.22)}$$

$$= N(E_c)f(E_c)/\beta$$

where $\beta = 1/kT$

therefore

$$n_{free} = N(E_c)f(E_c)/(1/kT) \qquad \text{(A2.23)}$$

so

$$\nu = T/T_c \qquad \text{(A2.24)}$$

but REL = $1/\nu$

so

$$\text{REL} = T_c/T \qquad \text{(A2.25)}$$

A3 Appendix 3

A3.1 Programmes Used.

Given below are examples of some of the programmes used in this work.

A3.1.1 Graph Plotting Programme.

```
      DIMENSION X(200,20),Y(200,20),X1(200)
      DIMENSION Y1(200),G(20),IDENT(20),NUM(20),NP(20)
      CHARACTER*10 FNAME
      CHARACTER*30 TITLE,XAXIS,YAXIS
      CHARACTER*5 IDENT
      CHARACTER*3 OPNX,OPNY,OPNACT,OPTIP
      DO 3 I=1,10
      NP(I)=0
3     CONTINUE
      WRITE(5,5)
5     FORMAT(' INPUT DATA FILE NAME')
      READ(5,15)FNAME
      OPEN(1,FILE=FNAME)
      READ(1,15)TITLE
      READ(1,15)XAXIS
      READ(1,15)YAXIS
      READ(1,15)OPNX
      READ(1,15)OPNY
      READ(1,15)OPNACT
15    FORMAT(A)
      READ(1,20)INUM
20    FORMAT(I5)
      DO 60 J=1,INUM
      READ(1,25)IDENT(J)
      READ(1,20)N
      NUM(J)=N
25    FORMAT(A)
      DO 30 I=1,N
      READ(1,*)X(I,J),Y(I,J)
30    CONTINUE
      DO 60 I=1,N
      IF (OPNX.EQ.'1/T') X(I,J)=1000./X(I,J)
      IF (OPNX.EQ.'LOG') THEN
      IF (X(I,J).LT.1.0E-37) THEN
      X(I,J)=-37.0
      ELSE
      X(I,J)=LOG10(X(I,J))
      ENDIF
      ENDIF
      IF (ONPY.EQ.'1/T') Y(I,J)=1000./Y(I,J)
      IF (OPNY.EQ.'LOG') THEN
```

```
      IF (Y(I,J).LT.1.0E-37) THEN
      Y(I,J)=-37.0
      ELSE
      Y(I,J)=LOG10(Y(I,J))
      ENDIF
      ENDIF
60    CONTINUE
      XMAX=X(1,1)
      XMIN=XMAX
      YMAX=Y(1,1)
      YMIN=YMAX
      DO 100 J=1,INUM
      N=NUM(J)
      DO 100 I=1,N
      IF (X(I,J).GT.XMAX) XMAX=X(I,J)
      IF (Y(I,J).GT.YMAX) YMAX=Y(I,J)
      IF (X(I,J).LT.XMIN) XMIN=X(I,J)
      IF (Y(I,J).LT.YMIN) YMIN=Y(I,J)
100   CONTINUE
      WRITE(5,1000)XMIN,XMAX
1000  FORMAT(' X AXIS IS ',E10.4,' TO ',E10.4)
      WRITE(5,1010)
1010  FORMAT(' DO YOU WANT TO ALTER IT (Y/N default = N)')
      READ(5,15)OPTIP
      IF (OPTIP.EQ.'y') OPTIP='Y'
      IF (OPTIP.NE.'Y') OPTIP='N'
      IF (OPTIP.EQ.'N') GOTO 1050
      WRITE(5,1030)
1030  FORMAT(' INPUT LOWER AND UPPER X BOUNDS')
      READ(5,*)XMIN,XMAX
1050  WRITE(5,1061)YMIN,YMAX
1061  FORMAT(' THE Y AXIS IS ',F10.4,' TO ',E10.4)
      WRITE(5,1010)
      READ(5,15)OPTIP
      IF (OPTIP.EQ.'y') OPTIP='Y'
      IF (OPTIP.NE.'Y') OPTIP='N'
      IF (OPTIP.EQ.'N') GOTO 1070
      WRITE(5,1060)
1060  FORMAT(' INPUT LOWER AND UPPER Y BOUNDS')
      READ(5,*)YMIN,YMAX
1070  WRITE(5,1080)
1080  FORMAT(' DO YOU WANT TO DELETE ANY OF THE CURVES')
      WRITE(5,1090)
1090  FORMAT(' (Y/N default=N)')
      READ(5,15)OPTIP
      IF (OPTIP.EQ.'y') OPTIP='Y'
      IF (OPTIP.NE.'Y') OPTIP='N'
      IF (OPTIP.EQ.'N') GOTO 1075
      WRITE(5,1100)
1100  FORMAT(' INPUT THE NUMBER OF
     1THE CURVE TO BE DELETED')
      READ(5,*)IZZ
      NP(IZZ)=1
      GOTO 1070
1075  WRITE(5,1110)
1110  FORMAT(' DO YOU WANT LINES OR
```

```
     1CHARACTERS (L/C default = L)')
      READ(5,15)OPTIP
      IF (OPTIP.EQ.'c') OPTIP='C'
      IF (OPTIP.NE.'C') OPTIP='L'
      IF (OPTIP.EQ.'C') THEN
      LT=1
      ELSE
      LT=0
      ENDIF
      CALL PAPER(1)
      CALL MAP(XMIN,XMAX,YMIN,YMAX)
      CALL CTRSET(4)
      DO 110 J=1,INUM
      SXY=0.0
      SX=0.0
      SY=0.0
      SX2=0.0
      N=NUM(J)
      DO 120 I=1,N
      X1(I)=X(I,J)
      Y1(I)=Y(I,J)
      SXY=(X1(I)*Y1(I))+SXY
      SX=X1(I)+SX
      SY=Y1(I)+SY
      SX2=(X1(I)*X1(I))+SX2
120   CONTINUE
      D=(NUM(J)*SX2)-(SX*SX)
      AM=((NUM(J)*SXY)-(SX*SY))/D
      C=((SX2*SY)-(SX*SXY))/D
      YS=AM*XMIN+C
      YE=AM*XMAX+C
      K=51+J
      IF (NP(J).EQ.1) GOTO 110
      IF (LT.EQ.1)CALL PTPLOT(X1,Y1,1,NUM(J),K)
      IF (LT.EQ.0)CALL PTPLOT(X1,Y1,1,NUM(J),-3)
109   G(J)=AM
110   CONTINUE
      IYS=6
      IF (G(1).GT.0.0) THEN
      IXS=10
      ELSE
      IXS=60
      ENDIF
        CALL CTRMAG(15)
        CALL SCALES
        IF (LT.NE.0) THEN
      CALL CTRSET(1)
      KK=IYS
      CALL PLACE(IXS,IYS)
      JJ=0
      DO 140 J=1,INUM
      IF (NP(J).EQ.0) JJ=JJ+1
      IF (NP(J).EQ.1) GOTO 140
      K=51+JJ
      CALL CTRMAG(20)
      CALL CTRSET(4)
```

```
      CALL TYPENC(K)
      CALL CTRMAG(15)
      CALL TYPECS('  ',2)
      CALL CTRSET(1)
      CALL TYPECS(IDENT(J),5)
      KK=6+JJ
      CALL PLACE(IXS,KK)
140   CONTINUE
        ENDIF
      CALL CTRSET(1)
      CALL PLACE(20,1)
      CALL TYPECS(TITLE,30)
      CALL PLACE(30,46)
      CALL CTRSET(1)
      CALL TYPECS(XAXIS,30)
      CALL PLACE(2,20)
      CALL CTRORI(1.0)
      CALL TYPECS(YAXIS,30)
      CALL BORDER
      CALL GREND
      STOP
      END
```

A3.1.2 Monte Carlo Simulation Programme.

```
#include stdlib
#include math
#include time
main()
{
 int pass=0,tim,n,m,no,x,j,d,f,imax,y,ittot;


 int iz,g[101],its[101],deep[101];
 double temp,tfree,ttrap,trapp,t20,rel,p,q,s,ts,v,w,to;
 double k=8.625e-5,tc=300,tmp,tmax,z,delta;

 double maxdelta,c,e,av,ttot,a[101];

/*  program runs twice
    first pass calculates t20%
    second pass calaculates max energy depth fastest 20% have
    been trapped at.


    input variable parameters
    trapp = mean free carrier trapping time (normalised =1)
    no = number of carriers
    to = number of trapping events per transit
    z = timestep between output values
    temp = temperature in K
*/

 printf("enter values for trapp,no,to,z,temp");
 scanf("%f %i %f %f %f",&trapp,&no,&to,&z,&temp);
 tmax = (double)99*z;
```

```
/* rel = unactivated portion of release time constant
         rel constant for this simulation */

 rel = trapp*((tc-(double)250)/(double)250);

/* only interested in carrier extraction so notify

   if none will be */

 if (tmax < to ) printf("No carriers will reach back electrode!");
 t20 = (double)0;

/* initialise random number generator */

 time(&tim);

/* main program loop */

 loop:
 srand(tim);
 printf(" pass %d ",pass);

/* initialise variables
   a[n] = number of free carriers averaged over
   time interval m*z to (m+1)*z
   n = number of current carrier    */

 for (n = 0;n <= 100; n++) {
  a[n] = (double)0;
  g[n] = 0;
  its[n] = 0;
  deep[n] = 0;
  }
 n = c = d = e = f = (double)0;

/* commence program for new carrier */

 ea:
  maxdelta = tfree = ttrap = (double)0;

/* calculate free carrier trapping time */

 m = 0;
 eb:
 p = (double)rand()/2147483647;
 w = -trapp*log(p);
 e +=w; f++;

/* calculate trap depth delta */

 q = (double)rand()/2147483647;
 delta = (double)-1*log(q)*k*tc;

/* maxdelta = deepest carrier has been trapped */
 maxdelta = (delta > maxdelta) ? delta : maxdelta;
```

```
/* calculate trapped carrier release time v */

 q = (double)rand()/2147483647;
 q = log(q);
 tmp = delta/(k*temp);
 tmp = exp(tmp);
 v = (double)-1.0*q*rel*tmp;
 c += v;
 d++;

/* upgrade array elements for the time period    over which the
carrier is free  */
 en:
 if (tfree+ttrap+w >= tmax) goto eh;
 if (tfree+w >= to) {
  if (ttrap+to <= t20 ) {
   imax = (int) (maxdelta*(double)500);
   imax = (imax < (double)100 ) ? imax : (double)100;
   deep[imax] += 1;
  }
  goto edd;
 } if (tfree+ttrap+w < ((double)(m+1)*z))
 {  a[m] += w;
  goto ef;
 }
 a[m] += ((double)(m+1)*z)-tfree-ttrap;
 ee:
 m++;
 if ((double)(m+1)*z > tfree+ttrap+w) {
  a[m] += tfree+ttrap+w-((double)m*z);
  goto ef; }
 a[m] += z;
 goto ee;

/* increment the values of total times free and trapped     check
if time limit exceeded */

 ef:
 tfree += w;
 ttrap += v;
 if (tfree+ttrap >= tmax) goto ec;
 eg:
 if ((double)(m+1)*z > tfree+ttrap) goto eb;
 m++;
 goto eg;

/* upgrade processes for alternative start/stop conditions */

 eh:
 a[m] += ((double)(m+1)*z)-tfree-ttrap;
 m++;
 eha:
 if (m > 99) goto ec;
 a[m] += z;
 m++;
 goto eha;
```

```
ed:
if ((double)(m+1)*z > ttrap+to)
{
 a[m] += to-tfree;
 goto ec;
}
a[m] += ((double)(m+1)*z)-tfree-ttrap;
eda:
m++;
if ((double)(m+1)*z > ttrap+to) {
a[m] += ttrap+to-((double)m*z);
goto ec;
}
a[m] += z;
goto eda;

/* next carrier if n < total allowed */

ec:
n++;
if (n < no ) goto ea;
goto ezz;
edd:
ttot = tfree+ttrap+(to-tfree);
ttot = ttot/tmax;
ittot = (int)(100*ttot);
for (iz = ittot;iz <= 100;iz++) its[iz] += 1;
goto ed;
ezz:
for (m = 1;m <= 100;m++) {
  if ((double)its[m]  <= ((double)0.2)*((double)n)) iz = m;
}
ttot =
(((double)0.2*(double)n-its[iz])/(double)(its[iz+1]-its[iz]));
ttot += iz;
ttot = (ttot/(double)100)*tmax;
if (pass == 0) {  t20 = ttot;
 pass++;
 goto loop; }

/* output rountine */
printf("transit pulse height vs time\n\n");
for (m = 0,j = 0;m <= 99;m++)  {
 printf(" %6.0f ",a[m]);
 if (j == 9) {
  j = -1;
  printf("\n");
 }  j+=1;
} printf("\n\n20%% transit time = %f ",ttot);
printf("\ntimestep used = %f",z);
printf("\ntemperature = %f",temp);
printf("\ne/f = av trapping time = %f",e/f);
printf("\nc/d = av release time = %f",c/d);
printf("\n\n");
for (m=0,j=0;m<=99;m++) {
 printf(" %5d ",its[m]);
```

```
  if (j == 9) {
   j = -1;
   printf("\n");
  }
  j++;
 }
 printf("\n\n");
 for (m = 0, j = 0,iz = 0; m <= 99; m++) {
  printf(" %5d ",deep[m]);
  iz += deep[m];
  if (j == 9) {
    j = -1;
    printf("\n");
  }
  j++;
 }
 printf("\n\nnumber of carriers collected = %5d",iz);
 printf("\nnumber of carriers that crossed sample in less");
 printf("\nthan  t20%%  but  not  included  in  above  output  =
%5d",deep[100]);
}
```

A3.1.3 Finite Difference Programme.

```
      IMPLICIT DOUBLE PRECISION (A-G,O-Z)
      PARAMETER(KE=21,KH=101)
      DOUBLE PRECISION G(KE),CG(KE),N1(KE),CE(KE),
     1TA(KH),T1(KH),TB(KH),T2(KH),
     2J1(KE),J2(KE),J3(KE),J4(KH),
     3K1(KE),K2(KE),K3(KE),K4(KH),
     4F(KH,KE),YM(KH,KE),YS(KH,KE),
     5DU(KH,KE),FL(KH),
     6X(10,1),Y(10,10),KT,
     7DAT(10,1)
      INTEGER H,HT,HL,IDAT(5,2)
      DO 5 I=1,KE
      DO 5 ID=1,KH
      J1(I)=0.0
      J2(I)=0.0
      J3(I)=0.0
      J4(ID)=0.0
      K1(I)=0.0
      K2(I)=0.0
      K3(I)=0.0
      K4(ID)=0.0
      DU(ID,I)=0.0
      YS(ID,I)=0.0
      YM(ID,I)=0.0
      F(ID,I)=0.0
      TA(ID)=0.0
      TB(ID)=0.0
      T2(ID)=0.0
      T1(ID)=0.0
5     CONTINUE
C     ***INPUT DATA***
```

```
      WRITE(5,*)'INPUT INITIAL TEMP., THE TEMP.
     1CHANGE AND NO. OF STEPS'
      READ(5,*)TI,TD,IT
750   FORMAT(2D10.4,I3)
      WRITE(5,*)'INPUT NT AND H (?) AND THE ENERGY'
      WRITE(5,*)'DEPTH OF DIST. AND RD(?) AND TC'
      READ(5,*)NT,H,ED,RD,TC
      KC=0
560   WRITE(5,480)
480   FORMAT(' INPUT STOP(1)/CONTINUE(2) ')
      READ(5,500)IC
500   FORMAT(I3)
      IF (IC.EQ.1) GOTO 520
      KC=KC+1
      WRITE(5,555)
555   FORMAT(' INPUT NUMBER OF TRAPPING
     1EVENTS PER TRANSIT')
      READ(5,*)DAT(KC,1)
760   FORMAT(D10.4)
      GOTO 560
      WRITE(5,820)TI,TD,ED,RD,VT
820   FORMAT(5D10.4)
520   KM=KC
      IM=IT
      HT=H+1
      HL=H-1
C     *      *
      NL=NT+1
C     *ARRAY FOR FLOAT(I)*
      DO 30 I=1,KH
      FL(I)=DBLE(I)
30    CONTINUE
C     ***FIELD LOOP (VT**
      DO 80 KY=1,KM
      VT=DAT(KY,1)
      AD=FL(H)/VT
      BD=RD*AD
      CD=AD+BD
C     **TEMPERATURE LOOP***
      DO 85 JT=1,IM
11    FORMAT(3I3)
      T=TI+TD*FL(JT-1)
      KT=8.625D-5*T
      DE=ED/(NT*KT)
C       *******DENSITY OF STATES*********
      S=0.0
      DO 20 I=2,NL
      G(I)=(T/250.)*DE*DEXP((-FL(I-1)*KT*DE)
     1/(8.625D-5*TC))
      S=S+G(I)
      N1(I)=DEXP(-FL(I-1)*DE)
20    CONTINUE
      C=1.0/S
      DO 40 I=2,NL
      CG(I)=C*G(I)
      CE(I)=C*N1(I)
```

```
40    CONTINUE
C     *INITIALISE*
      DT=0.01
      TL=1.0D-3
      TT=0.0
      DO 50 ID=1,HT
      DO 50 I=1,NL
      YS(ID,I)=0.0
50    CONTINUE
      YS(1,1)=1.0
C     *INITIAL JACOBIAN SET UP*
      DO 110 ID=1,HT
      DO 110 I=1,NL
      YM(ID,I)=YS(ID,I)
110   CONTINUE
      DO 125 ID=1,H
      S1=0.0
      S2=0.0
      DO 120 I=2,NL
      J2(I)=CG(I)
      S1=S1+J2(I)
      J3(I)=-CE(I)
      S2=S2-YM(ID,I)*J3(I)
      J1(I)=-J3(I)
120   CONTINUE
      J4(ID)=-S1-(1.0+2.0*RD)*AD
125   CONTINUE
      J4(1)=-S1-(1.0+RD)*AD
      J4(HT)=0.0
C     TRIDIAG ELEMENTS
      DO 300 ID=2,HT
      TA(ID)=(1.0+RD)*AD
300   CONTINUE
      DO 310 ID=1,HL
      TB(ID)=BD
310   CONTINUE
C     *ITERATION*
      L=0
650   CONTINUE
      DO 60 ID=1,HT
      DO 60 I=1,NL
      YM(ID,I)=YS(ID,I)
60    CONTINUE
      S5=0.0
      DO 430 ID=1,H
      S5=S5+YS(ID,1)
430   CONTINUE
      IF (L.EQ.0) GOTO 90
90    CONTINUE
      TT=TT+DT
C     ***MATRIX ROUTINES***
C     *MODIFIED JACOBIAN*
      DO 130 I=2,NL
      K1(I)=-DT*J1(I)
      K2(I)=-DT*J2(I)
      K3(I)=1.0-DT*J3(I)
```

```
130   CONTINUE
      DO 135 ID=1,HT
      T1(ID)=-DT*TA(ID)
      T2(ID)=-DT*TB(ID)
135   CONTINUE
400   DO 460 ID=1,HT
      K4(ID)=1.0-DT*J4(ID)
460   CONTINUE
C     ***RHS FUNCTION***
      DO 145 ID=1,H
      S3=0.0
      S2=0.0
      DO 140 I=2,NL
      F(ID,I)=YM(ID,1)*CG(I)-YM(ID,I)*CE(I)
      S2=S2-YM(ID,I)*J3(I)
      DU(ID,I)=DT*F(ID,I)-YM(ID,I)+YS(ID,I)
140   CONTINUE
      IF (ID.EQ.H) GOTO 340
      IF (ID.EQ.1) GOTO 350
      F(ID,1)=YM(ID,1)*J4(ID)+S2+CD*
     1YM(ID-1,1)+BD*YM(ID+1,1)
      GOTO 360
350   F(1,1)=YM(1,1)*J4(1)+S2+BD*YM(2,1)
      GOTO 360
340   F(H,1)=YM(H,1)*J4(H)+S2+CD*YM(H-1,1)
360   DU(ID,1)=DT*F(ID,1)-YM(ID,1)+YS(ID,1)
145   CONTINUE
      F(HT,1)=YM(H,1)*CD
      DU(HT,1)=DT*F(HT,1)-YM(HT,1)+YS(HT,1)
C     ****DIAGONALISATION***
      DO 155 ID=1,H
      S3=0.0
      S4=0.0
      DO 150 I=2,NL
      E1=-K1(I)/K3(I)
      S3=S3+DU(ID,I)*E1
      S4=S4+K2(I)*E1
150   CONTINUE
      K4(ID)=K4(ID)+S4
      DU(ID,1)=DU(ID,1)+S3
155   CONTINUE
C     ELIMINATE TRIDIAG ELEMENTS
C     ELIMINATE T1(ID)
      DO 380 ID=1,H
      E3=T1(ID+1)/K4(ID)
C      WRITE(5,900)E3,ID
C900   FORMAT(' E3=',D10.4,' ID=',I3)
      K4(ID+1)=K4(ID+1)-E3*T2(ID)
C      WRITE(5,910)K4(ID+1)
C910   FORMAT(D10.4)
      DU(ID+1,1)=DU(ID+1,1)-E3*DU(ID,1)
C      WRITE(5,920)DU(ID+1,1)
C920   FORMAT(D10.4)
380   CONTINUE
C     ELIMINATE T2(ID)
      DO 390 IN=1,HL
```

```
      IH=H-IN
      IT=HT-IN
      E4=T2(IH)/K4(IT)
      DU(IH,1)=DU(IH,1)-E4*DU(IT,1)
390   CONTINUE
C     ELIMINATE FIRST COLS
      DO 160 ID=1,H
      E2=DU(ID,1)/K4(ID)
C     IF(E2.LT.1.0D-30)E2=0.0
      DO 160 I=2,NL
      DU(ID,I)=DU(ID,I)-E2*K2(I)
C      WRITE(5,930)DU(ID,I),E2,K2(I)
C930   FORMAT(' DU,E2,K2,',3D10.4)
160   CONTINUE
      DO 175 ID=1,HT
      DO 170 I=2,NL
      DU(ID,I)=DU(ID,I)/K3(I)
170   CONTINUE
      DU(ID,1)=DU(ID,1)/K4(ID)
175   CONTINUE
      DO 190 ID=1,HT
      DO 190 I=1,NL
      YM(ID,I)=YM(ID,I)+DU(ID,I)
190   CONTINUE
C     ***TEST TOLERANCES***
      ER1=DABS(DU(1,1))+DABS(DU(HT,1))
      ER2=DABS(YM(1,1))+DABS(YM(HT,1))
      ERR=ER1/ER2
      IF (ERR.GT.TL) GOTO 400
C     **UPDATE VARIABLES**
      YD=YS(HT,1)
      DO 210 ID=1,HT
      DO 210 I=1,NL
      YS(ID,I)=YM(ID,I)
210   CONTINUE
C     **END ITERATION IF 20% THRU**
      AYS=0.2-YS(HT,1)
      AY=DABS(AYS)
      IF (AY.GT.0.00001) GOTO 660
      Y(JT,KY)=TT
      X(JT,1)=1.E3/T
      L=0
      GOTO 87
C     ***STEP LENGTH STRATEGY***
660   IF (YS(HT,1).LT.0.01) GOTO 600
      IF (YS(HT,1).LT.0.1) GOTO 610
      DT=0.5*(0.2-YS(HT,1))*DT/(YS(HT,1)-YD)
      GOTO 620
610   DT=0.1*TT
      GOTO 620
600   DT=0.2*TT
620   L=L+1
      WRITE(5,800)TT,YS(HT,1),T,KY
800   FORMAT(2X,1PD14.6,4X,1PD10.4,4X,1PD10.4,4X,I3)
      GOTO 650
87    CONTINUE
```

```
85     CONTINUE
80     CONTINUE
       DO 1020 I=1,IM
       DO 1020 K=1,KM
       Y(I,K)=LOG(Y(I,K))
1020   CONTINUE
       DO 2000 K=1,KM
       SX=0.0
       SY=0.0
       SXY=0.0
       SX2=0.0
       DO 1040 I=1,IM
       SX=X(I,1)+SX
       SX2=SX2+X(I,1)*X(I,1)
       SY=SY+Y(I,K)
       SXY=SXY+Y(I,K)*X(I,1)
1040   CONTINUE
       D=(FL(IM)*SX2)-(SX*SX)
       AM=((FL(IM)*SXY)-(SX*SY))/D
       ACTE=AM*8.625D-5*1000.
       WRITE(5,1050)DAT(K,1),ACTE
1050   FORMAT(' TR/TF= ',F6.1,' DRIFT ACT
      1ENERGY IS ',1PD14.6,' EV')
2000   CONTINUE
       STOP
       END
```